Strömgren Color-Temperature Relations for Cool Stars

by
James Lewis Clem
B.Sc., University of Arkansas, 1998

A Thesis Submitted in Partial Fulfillment of the
Requirements for the Degree of

MASTER OF SCIENCE

in the Department of Physics and Astronomy

We accept this thesis as conforming
to the required standard.

[redacted]

Dr. D. A. VandenBerg, Supervisor (Department of Physics & Astronomy)

[redacted]

Dr. C. J. Pritchet, Departmental Member (Department of Physics & Astronomy)

[redacted]

Dr. F. El Guibaly, Outside Member (Department of Electrical & Computer Engineering)

[redacted]

Dr. F. Grundahl, Outside Member (Aarhus University, Denmark)

[redacted]

Dr. J. E. Hesser, External Examiner (The Herzberg Institute for Astrophysics)

Supervisor: Dr. D A. VandenBerg

Abstract

Color temperature relations and bolometric corrections are commonly employed not only to infer the physical properties of a star from its photometric color indices, but more importantly to translate stellar evolutionary tracks and isochrones from the theoretical temperature-luminosity plane to the observational color-magnitude plane. The current work discusses the efforts to develop a new and extensive grid of synthetic Strömgren colors applicable to cool, low mass stars (i.e., those having $3000\,\mathrm{K} \leq \mathrm{T_{eff}} \leq 8000\,\mathrm{K}$, $-0.5 \leq \log g \leq 5.0$, and $-3.0 \leq [\mathrm{Fe/H}] \leq +0.5$). These purely theoretical colors, based on the latest versions of the MARCS model atmosphere and SSG spectral synthesis codes, are placed onto the observational systems by applying color calibrations derived from the *uvby* photometry of field stars having accurate *Hipparcos* parallaxes and effective temperatures determined using the infrared flux method. The resultant color transformations are able to reproduce the observed colors of the classic Population II subdwarfs quite satisfactorily, as well as yield a very good fit of a 4 Gyr isochrone, whose $\mathrm{T_{eff}}$ scale is normalized to the Sun, to the observational color-magnitude diagram of the open cluster M 67. To supplement this investigation, recent photometric observations in the *uvby* filter system of the open clusters NGC 188 and NGC 6819 were obtained to further constrain the accuracy of the new Strömgren color-temperature relations for solar metallicities. Moreover, when the latest theoretical isochrones of Bergbusch & VandenBerg (2001) are transformed to the various Strömgren color planes, they provide superb fits to the CMDs of such globular clusters as M 92, M 13, NGC 288, and 47 Tuc when reasonable estimates for the basic cluster parameters (i.e. distance, reddening, and metallicity) are assumed.

Examiners:

[redacted]

Dr. D. A. VandenBerg, Supervisor (Department of Physics & Astronomy)

[redacted]

Dr. C. J. Pritchet, Departmental Member (Department of Physics & Astronomy)

[redacted]

Dr. F. El Guibaly, Outside Member (Department of Electrical & Computer Engineering)

[redacted]

Dr. F. Grundahl, Outside Member (Aarhus University, Denmark)

[redacted]

Dr. J. E. Hesser, External Examiner (The Herzberg Institute for Astrophysics)

Table of Contents

List of Tables

List of Figures

Acknowledgments

While it seems such a trivial task to acknowledge those people who have supported and/or encouraged me throughout the time leading up to and including the writing of this thesis, I find it somewhat impossible to express how thankful I truly am to all of them on just a few pages. In truth, my appreciation goes well beyond whatever is written here, and I must emphasize that the people I list in the following paragraphs deserve much more recognition than I can rightly give them with just a few simple words on paper.

To those people who have made my research possible, I would foremost like to thank my supervisor, Don VandenBerg, for his insightful discussions, advice, motivation, guidance, and generous financial support during my study. His knowledge of stellar structure and evolution far outweighs anything which could be found in a textbook, and his enthusiasm towards my own research made the whole process more exciting (and even more bearable) for me. Also, I am indebted to Frank Grundahl who graciously provided the majority of superb photometric data used for this thesis, as well as his vast knowledge and many useful discussions on photometry and data reduction. Finally, much thanks is extended to Roger Bell of the University of Maryland for the use of the programs employed to generate the synthetic Strömgren colors.

Over the past three years, a number faculty and staff members here in the department have offered their words of advice and/or lended an ear when I needed to ask a question or vent some frustration. In particular, Russ Robb always had his door open and the time to listen to whatever I had to say. I would also like to thank Mr. David Balam (a.k.a. Uncle Dave) for every light-hearted, but wise, word of advice he has offered to me as well as having a sense of humor (slightly) more twisted than my own. In addition, his patience and guidance during my observing time at the Plaskett

telescope made the entire experience extremely rewarding and less stressful for me. To Stephenson Yang, I want to express my appreciation for all the time, energy, and devotion in keeping the computers operating smoothly here on the fourth floor of the Elliot Building.

Of course, I can't exclude (for concerns of my own personal safety) my fellow graduate students, both past and present, from this list - those people with whom I've shared many laughs, many beers, and many strange stories. I have to admit that despite the onslaught of jokes concerning my nationality, and particularly my home state - not to mention persistent attempts to assimilate me into the Canadian culture - no other group of people has made me feel more comfortable and more welcome during my stay in Canada. From Friday afternoon beer time to Mr. Gwyn's infamous boat drinks parties where anything that you couldn't possibly imagine happening, inevitably did, my life as a graduate student has been a fun and rather interesting one. To those people (and you know who you are), I want to extend my deepest gratitude.

On a personal level, I have been, and will forever be, indebted to my parents, Donald and Arlene Clem, for their endless love and support throughout my life. While they admittedly never fully understood what exactly I was studying at a Canadian university, they always were willing to provide whatever I needed to get me through the good - and not so good - times. Finally, and most certainly not the least, to the person who has shown much patience, sacrifice, understanding, and love to me throughout the time I have known her, I cannot truly express the amount of gratitude, appreciation, and love I have in my heart for you, Melissa. You have always been there to show an interest in what I was doing as well as lend a supporting and caring ear to my troubles and frustrations. I thank you for what you have done for me, and I am extremely happy to have had you as a part of my life for the past three years.

Chapter 1

Introduction

Given all the observational and empirical tools astronomers have at their disposal, the Hertzsprung-Russell (HR) diagram has proven to be one of the most valuable in our quest to understand the physical and evolutionary properties that govern the nature of stars. Ideally, the best way to ascertain a star's position within the HR diagram is to obtain high-resolution observations of the stellar spectral energy distribution and derive estimates for its basic physical properties such as effective temperature, surface gravity, and chemical composition ($T_{\rm eff}$, $\log g$, and [Fe/H], respectively). In practice, however, this method of study is very time consuming and feasible for only the brightest stars. For example, the idea of obtaining individual spectra for each member of a stellar cluster which could contain hundreds or thousands of stars would require an overwhelming amount of observing time (even assuming the stars are bright enough to get usable spectra). Thus, for the study of a large number of fainter objects, astronomers must resort to lower resolution techniques such as multicolor photometry. The method of photometry typically involves the use of filters to allow observations of an object to be made in specific wavelength regions. If the photometric system used is well designed and calibrated, it can provide an accurate means for investigating the physical characteristics of a multitude of stars where higher resolution data are not

available. One of the benefits of this type of study is the creation of the photometric equivalent to the HR diagram, the color-magnitude diagram (CMD). By plotting a star's color (i.e. the difference of its brightness through two different filters) versus its magnitude, the resulting CMD still retains the same basic information as an HR diagram, but obtained with much less time and effort.

1.1 The Strömgren Photometric System

Among all the photometric systems available today, the two most widely used are the UBV system of Johnson and Morgan (1953) and the *uvby* system of Strömgren (1963). While both systems were born out of the desire to develop a framework for classifying stars on the basis of photoelectric indices, certain aspects of the *uvby* system set it apart from its UBV counterpart. Namely, the four Strömgren filters (u, b, v, and y) are characterized by their intermediate bandwidths ranging from 180 to 300 Å as compared to the broader ($\approx$ 700-950 Å) UBV filters. Table 1.1 lists the specifics regarding the central wavelengths, bandwidths, and transmissions for the two filter sets whereas Figure 1.1 plots a comparison of their location and spectral coverage.

As seen in the figure, the four Strömgren filters sample the same spectral region as the broadband system, only more finely. The narrowness of each filter together with their wide spectral coverage as a whole gives the *uvby* system several advantages over the broader UBV filters. The Strömgren y (yellow) filter is centered in the middle of the visual part of the electromagnetic spectrum and closely corresponds to the Johnson V filter. Indeed, early calibrations showed that stellar magnitudes determined through the Strömgren y filter can be equated to V in photometric studies. Also, the filter transmits no strong spectral features in stars of most spectral types. Likewise, the b (blue) filter sits in a region where the effects of line absorption are not particularly strong for early type stars. The next filter, v (violet), is positioned

Table 1.1: The filters used to define the *uvby* and *UBV* photometric systems. All information presented in this table as well as the filter response functions plotted in Figure 1.1 are taken from Crawford & Barnes (1970b) and Strömgren (1963) for the *uvby* filters and Johnson & Morgan (1951) for the *UBV* filters.

Filter	Central Wavelength (Å)	Bandwidth (Å)	Maximum Transmission (%)
u	3500	300	44
v	4110	190	46
b	4670	180	47
y	5470	230	52
U	3600	690	60
B	4400	960	55
V	5500	900	43

above the Balmer discontinuity limit in a region which is strongly affected by line blanketing in stars of all spectral types. Finally, the u, or ultraviolet, filter is confined completely within the region defined by the Balmer discontinuity to the red and the cutoff imposed by the Earth's atmosphere at shorter wavelengths.

To illustrate how the Strömgren filters serve to isolate important features in a stellar spectrum, Figure 1.2 presents a synthetic spectrum of a normal main sequence star of spectral type F 5 and its corresponding theoretical continuum represented by a dotted line overplotted with spectral coverage of each *uvby* filter from Table 1.1. From the locations of the b and y filters it is obvious that neither filter suffers from any significant absorption features. Therefore, it follows that the color index $(b-y)$ is particularly insensitive to the effects of line absorption in this portion of the spectrum and can be considered as an accurate estimator of continuum slope. For this reason, the $(b-y)$ index is a good indicator of stellar effective temperature ($T_{\rm eff}$) akin to the $(B-V)$ index in broadband photometry.

The same does not hold true for the difference in flux between the v and b filters, however. The $(v-b)$ index is strongly affected by the prominent absorption features

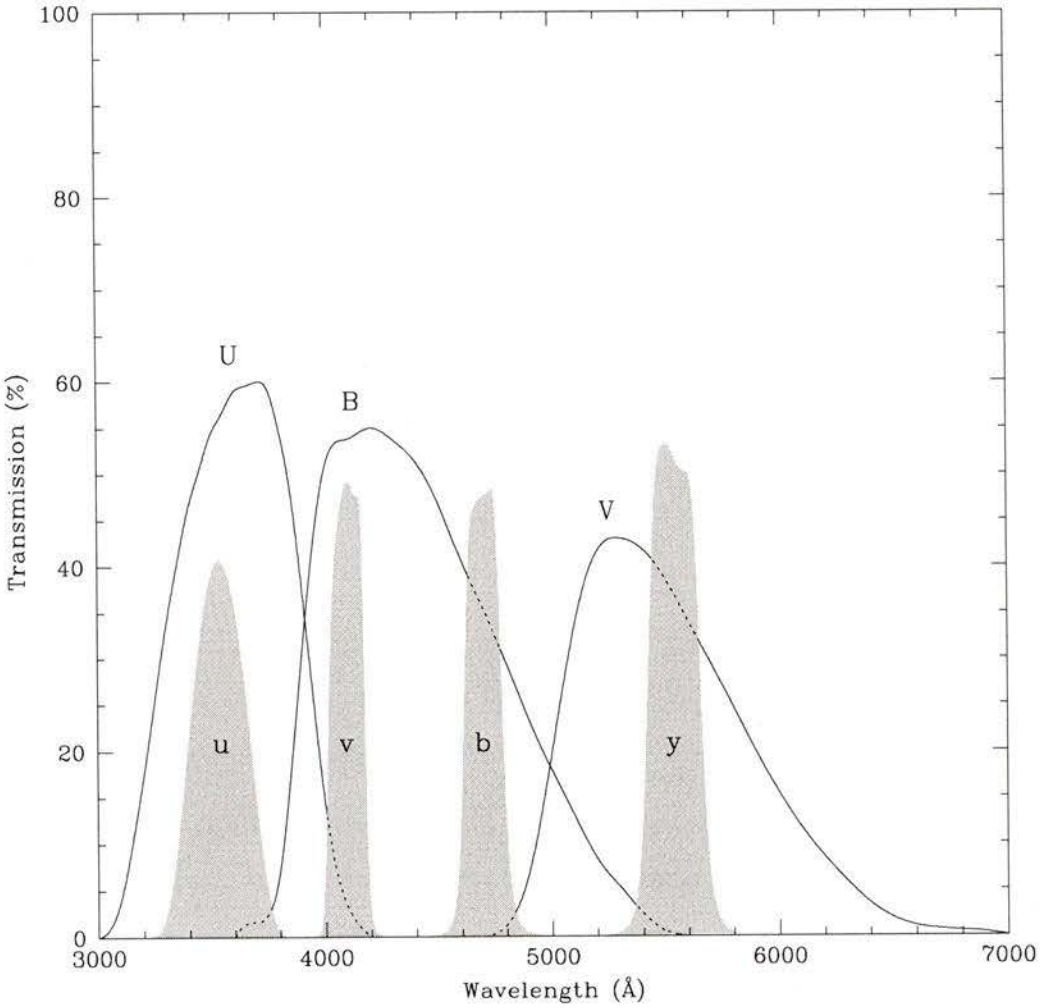

Figure 1.1: The transmission curves of the Strömgren *uvby* filter set compared to the *UBV* filters of Johnson & Morgan.

in the v band. Thus, a new quantity m_1 $[=(v-b)-(b-y)]$ is defined to measure the intensity of the line blanketing in the v filter relative to the color gradient in the b and y regions. Indeed, the Strömgren m_1 index is generally considered to be an accurate photometric measurement of the abundance of heavy elements (i.e. elements heavier than helium) in a star's atmosphere due to the fact that a higher abundance of metals results in increased absorption in the v band. In his seminal paper discussing the benefits of the *uvby* system, Strömgren (1966) presented a simple correlation between m_1 and the stellar abundance parameter, [Fe/H]. While his analysis was based on only a few main sequence stars, it presented the first real evidence that m_1 could successfully be calibrated against [Fe/H]. Since that time, numerous such calibrations for both main sequence and giant stars have surfaced in the literature (e.g., see Schuster & Nissen 1989 and Hilker 2000 and references therein) which report both well defined and consistent relations between photometric and spectroscopic abundance determinations.

As mentioned earlier, the Strömgren u filter lies almost completely below the Balmer discontinuity at 3647 Å. For this reason, the $(u-v)$ index can be considered as a measurement of both the height of this discontinuity plus the fraction of line blanketing as measured by the $(v-b)$ index. Taking the difference between these two color indices leads to the quantity c_1 $[=(u-v)-(v-b)]$ which accounts solely for the size of the Balmer jump and is commonly considered to be an accurate indicator of stellar surface gravity in most stars (specifically mid-B to early-G type stars). A star's gravity (commonly expressed logarithmically as $\log g$) is dependent on its evolutionary state. Main sequence stars (classes IV and V in the Morgan-Keenan classification scheme) have the highest values for $\log g$ while giants (classes I, II, and III) of the same spectral type typically have much smaller values due to their large size. A difference in $\log g$ correlates with Balmer discontinuity because the size of the jump is less in giants than in main sequence stars due to pressure effects. As with the m_1 parameter, Strömgren recognized the usefulness of the c_1 index in distinguishing

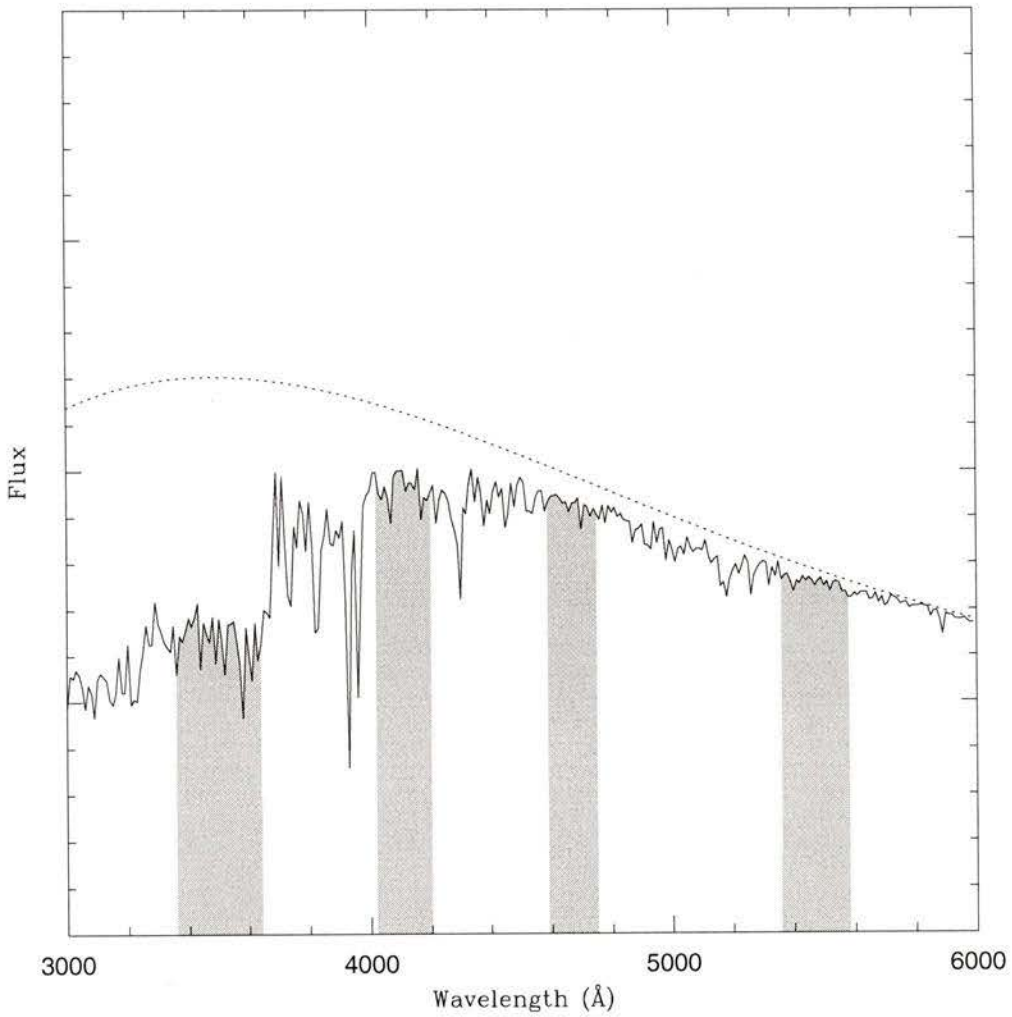

Figure 1.2: The spectral coverage of each *uvby* filter overplotted on a theoretical spectrum corresponding to an F5 V star to illustrate how each filter isolates certain important spectral features. The dotted line represents the theoretical continuum level of a star of the same spectral type.

between giants and dwarfs having the same spectral type, and a number of studies have addressed the c_1 - $\log g$ correlation both theoretically (Relyea & Kurucz 1978 and Moon & Dworestsky 1985) and observationally (Castelli 1991 and Napiwotzki et al. 1993) .

In summary, the Strömgren *uvby* photometric system can provide precise photometric estimates of star's effective temperature, surface gravity, and chemical composition via the definition of the $(b-y)$, m_1, and c_1 color indices, respectively. It is this ability that sets Strömgren intermediate-band photometry apart from standard broadband UBV photometry. The broadness of the UBV filters greatly limits the amount of information that can be obtained photometrically for a star. While the $(B-V)$ index is quite similar to the Strömgren $(b-y)$ index in providing T_{eff} information, it cannot be used (like the m_1 index) to infer the metallicity of a star. Furthermore, the four color system is almost completely filter defined and is barely affected by detector sensitivity or atmospheric limitations. The same cannot be said for the broadband U filter, which can be compared to the Strömgren u filter through the fact that they are both centered at roughly the same wavelength and the $(U-B)$ index can be used to estimate the size of the Balmer jump. Due to its large bandwidth, however, it is not fully contained between the Balmer discontinuity to the red and the atmospheric cutoff towards shorter wavelengths like the u filter, and photometric observations and reductions involving the U filter are affected by both the instrumentation and observing location.

Despite all of the advantages and potential that the Strömgren *uvby* system brings to our understanding of the nature of stars, many researchers still adopt the UBV filters as their photometric system of choice. This fact can likely be attributed to the following reasons. First, observations using the *uvby* filters typically require longer integration times due to their narrower bandwidths. This problem has been mostly overcome, however, with the modern use of CCD detectors which offer both superb sensitivity over a wide spectral range and the ability to simultaneously observe a

large number of stars within the same field compared to the older photon counting instruments which were limited to observing one star at a time. Second, in order to use the Strömgren system to its full potential, observations should be made through each of the four *uvby* filters. This, along with the aforementioned longer integration times, poses a problem for astronomers who are limited by their observing time budget, and many may choose to sacrifice the information which could be obtained using the four-color system for the expedience of the UBV filters. The final reason derives from the fact that direct comparisons of theoretical stellar models to Strömgren photometric data have been difficult in the past owing to the lack of modern and precise *uvby* color-temperature relations and bolometric corrections which are needed to transform these models to the observations. While this problem will be addressed in detail throughout the present work, it suffices to say here that this current inability to accurately relate theoretical models to *uvby* data is a significant reason why the UBV system has remained the dominant photometric system for observers and theorists.

1.2 The Role of Color-Temperature Relations

One area where astronomical photometry plays a crucial role is the study of star clusters. These stellar populations are composed of multitude of stars with a wide range in mass but with essentially the same age and chemical composition. For this reason, clusters and their associated photometric CMDs offer ideal testing grounds for many aspects of stellar evolution theory. The most popular way to compare the theory with photometric observations is by computing numerous stellar evolutionary tracks as a function of mass, determining a position on each track corresponding to a specific age, and comparing the resulting curve connecting these positions (i.e. an *isochrone*) to the actual distribution of stars in a cluster CMD. This so-called "isochrone fitting" technique has been widely used in the past to not only test the overall accuracy of the stellar models, but also to yield estimates for the cluster's

distance, reddening, and age provided an isochrone modeled with the same chemical composition as the cluster is employed.

However, there is a crucial step in this type of confrontation between theory and observations. Specifically, how do the model evolutionary tracks and isochrones, computed in terms of stellar temperature and luminosity, get transferred to their observational equivalents of photometric color and magnitude? For this purpose, a set of predefined color-temperature (C-T) relationships and bolometric corrections (BCs) are required to link photometrically determined indices with the fundamental stellar parameters of effective temperature, surface gravity, and chemical composition. In a time when extremely precise cluster photometry and recent stellar models which account for the most up-to-date physics are becoming readily available, these C-T relations and BCs play an increasingly important role in bridging the gap between theory and observation. Not only are extremely precise and consistent relations needed to check the accuracy of the stellar models in interpreting photometric data, but they must also ensure that reasonable estimates for a star's T_{eff}, $\log g$, and chemical composition can be obtained from just knowing its photometric indices.

Typically, C-T relations and BCs for any photometric system can be derived by using either theoretical or empirical methods. Whereas theoretical grids of synthetic colors are produced by convolving models of photometric filter transmission profiles with synthetic spectra of stars having a wide range of effective temperatures, surface gravities, and chemical compositions, empirical methods rely on calibrating photometric colors against stars having precise estimates for their basic parameters. Both methods have their advantages and disadvantages. For instance, the production of large grids of theoretical colors are ideal for transforming isochrones and evolutionary tracks to the observational plane owing to the fact that a color and magnitude can be readily computed for any stellar model. However, the accuracy of the synthetic colors tend to rely on how well the input synthetic atmospheres and spectra are able to reproduce the observed spectrum of an actual star. Empirical C-T relations, on the

other hand, overcome this problem because they are largely model independent, but they are restricted to a very limited sample of stars with well-determined values for T_{eff}, log g, and [Fe/H]. While some considerable effort has been devoted over the years to deriving such C-T relations for the Strömgren system using both techniques (see, e.g., the discussions of Relyea & Kurucz 1978, Moon & Dworetsky 1985, VandenBerg & Bell 1985, Kurucz 1991, Gratton et al. 1996, and Alonso et al. 1996b), and the results appear to show reasonable agreement for some cases (often for warmer effective temperatures) but usually fail to reproduce the photometric data to a high degree of accuracy over the entire range in temperatures; a fact that is generally exemplified by inadequate isochrone fits to cluster *uvby* CMDs (Grundahl et al. 1998, 2000).

1.3 Scope of the Present Study

Given that currently available C-T relations and BCs for the *uvby* system appear to provide a limited degree of success in relating stellar evolutionary models to *uvby* observations, this study undertakes the task of deriving a new, more extensive, and internally consistent grid of synthetic Strömgren colors on the basis of theoretical stellar spectra but constrained to satisfy empirical data. While Chapter 2 outlines the basic concepts and programs involved in computing the theoretical Strömgren colors, Chapter 3 will seek to constrain the accuracy of the resultant synthetic colors by testing them against a number of field stars with well-determined values for T_{eff}, log g, and [Fe/H] and accurate *Hipparcos* parallaxes. Chapter 4 will serve two purposes. First, the testing of the theoretical Strömgren colors will continue by transforming a number of isochrones to the observational color-magnitude plane and fitting them to the *uvby* CMDs of a large sample of open and globular clusters with various ages and metallicities. Secondly, the consistency between such fits to the four color CMDs and those obtained from broadband CMDs will be investigated to determine whether or not the same isochrone yields the same interpretation of the data regardless of which

photometric color is used. Finally, concluding remarks are presented in Chapter 5.

Chapter 2

The Synthetic Colors

In any ground-based photometric system light from a star passes through the Earth's atmosphere, is reflected by the optics in a telescope, passes through a filter, and is collected at the focal plane by a photon detecting device. To allow intercomparisons of observations made using different equipment (i.e. telescopes, filters, and detectors), a number of stars are observed that have colors defined on a standard system. The observed data are then transformed to the standard system by forcing the standard and observed colors to agree. In order to generate a set of synthetic colors, one must not only be able to model the spectrum of a star, but also construct a theoretical photometric system which accurately accounts for all of the principles mentioned above (such as the transmission of the atmosphere, the reflectivity of the telescope mirrors, transmission of the filters, sensitivity of the detector, and the adoption of suitable standard stars).

The following chapter outlines the basic ideas and procedures involved in constructing a set of synthetic Strömgren colors via the following steps: 1) Create a unique theoretical model atmosphere corresponding to a star having a specific effective temperature, surface gravity, and chemical composition ($T_{\rm eff}$, $\log g$, and [Fe/H], respectively), 2) employ this model atmosphere in the generation of a synthetic stel-

lar spectrum, and 3) convolve the resulting synthetic spectrum with the response functions of the *uvby* filters. Repeating these steps for a number of stellar models covering a wide range in temperature, gravity, and abundance results in a composite grid of synthetic colors suitable for either transforming theoretical stellar models to the observational plane or estimating the basic properties for a star basely solely on its observed photometric indices.

2.1 Stellar Atmosphere Models

The MARCS program (Gustafsson et al. 1975) has been widely used in the past for the construction of model stellar atmospheres. The current version of the MARCS program computes a flux-constant, homogeneous, plane-parallel atmosphere assuming hydrostatic equilibrium and local thermodynamic equilibrium. The solar abundance scale adopted for the models follows that given by Anders & Grevesse (1989) with small modifications to the carbon and nitrogen abundances reported by Grevesse et al. (1990, 1991). Furthermore, enhancements to the α process elements (O, Ne, Mg, Si, S, Ar, Ca, and Ti) by +0.4 dex relative to the solar value were considered for models with [Fe/H] $\leq$ -1.0 and +0.25 for [Fe/H] = -0.5. For models with solar and super-solar abundances, no α enhancements were considered in the mix. These enhancements in the model atmospheres reflect recent spectroscopic evidence (Zhao & Magain 1990, Kraft et al. 1998, and Carney 1996) which suggest an overabundance of the α elements relative to solar (commonly denoted as [α/Fe]) of at least +0.3 dex is present in the most metal poor halo and globular cluster stars. Table 2.1 presents the chemical abundance mix adopted for not only the MARCS atmospheres, but also for the generation of the synthetic spectra which will be described in the next section.

The tabulated values listed in Table 2.1 are given on the logarithmic scale usually adopted by astronomers in which the abundance of each element is expressed relative to the number abundance of Hydrogen by $A_{el} = log N_{el}/N_H + 12.0$. Elements marked

Table 2.1: Solar elemental abundances considered in the generation of the model atmospheres and synthetic spectra taken from Anders & Grevesse (1989) with small modifications to the abundances of C and N given by Grevesse et al. (1990, 1991). Elements flagged by double asterisks are those required as input to the MARCS atmosphere program.

Element	Abundance	Element	Abundance	Element	Abundance
01 **H** **	12.00	29 **Cu**	4.21	58 **Ce**	1.55
02 **He** **	10.99	30 **Zn**	4.60	59 **Pr**	0.71
03 **Li**	1.16	31 **Ga**	2.88	60 **Nd**	1.50
04 **Be**	1.15	32 **Ge**	3.41	62 **Sm**	1.00
05 **B**	2.60	33 **As**	2.37	63 **Eu**	0.51
06 **C** **	8.60	34 **Se**	3.35	64 **Gd**	1.12
07 **N** **	8.00	35 **Br**	2.63	65 **Tb**	-0.10
08 **O** **	8.93	36 **Kr**	3.23	66 **Dy**	1.10
09 **F**	4.56	37 **Rb**	2.60	67 **Ho**	0.26
10 **Ne** **	8.09	38 **Sr**	2.90	68 **Er**	0.93
11 **Na** **	6.31	39 **Y**	2.24	69 **Tm**	0.00
12 **Mg** **	7.58	40 **Zr**	2.60	70 **Tb**	1.08
13 **Al** **	6.48	41 **Nb**	1.42	71 **Lu**	0.76
14 **Si** **	7.55	42 **Mo**	1.92	72 **Hf**	0.88
15 **P**	5.57	44 **Ru**	1.84	73 **Ta**	0.13
16 **S**	7.27	45 **Rh**	1.12	74 **W**	1.11
17 **Cl**	5.27	46 **Pd**	1.69	75 **Re**	0.27
18 **Ar**	6.56	47 **Ag**	0.94	76 **Os**	1.45
19 **K** **	5.12	48 **Cd**	1.86	77 **Ir**	1.35
20 **Ca** **	6.34	49 **In**	1.66	78 **Pt**	1.80
21 **Sc**	3.10	50 **Sn**	2.00	79 **Au**	1.01
22 **Ti** **	4.93	51 **Sb**	1.00	80 **Hg**	1.09
23 **V**	4.00	52 **Te**	2.24	81 **Tl**	0.90
24 **Cr** **	5.68	53 **I**	1.51	82 **Pb**	1.85
25 **Mn**	5.53	54 **Xe**	2.23	83 **Bi**	0.71
26 **Fe** **	7.51	55 **Cs**	1.12	90 **Th**	0.12
27 **Co**	4.92	56 **Ba**	2.13	93 **U**	-0.47
28 **Ni** **	6.25	57 **La**	1.22		

by double asterisks indicate those abundances which are required as input in the MARCS program. MARCS accounts for atmospheres with differing chemical compositions by multiplying all abundances except H and He by $10^{-0.5}$, 10^{-1}, 10^{-2}, *etc.* to obtain the metallicities denoted by [M/H][1] $= -0.5$, -1.0, and -2.0, respectively.

The treatment of convective energy transport in the atmospheric models follows the variant of the mixing-length theory given by Henyey et al. (1965). For all models, the mixing length ℓ was set to a value of 1.6 the pressure scale height H_p ($\ell = 1.6H_p$). Furthermore, the y parameter describing the transparency of convective bubbles was set to $3/(4\pi^2) \approx 0.076$ which corresponds to the temperature structure of a convective element that results from the diffusion approximation.

The MARCS program incorporates opacity distribution functions (ODFs) to represent the opacity due to atomic and molecular lines as a function of wavelength. The specifics regarding the concepts and construction of ODFs are explained extensively in Gustafsson et al. (1975, sec. IIIb). For the sake of brevity, however, only a basic outline of how MARCS uses an ODF to compute a model atmosphere will be presented here. The ODFs are produced from the latest lists of spectral lines which contribute significantly to the line opacity. In general, an ODF is set up in the form of a look-up table for interpolating the opacity in a certain wavelength region as a function of both the temperature and electron pressure derived from MARCS. Obviously, a different ODF must be computed for different chemical abundance mixes (i.e. different metallicities) owing to the fact that a higher abundance would mean that the overall line spectrum will be richer.

[1]Past literature devoted to theoretical atmosphere studies typically adopt [M/H] or [A/H] to logarithmically express the number abundance ratio of *all* metals to hydrogen relative the sun. However, the most convenient way of quantifying a star's chemical composition observationally is its iron to hydrogen abundance ratio relative to the sun, or [Fe/H]. While there are distinct differences between these two values, both in their meaning and function, they will be used interchangeably throughout the present work to refer to the "metallicity" of a star and/or model.

2.2 The Synthetic Spectra

The SSG spectral synthesis code (Bell & Gustafsson 1978, 1989) uses the generated MARCS stellar atmosphere together with spectral line data, a Doppler broadening velocity (which includes both a thermal and microturbulent term), and the elemental abundances presented in Table 2.1 to compute a synthetic stellar spectrum. The synthetic spectra presented here have been computed at 0.1 Å resolution covering an optical wavelength range of 3000 - 8000 Å . SSG uses the most up-to-date atomic and molecular line lists (described in Bell et al. 1994) together with an additional TiO line list for all spectra with $T_{eff} \leq 4000$ K to accommodate for the increased strength of TiO molecular absorption features in cool stars (Houdashelt et al. 2000). Furthermore, the microturbulent velocity, ξ, is assumed to vary as a function of surface gravity using the relation $\xi = 2.22 - 0.322 \log g$ (Gratton et al. 1996). To account for the continuum opacity due to H^-, SSG assumes the Wishart (1979) and Bell & Berrington (1987) bound-free and free-free cross-sections for the H^- ion, respectively.

2.3 Synthetic Photometry

As mentioned at the beginning of this chapter, the process of computing synthetic magnitudes and colors typically involves using a synthetic stellar spectrum as input into a theoretical photometric system. This system convolves the spectrum with not only the transmission profiles for a specific filter set, but also the detector sensitivity function, and an atmospheric extinction profile. By definition, the computed magnitude m_i for a particular filter or passband is given by:

$$m_i = -2.5log \int_{\alpha_i}^{\beta_i} F_\lambda S_i(\lambda) A(\lambda) d\lambda, \tag{2.1}$$

where F_λ is the computed monochromatic flux at the stellar surface, $S_i(\lambda)$ is the sensitivity function describing the fraction of the star's flux that is detected at wavelength

λ,[2] $A(\lambda)$ is the transmission of Earth's atmosphere, and α_i and β_i give the wavelength interval of $S_i(\lambda)$. From this formalism the photometric color indices are simply expressed as the difference between the magnitude of a star in two different spectral regions (i.e. through two different filters i and j). However, the synthetic indices cannot be directly compared to the observed indices of a star due to the fact that the computation of synthetic magnitudes involve the flux at the stellar surface, whereas observed stellar colors always involve apparent magnitudes. In practice, each computed index can correctly be related to the corresponding observed index by means of an additive constant:

$$(m_i - m_j)_{obs} = (m_i - m_j)_{calc} + C. \tag{2.2}$$

The most practical way to derive this constant C is by forcing a fit between computed and observed colors for a given star or sample of stars well reproduced by the stellar models.

A bolometric correction BC_i is described as the correction required to reduce a magnitude in a given bandpass to a bolometric magnitude. In other words, the computed BC_i is:

$$BC_i = (m_{bol} - m_i)_{calc} + K, \tag{2.3}$$

where, by definition, m_{bol} is the apparent magnitude of a star measured over all wavelengths:

$$m_{bol} = -2.5log \int_0^\infty F_\lambda d\lambda = -2.5log(\sigma T_{\rm eff}^4). \tag{2.4}$$

Thus, the bolometric correction BC_V relative to the broadband Johnson V magnitude reduces to:

$$BC_V = -2.5 \left[log(\sigma T_{\rm eff}^4) - log \int_{\alpha_V}^{\beta_V} F_\lambda S_V(\lambda) A(\lambda) d\lambda \right] + K. \tag{2.5}$$

where the constant K is required to match the adopted solar BC_V.

[2] $S_i(\lambda)$ can include such factors as the transmission of the photometric filters and other optical components used, the detector response, and the reflectivity of the telescope mirrors.

The IRCONVABS program serves as the virtual photometric system which is employed to calculate the synthetic Strömgren photometric indices and bolometric corrections given a theoretical stellar spectrum as input. IRCONVABS proceeds to compute the *uvby* magnitudes, color indices, and bolometric corrections by convolving the spectrum with the *uvby* filter transmission curves given by Crawford & Barnes (1970b) while accounting for atmospheric extinction due to Rayleigh scattering by molecules and scattering by aerosols using the treatment of Hayes & Latham (1975). At wavelengths longward of 7600 Å the effects of terrestrial line absorption are also included by considering the Manduca & Bell (1979) computations of Kitt Peak winter extinctions.

As a final step, the synthetic colors must be related to the observed Strömgren system by forcing agreement between the observed and calculated indices for a standard star. The most common way of doing this is to construct a synthetic flux model for a suitable standard like Vega, which is assumed to have $T_{\rm eff} = 9650$, $\log g = 3.90$, and $[{\rm Fe/H}] = 0.0$ (Dreiling & Bell 1980), and then compare it to the observed flux distribution. A significant amount of work has been devoted to this type of comparison (see, e.g., the discussions of Dreiling & Bell 1980 and Castelli & Kurucz 1994), and good agreement between the models and the data has generally been found. A set of zero point corrections, defined as the difference between the observed and calculated color indices for Vega, can then be applied to each subsequent set of colors to ensure they correspond to observational Strömgren colors.

The final composite grid of synthetic Strömgren colors computed using the programs and methods mentioned above covers a range in $T_{\rm eff}$ from 3000 to 8000 K in 250 K intervals and $\log g$ from -0.5 to 5.0 in increments of 0.5 dex for the abundances of $[{\rm M/H}] = -3.0$, -2.5, -2.0, -1.5, -1.0, -0.5, 0.0, and $+0.5$. While this particular grid is only applicable to cool, low mass dwarf and giant stars, an extension of the colors to higher temperatures is accomplished by melding this grid with

the synthetic Strömgren colors computed by F. Castelli at a temperature of 8000 K[3]. Furthermore, the bolometric corrections derived by P. R. Wood & M. S. Bessell (1994, private communication) from the Kurucz (1993) synthetic spectra are favored over those computed here in order to ensure consistency when comparing isochrone fits on various Strömgren CMDs with those presented in VandenBerg (2000) on various broadband CMDs.[4]

[3]The entire grid of Strömgren colors, based on a revised treatment of convection in the ATLAS9 model atmospheres discussed by Castelli et al. (1997), are currently available only on the homepage of R. L. Kurucz `http://cfaku5.harvard.edu`

[4]Indeed, the bolometric corrections derived here from the MARCS-SSG models show good agreement with those of Wood & Bessel in a systematic sense. The only mentionable differences between the two lie in a small zero point offset due to the adoption of slightly different normalization values for the sun.

Chapter 3

Calibrating and Testing the Synthetic Colors

The first step in testing the accuracy of the synthetic Strömgren colors is to assess how well they reproduce the observed colors of stars having various temperatures, gravities, and metal abundances. To facilitate this, one may use the colors to transform a theoretical isochrone to the observational plane and compare it to the color-magnitude diagram (CMD) of a cluster of stars. The two main purposes of fitting an isochrone to photometric data are check to the consistency of the theoretical models with the observations when best estimates of the cluster distance, reddening, and metallicity are assumed, and to derive the cluster age. However, inaccuracies in the synthetic colors as well as in the stellar models (due, for example, to the treatment of convection or the atmospheric boundary conditions) could easily lead to poor fits to the CMDs. Also, in clusters younger than ≈ 5 Gyr, the morphology of the main sequence turnoff is highly sensitive to the effects of convective overshooting in the stellar interior. Thus, it is important to first test the colors by using stars in the solar neighborhood having accurate parallaxes, low reddenings, and spectroscopically determined abundances. When the colors are constrained in this way, they should

not be a large source of error in the CMD fits.

This chapter will discuss how the Strömgren colors measured directly from synthetic spectra are tested using a sample of local field stars selected from the literature which have accurate *Hipparcos* parallaxes and well-determined effective temperatures, surface gravities, and metallicities. By comparing the calculated colors with the actual photometry for these field stars, a set of color calibrations are derived and used to correct the synthetic colors so they may be placed onto the observational system.

3.1 Synthetic Color Calibrations

The method of correcting synthetic colors by deriving a set of color calibrations from a sample of field stars with well-determined physical properties was most recently described by Houdashelt, Bell, & Sweigert (2000b, hereafter HBS). While their work was concerned with various broadband ($UBVRIJHK$) colors, their techniques can be easily adapted to calibrate the synthetic Strömgren indices. Two major differences between the present work and that of HBS should be mentioned. First, this work not only makes use of the sample of field stars employed by HBS (their Table 2), but also greatly expands on this list by including stars from Alonso, Arribas, & Martínez-Roger (1996, hereafter AAM96) and Alonso, Arribas, & Martínez-Roger (1999, hereafter AAM99). All of the stars in these three samples effectively cover the temperature, gravity, and metallicity range of the synthetic Strömgren colors presented here (see Figure A.1). Furthermore, reasonably accurate estimates of T_{eff} for these stars have been derived using the infrared flux method (IRFM) of Blackwell & Shallis (1977). Since effective temperature is the most crucial determinant of stellar color, it is important to have a stellar sample whose temperatures have been determined in an accurate and self-consistent way. Second, HBS choose to calculate an individual synthetic spectrum for each star in their list and use that spectrum to

derive the model colors. While this is certainly valid and feasible for the moderate number of field stars in their sample, the final list (see Table A.1) presented in this work contains over 500 field stars, and it would be impractical to compute individual model atmospheres, synthetic spectra, and colors for the entire sample presented here. Thus, Strömgren colors for each star in the listed in Table A.1 having a particular $T_{\rm eff}$, log g, and [Fe/H] are calculated by interpolating in the composite grid of synthetic colors.

To illustrate the need for these color calibrations, CMDs of the Galactic open cluster M 67 overplotted with a 4 Gyr, near-solar metallicity isochrone (see VandenBerg & McClure, in preparation) are presented in Figure 3.1. The *uvby* photometry for M 67 is provided by F. Grundahl (private communication) and has been corrected for a reddening of $E(b-y) = 0.029$ (corresponding to $E(B-V) = 0.04$ derived from the reddening maps of Schlegel et al. 1998). A slight sub-solar metallicity of [Fe/H] $= -0.04$ is adopted for the cluster which is consistent with recent spectroscopic studies (Tautvaisiene, Edvardsson, & Tuominen 2000 and Shetrone & Sandquist 2000). Finally, the absolute magnitudes of the M 67 stars are derived assuming a distance modulus of $(m-M)_V = 9.60$ (Nissen et al. 1987, Montgomery et al. 1993, Dinescu et al. 1995, and Fan et al. 1996). The 4 Gyr isochrone has been transformed to the indicated color planes in the figure by interpolating in the final, uncalibrated grid of synthetic colors for the set of temperature-gravity combinations lying along it.

While the isochrone appears to match the data quite well for the $(b-y)$ index if a small redward shift were applied, the fits to the data on the $(v-b)$ and $(u-v)$ color planes are not very satisfactory. It is difficult to ascertain what might be causing such discrepancies between the isochrone and the CMDs and why the colors measured directly from the synthetic spectra do not appear to be on the same system as the photometric data. Indeed, as mentioned earlier, errors in the isochrones could lead to a mismatch between models and the data. However, similar isochrone fits to M 67 in the broadband $(UBVRI)$ system yield very acceptable fits to all components of

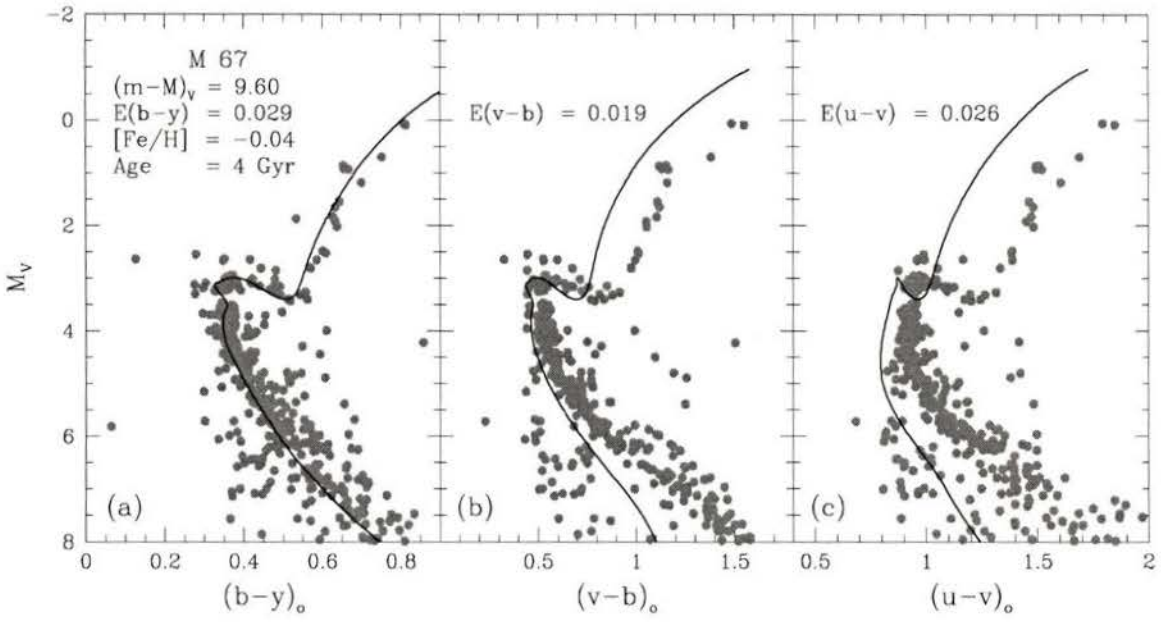

Figure 3.1: Strömgren photometry of stars in the open cluster M 67. The colors have been corrected for reddening and distance by the values indicated in the plots. The 4 Gyr, [Fe/H] = −0.04 isochrone overlayed on the CMDs has been transformed to the various color planes using the uncalibrated colors derived directly from the synthetic spectra.

the M 67 CMD (see HBS). Ruling out possible errors in the model isochrones, the only other possible explanation are inaccuracies in the synthetic colors. To expand on this problem, Bessel et al. (1998) have touched on possible reasons why synthetic photometric colors fail to match their observed counterparts and conclude that, "As the standard systems have been established from natural system of colors using linear and nonlinear corrections of at least a few percent, we should not be reluctant to consider similar corrections to synthetic photometry to achieve good agreement with the standard system across the whole temperature range of the models."

3.1.1 The $(b-y)$ index

To begin the calibration of the synthetic colors, Strömgren photometry for the field stars listed in Table A.1 has been compiled from the *uvby* catalog of Hauck & Mermilliod (1998). In addition, parallaxes and broadband colors for the entire sample are taken from the *Hipparcos* catalog (Perryman et al. 1997)[1]. Finally, the effects of reddening on the field star photometry cannot be ignored despite the fact that all of them are relatively nearby. Therefore, the *uvby* colors for stars listed by AAM96 and AAM99 have been corrected for reddening by the $E(B-V)$ values[2] provided in their studies, whereas stars taken from HBS were reddening corrected by obtaining individual $E(B-V)$ values from the reddening maps of Schlegel et al. (1998) and multiplying by a factor $[1-\exp(-|d \sin b|/h)]$, where d is the star's distance, b its galactic latitude, and h the scale height of the typical dust layer, which was assumed to be 125 pc (Bonifacio et al. 2000).

Figure 3.2 presents the plot of the synthetic versus observed $(b-y)$ indices for the 541 stars listed in Table A.1. Stars in the plot are divided into two classes according to

[1]Both catalogs were accessed online via the *VizieR* database at the Canadian Astronomical Data Center at `http://vizier.hia.nrc.ca/viz-bin/VizieR`.

[2]The $E(b-y)$ values listed in Table A.1 are derived assuming $E(b-y) = 0.732\, E(B-V)$. Therefore, it follows that the reddening corrected Strömgren indices take the form $(b-y)_o = (b-y) - E(b-y)$, $m_o = m_1 + 0.347\, E(b-y)$, and $c_o = c_1 - 0.228\, E(b-y)$ (Schlegel et al. 1998).

their surface gravities. Filled circles represent dwarf and subgiant stars ($\log g \geq 3.5$), while open circles are the giants and supergiants ($\log g < 3.5$). In addition, the equality between the synthetic and photometric indices is indicated by the dashed line. From initial inspection, the plot shows that the synthetic $(b-y)$ colors appear to adequately reproduce the observed colors for these field stars over a broad color range. Fitting a least-squares relation (solid line) to the field star data using the photometric color as the dependent variable and the synthetic color as the independent variable, the result does in fact show that the relation between the two is approximately equal if a small zero point difference is applied. This result is also evident in the left-hand panel of Figure 3.1 where the isochrone fit to the M 67 $(b-y)$ CMD appears to follow the same trend as the photometric data from the main sequence through the giant branch, but doesn't quite adequately match due to an apparent small difference in color.

3.1.2 The m_1 index

Owing to the importance of the Strömgren m_1 index in providing a photometric indicator of stellar metallicity, it is imperative for the synthetic m_1 colors to accurately reproduce their observed counterparts. Therefore, following the same procedure mentioned in the previous section, Figure 3.3 presents the resulting plot of synthetic versus observed colors for the Strömgren m_1 index. However, this index is somewhat more problematic and shows a significant systematic deviation between the synthetic and observed colors for the field stars. This deviation is consistent with the discrepancy between the isochrone and the M 67 CMD shown in the middle panel of Figure 3.1. Given that the m_1 index contains the Strömgren v filter [recall $m_1 = (v-b)-(b-y)$; see Chapter 1], which is located in a heavily line blanketed region of stellar spectra, the synthetic spectra used to calculate the models colors may not fully account for the number of atomic and molecular lines in this region, thus underestimating the

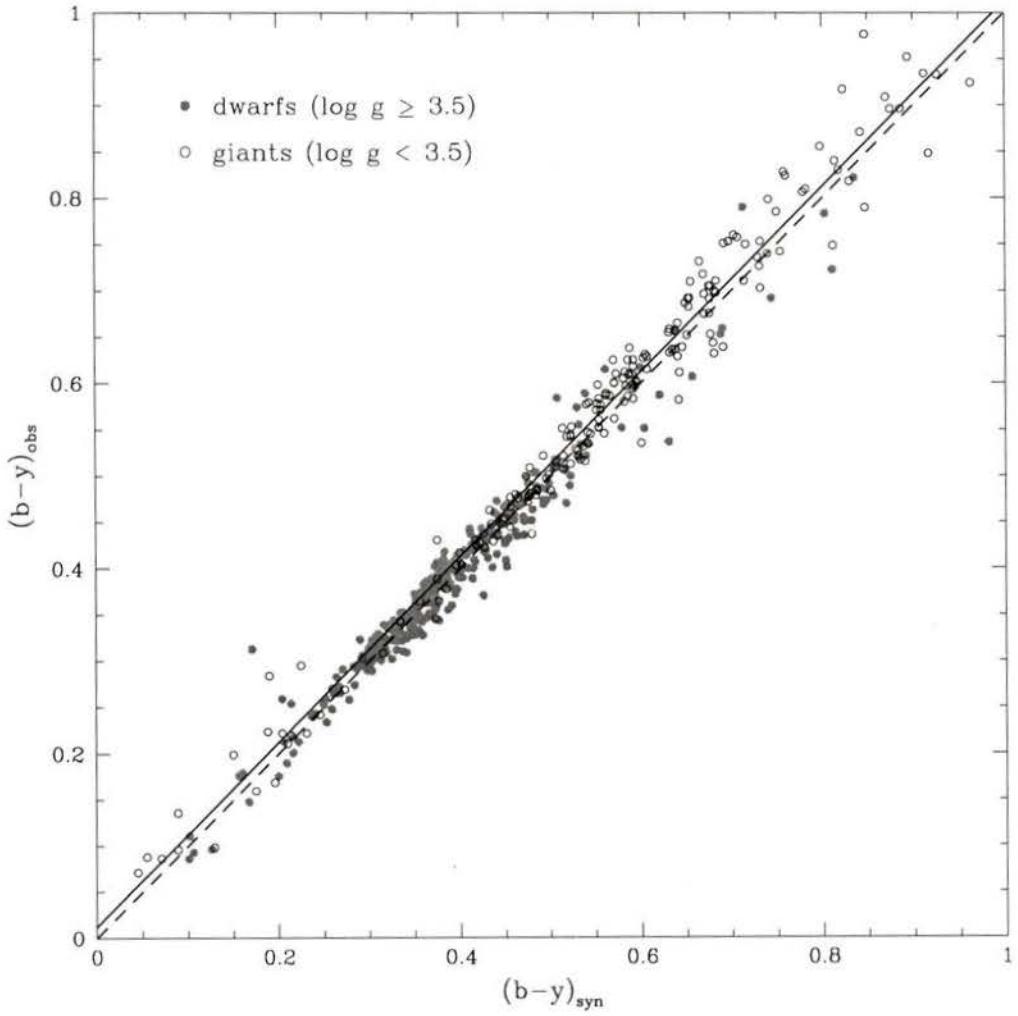

Figure 3.2: The synthetic versus observed colors for the $(b-y)$ index. Filled circles represent all dwarfs stars from the field star sample with $\log g \geq 3.5$, and open symbols are all giants and supergiants ($\log g < 3.5$). The solid line gives the linear, least-squares fit to the data which is required to put the synthetic colors onto the observational system, whereas the dashed line represents the one-to-one relation between the synthetic and photometric colors.

amount of absorption in the v filter. This would systematically shift the colors bluer for cooler stars. Whatever the reason, the focus of this study is to determine the best way to derive the calibration necessary to put the synthetic m_1 colors onto the observed system rather than delve into the source of the problem.

By inspection of Figure 3.3, it appears that the dwarf stars in the sample follow a different trend than the giant stars. Furthermore, the coolest dwarf stars show a hint that a higher order polynomial may fit the data better than a straight line. To elaborate on this, Figure 3.4 divides the field stars into different temperature and gravity regimes in an effort to derive a separate and distinct color calibration for each set of stars. The stars classified as "warm dwarfs" ($5250\,\mathrm{K} \leq \mathrm{T_{eff}} \leq 8000\,\mathrm{K}$; $\log g \geq 3.5$) are plotted in the left-hand panel of Figure 3.4. As illustrated in this panel, a simple least-squares relation appears to fit the data reasonably well. Stars identified as "cool dwarfs" ($3000\,\mathrm{K} \leq \mathrm{T_{eff}} \leq 5500\,\mathrm{K}$; $\log g \geq 3.5$) and the "giants" ($3000\,\mathrm{K} \leq \mathrm{T_{eff}} \leq 8000\,\mathrm{K}$; $\log g < 3.5$) are given in panels (b) and (c), respectively. While there is a rather large scatter in the data for the giants, another linear fit is used to calibrate their colors, whereas a second order polynomial is employed to fit the cool dwarfs. Stars excluded from the m_1 color calibrations due to their anomalous locations in the plots are indicated as asterisks. The corresponding coefficients for the each m_1 calibration together with those from the $(b-y)$ calibration are provided in Table 3.1.

This type of calibration of the m_1 index is not unreasonable. For comparison, HBS proposed that a separate calibration is necessary for some of the coolest dwarfs in their sample, particularly for the $(B-V)$ colors. They chose to meld their two calibrations at a temperature corresponding to a 5000 K dwarf. For the m_1 dwarf calibrations presented here, a temperature of 5500 K is chosen as the intersection point. In addition, their cool dwarf calibration is a linear relation and based on only three field stars with near solar metallicities, whereas the present calibrations are based on a larger sample of cool dwarfs covering a much wider metallicity range from [Fe/H]≈ -3.0 to $+0.3$.

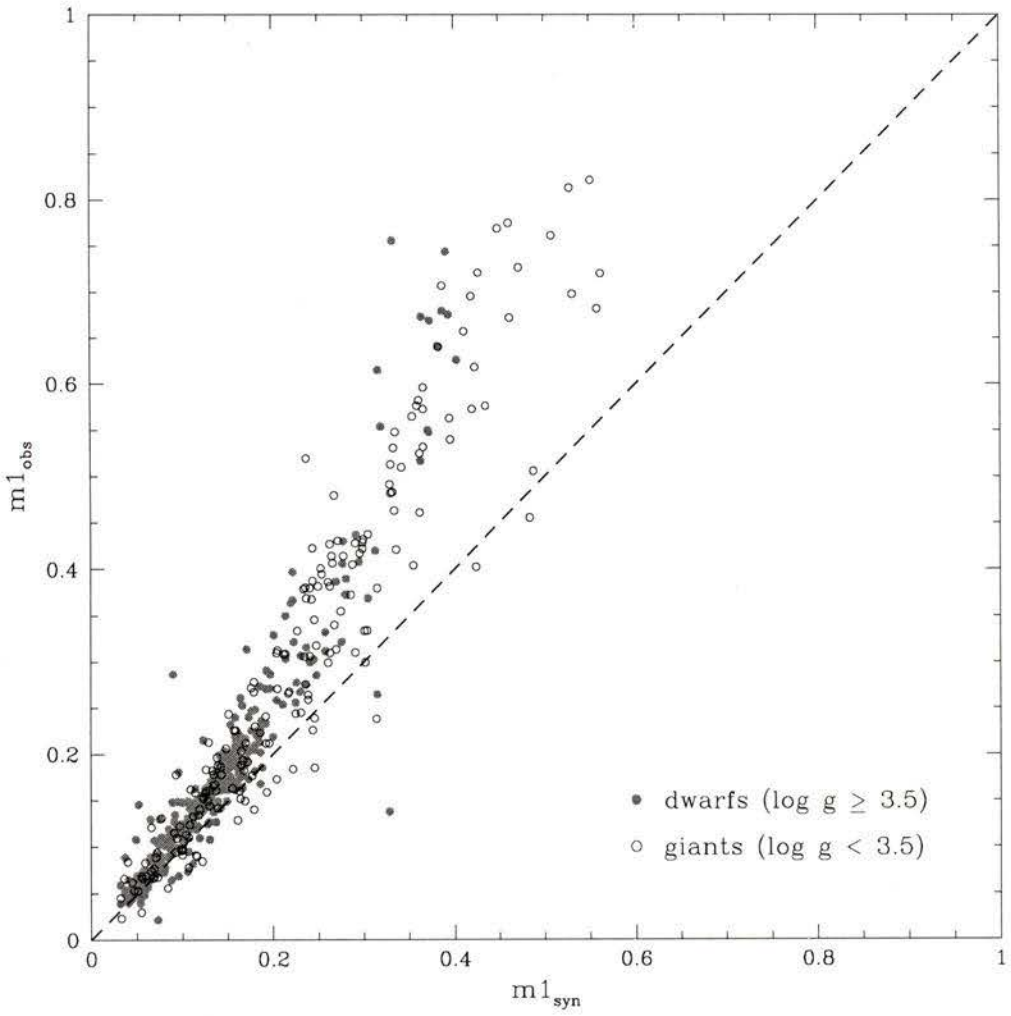

Figure 3.3: Similar to Figure 3.2 except for the m_1 index. The dashed line again represents the one-to-one relation between the synthetic and observed m_1 colors. The fit required to correct the colors is not plotted because the dwarfs stars appear to follow a different relation than the giants.

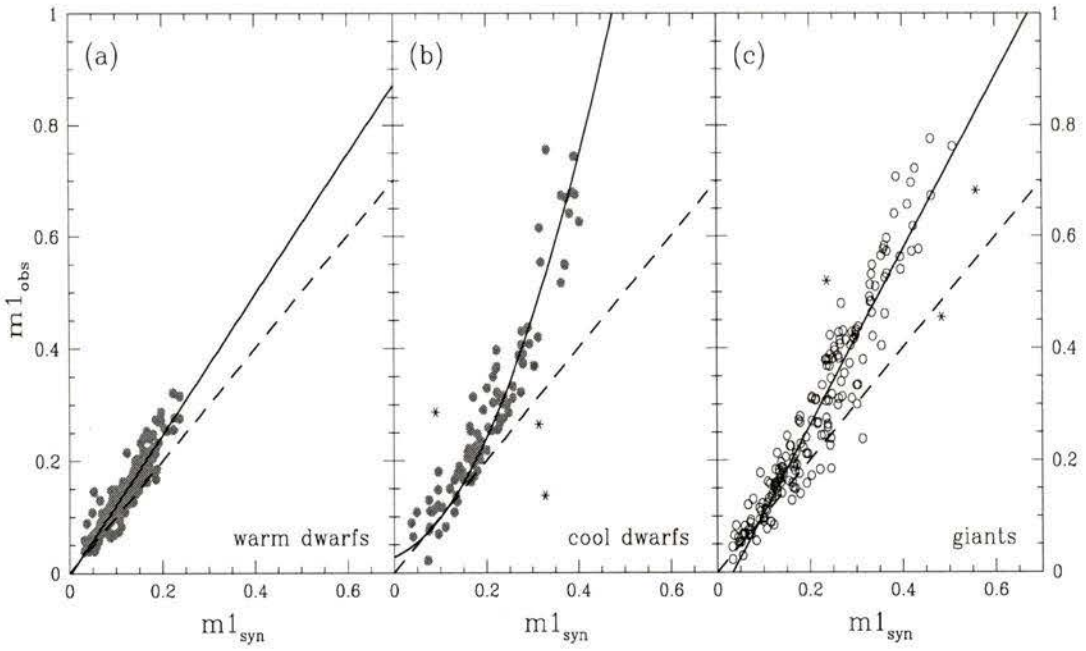

Figure 3.4: Similar to the previous figure except the field stars have been divided into different temperature and gravity regimes in an effort to illustrate the need for separate calibrations. The specifics of how the stars are classified are given in the text. In all panels the solid line represents the color calibrations derived from fits to the data while the dashed line again shows the one-to-one relations for reference. The fits in panels (*a*) and (*c*) indicate that a least-squares relation is sufficient to correct the colors for the warm dwarf stars and giants, respectively. However, the cooler dwarfs in panel (*b*) appear best fit by a second-order polynomial.

Table 3.1: Regression coefficients for calibrations between synthetic and observed color. The colors calibrations are based on the synthetic color as the independent variable and take the form $y = A + Bx + Cx^2$. The number of stars used to derive each calibration equation, N, as well as the resulting standard deviations are also provided.

Color Index	A	B	C	N	σ
$(b-y)$:					
dwarfs & giants	0.011	1.001		536	0.039
m_1:					
cool dwarfs	0.028	0.346	3.573	97	0.053
giants	-0.052	1.568		178	0.054
warm dwarfs	-0.005	1.253		275	0.020

3.1.3 The c_1 index

From inspection of Figure 3.5, it would appear the Strömgren c_1 index poses even more of a problem to calibrate than the aforementioned m_1 index. While the dwarf field stars are fairly well defined in the plot, they indicate that a high order calibration would likely fit the trend better at lower c_1 values. However, the giants show a significant scatter and do not seem to follow any specific trend. The cause for this extreme discrepancy could lie in the Strömgren u filter which comprises the c_1 index [recall $c_1 = (u - v) - (v - b)$; see Chapter 1]. For example, in late-type field stars (specifically late-G through M types) the flux through the u filter is no longer dominated by the Balmer discontinuity, but rather by a large number of stellar absorption lines which begin to appear at cooler temperatures. Therefore, the c_1 index could suffer from the same flux problems as the m_1 index due to the inability of the synthetic models to fully account for the absorption. Furthermore, the inability of stellar flux models to fit the observed ultraviolet flux for solar-like stars (the so-called "missing UV opacity problem") could result in problems deriving the c_1 colors from the synthetic spectra. In a recent study of the UV problem, Bell, Balachandran, & Bautista (2001) suggest that the bound-free transitions in Fe I is the main suspect

as an additional absorption source in the wavelength range of 2000-4000Å. However, this opacity source does not pose a significant problem for stellar models of hotter stars due to the greater ionization of Fe I. Nor should it be a problem for models with sub-solar metallicities because of the decreased abundances of iron. In light of this evidence, it would seem that the c_1 colors derived from synthetic spectra of cool, solar-type stars would be in error the most. To complicate matters further, Grundahl et al. (2000b) cite evidence of significant scatter in the c_1 colors of globular cluster giant stars due to variations in carbon and nitrogen abundances. The most likely candidate for causing such variations is the ultraviolet NH molecular band at 3360Å. Therefore, since the synthetic c_1 colors presented here are derived from models with scaled-solar C and N abundances, it is unlikely they would be able to adequately reproduce the observed colors of field stars with anomalous abundances of these elements.

Given the uncertainties inherent to the synthetic c_1 colors, possibly due to the aforementioned evidence as well as the obvious lack of agreement between the synthetic and observed indices in Figure 3.5, it would seem to be difficult to derive a set of color calibrations that would adequately correct the c_1 colors. In an effort to clarify this problem, it is worthwhile to investigate if the problems lie solely in the c_1 colors or in one of its component colors (i.e. the $(u-v)$ or the $(v-b)$ indices). Sections 3.1.1 and 3.1.2 illustrated how different first- and second- order fits are needed to calibrate the synthetic $(b-y)$ and m_1 colors. Based on the fact that m_1 is comprised of two other color indices, namely $(b-y)$ and $(v-b)$, would the $(u-v)$ colors be significantly in error if the $(v-b)$ and $(b-y)$ indices are correctly calibrated? Figure 3.6 presents two plots of the observed versus synthetic $(u-v)$ colors for the field stars using the fact that $(u-v) = c_1 + m_1 + (b-y)$. However, the two panels differ from each other in the fact that the synthetic $(u-v)$ colors in panel (a) are derived using the uncalibrated m_1 and $(b-y)$ indices and those in panel (b) make use of the *calibrated* m_1 and $(b-y)$ colors. The trend in the right-hand panel of Figure 3.6 appears to indicate that the majority of disagreement in panel (a) is nearly removed

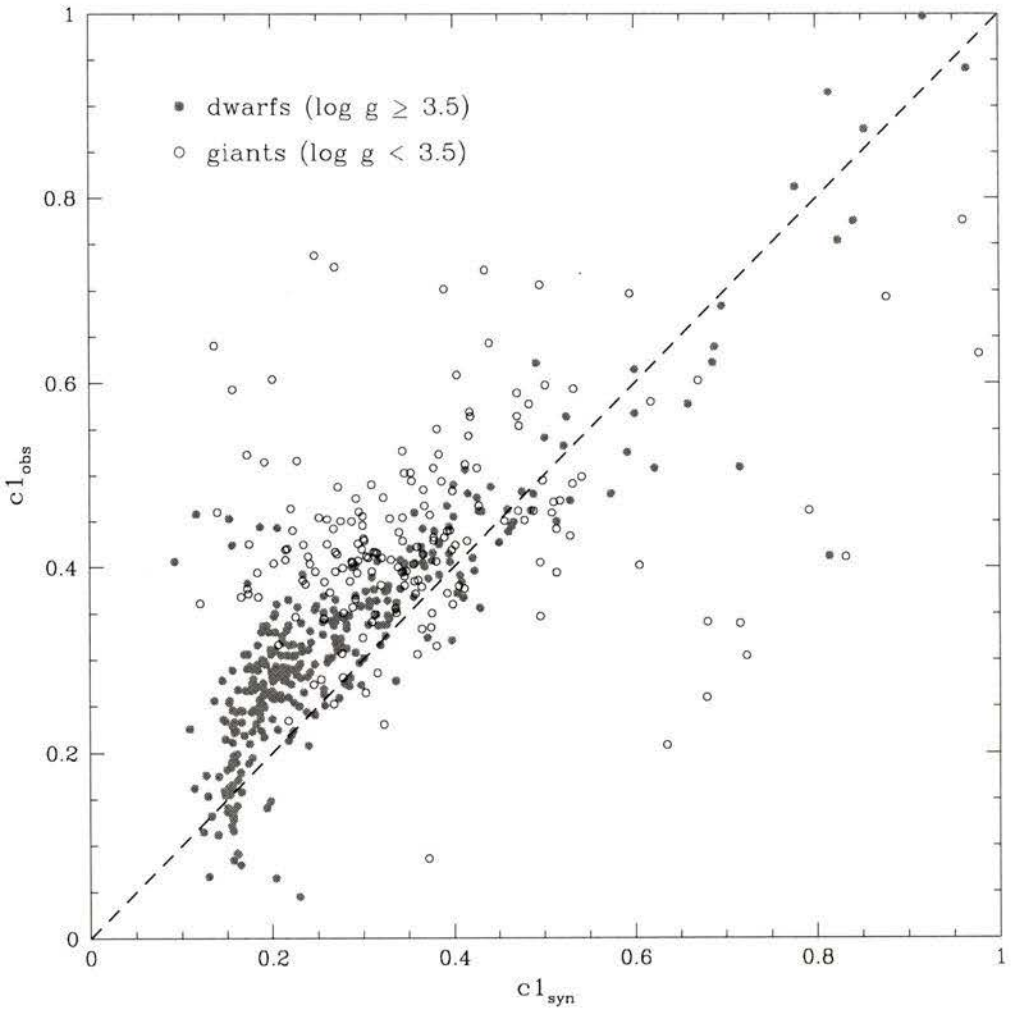

Figure 3.5: Similar to Figures 3.2 and 3.3 except for the c_1 index.

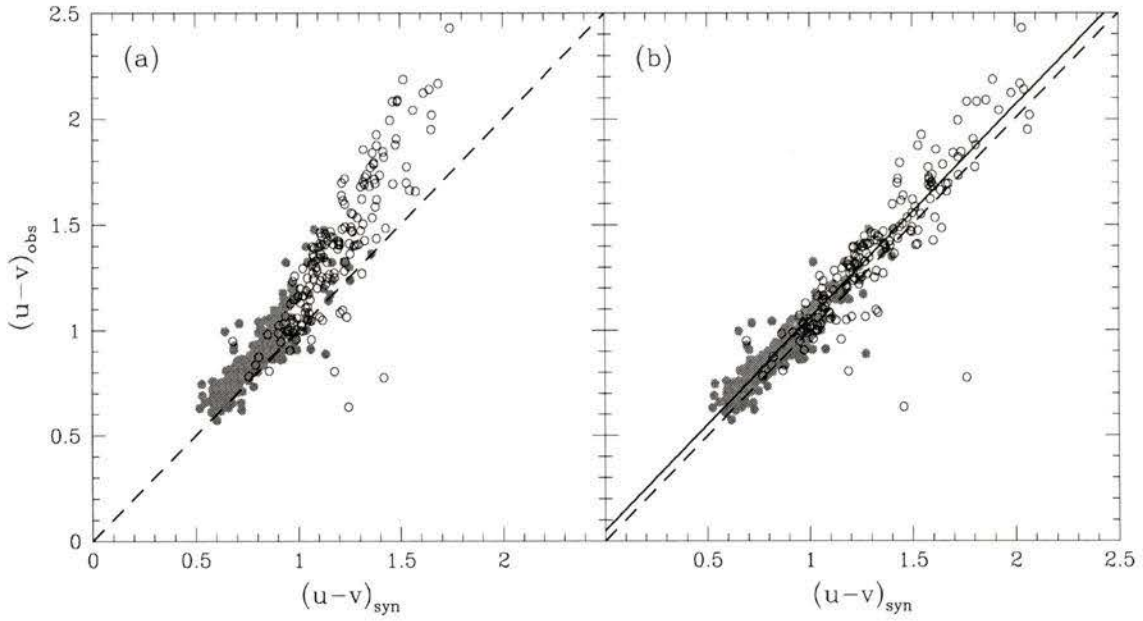

Figure 3.6: Plots of the synthetic versus observed $(u-v)$ colors for the field stars. Panel (a) gives the results when the uncalibrated m_1 and $(b-y)$ colors are used to derive $(u-v)$ [using $(u-v) = c_1 + m_1 + (b-y)$], whereas panel (b) uses the calibrated m_1 and $(b-y)$ colors. Dwarf stars are again represented by filled circles and giants by open circles. The disagreement for the synthetic colors in the left-hand panel is largely removed when the calibrated m_1 and $(b-y)$ colors are used to determine $(u-v)$ in panel (b). The solid line in the right-hand panel gives the resulting linear fit derived from the data while the dashed lines again represents the equality between synthetic and observed colors.

when using the calibrated m_1 and $(b-y)$ colors. While the coolest giants appear to deviate slightly from a linear fit, applying a least-squares fit to the entire data set (both dwarfs and giants) yields a slope of 1.009 ± 0.012 and intercept of 0.047 ± 0.012 with $\sigma = 0.082$. Therefore, apart from a zero-point offset between the synthetic and observed $(u-v)$ colors, the discrepancies in c_1 seem to lie predominantly in the synthetic $(v-b)$ indices.

3.2 Accuracy of the Calibrated *uvby* Colors

As mentioned at the beginning of this chapter, one way of testing the accuracy of the corrected Strömgren colors is to transform a theoretical temperature-luminosity isochrone to the observational color-magnitude plane and compare it with photometric data for a cluster of stars. While Figure 3.1 presented the resulting fits to the CMD of M 67 using the uncalibrated colors to transform the isochrone, Figure 3.7 gives the revised fits using the newly calibrated synthetic *uvby* colors. In both panels of this figure, the uncalibrated isochrone is shown as a dotted line while the calibrated isochrones are represented by a solid curve. Overall, the isochrone fits to the CMDs using the calibrated colors in Figure 3.7 are substantially improved compared with those using the uncalibrated indices. The fit to the $(b-y)$ plane in panel (a) indeed shows that a small zero-point correction to the colors was all that was needed to correct the synthetic $(b-y)$ index. However, the $(v-b)$ colors in panel (b) required three different calibrations (see § 3.1.2), both linear and non-linear, to place the synthetic colors onto the observed system. Despite this fact, the calibrated colors appear to correctly reproduce the CMD for M 67 on this color plane.

From the comparisons of the new, 4 Gyr, solar-metallicity isochrone with the CMDs of M 67 in Figure 3.7, the calibrated Strömgren colors appear to be appropriate for field and cluster stars with near solar metallicities. While the field star sample covers a wide range in metallicity, there is no evidence from their photometry that the synthetic color calibrations depend upon chemical composition. Therefore, one should expect the same good agreement between the isochrones and the CMDs of globular clusters with sub-solar metallicities provided reasonable values for the cluster distance, reddening, and age are chosen. This examination and discussion of isochrone fits to a number of metal deficient globular clusters is reserved until the next chapter, while the present discussion will proceed with testing these newly calibrated colors against the field stars used to derive them.

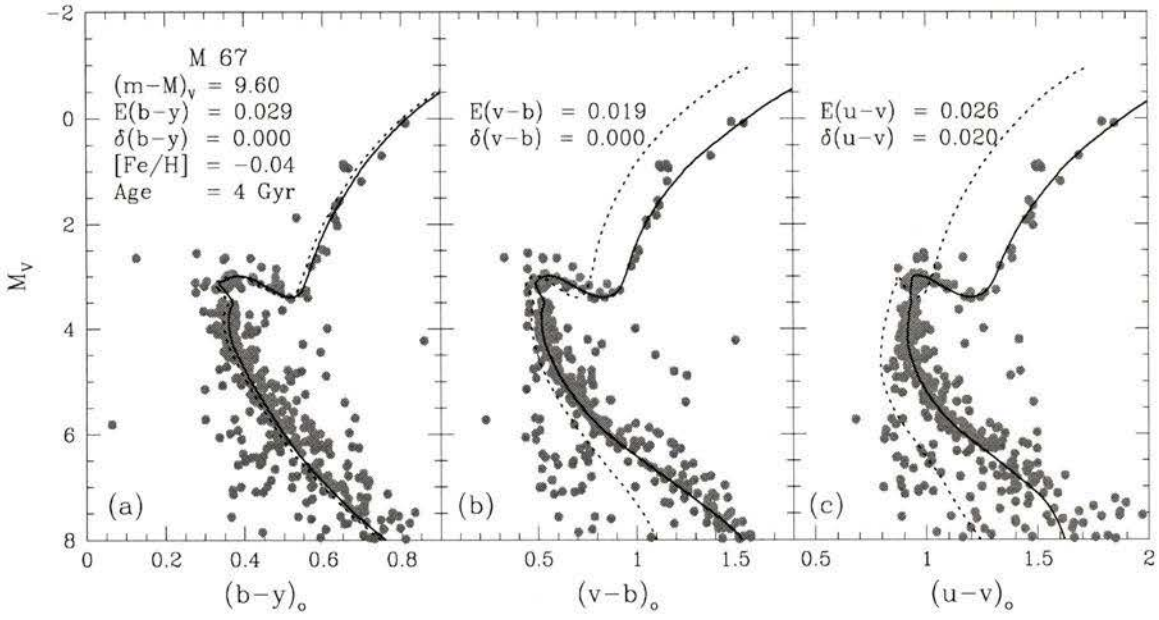

Figure 3.7: Similar to Figure 3.1 except the solid lines now indicate the 4 Gyr isochrone fits using the calibrated colors while the dotted lines are the uncalibrated isochrones. In each panel the color shifts needed to provide the best fits to the data are indicated by $\delta(b-y)$, $\delta(v-b)$, and $\delta(u-v)$.

3.2.1 Testing the Calibrated Colors Using the Field Star Sample

The large number of field stars listed in Table A.1 used to place the synthetic colors onto the observational system also provide an ideal photometric sample to test the resulting calibrated colors due to their broad coverage in T_{eff}, log g, and [Fe/H]. To begin this examination, Figure 3.8 plots various *uvby* CMDs of the field stars from Table A.1 which have $\log g \leq 3.5$ and near solar metallicities ($-0.20 \leq$ [Fe/H] $\leq +0.12$). Absolute magnitudes are derived using the star's apparent visual magnitude V along with its corresponding *Hipparcos* parallax. In addition, the stellar colors are corrected for reddening using the $E(b-y)$ values listed in A.1. Superimposed on the observations are two zero age main sequence (ZAMS) models (VandenBerg, private communication) having [Fe/H] $= -0.20$ and $+0.12$ transformed to the indicated color-magnitude planes using the newly calibrated Strömgren colors. For the sake of clarity, the sequence of stars encompassed by the two ZAMS loci in the left-hand panel of the figure are represented by filled circles in panels (b) and (c) while all others are shows as asterisks. The resulting fits show that a large number of stars define a tight sequence which lie consistently between the two ZAMS models in all the color planes while the number of the remaining stars lying above the [Fe/H] $= +0.12$ ZAMS are most likely evolved turnoff stars and sub-giants. From this type of plot one can see that the same stars are confined between the two ZAMS models in each panel to within reasonable uncertainties in their photometry and absolute magnitudes. This result lends good support to the accuracy of both the calibrated *uvby* colors as well as the bolometric corrections for models with near-solar metallicities.

Figure 3.9 presents two color-color plots of the same set of stars which are located between the two ZAMS in the previous figure. Panels (a) and (b) now plot $(b-y)_o$ versus the dereddened m_o and c_o indices for the solar metallicity dwarfs, respectively, with the majority of stars still lying between the same two ZAMS models in each

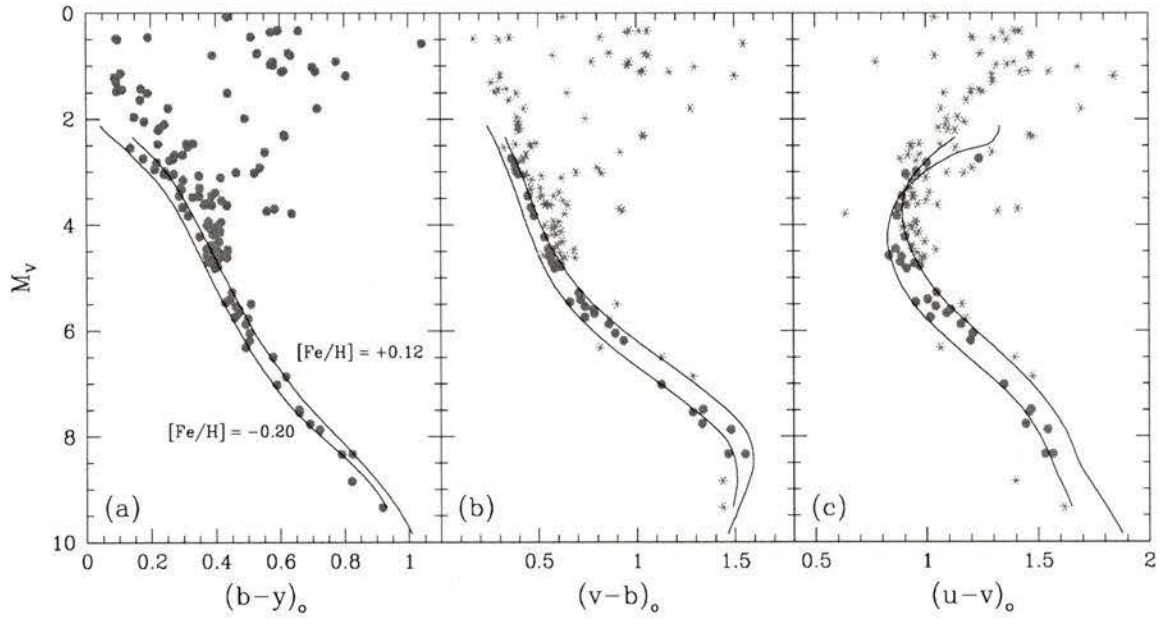

Figure 3.8: Fits of two ZAMS models corresponding to metallicities of [Fe/H] = +0.12 and -0.20 to the *uvby* CMDs of all solar metallicity dwarfs stars taken from the field star sample. The stars confined between the ZAMS in panel (a) are represented by solid circles in panels (b) and (c).

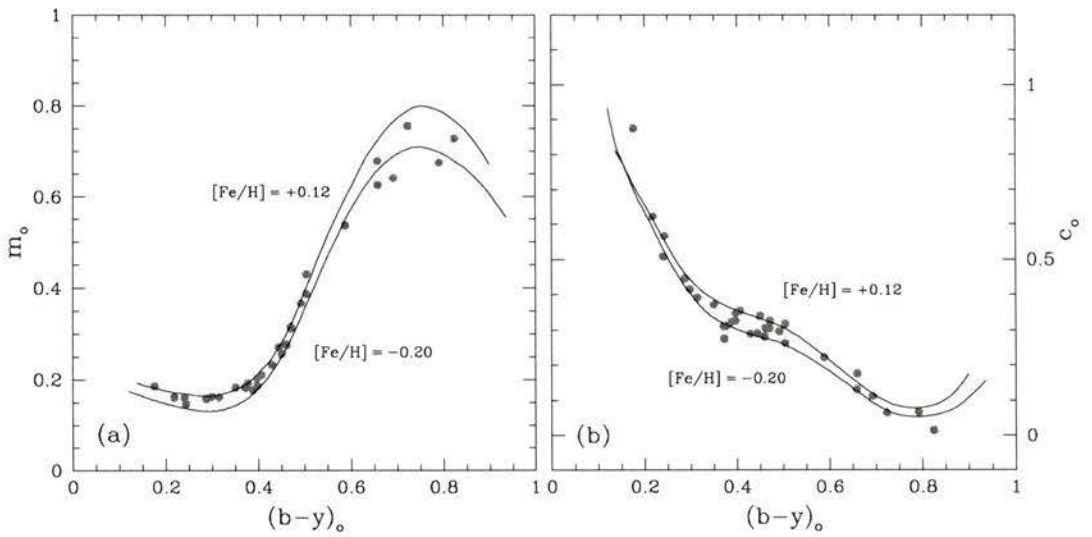

Figure 3.9: Color-color diagrams of stars confined between the same two ZAMS models from the previous figure.

case. Furthermore, the two calibrated ZAMS also do an excellent job of reproducing the general trend of the field stars over the entire color range plotted, thus lending even more support to the validity of the calibrated colors.

Finally, Figure 3.10 presents a color-temperature and a color-color plot for the field dwarfs that have been divided into separate metallicity bins as indicated by the different symbols. The three ZAMS models overplotted as solid lines are calculated for metallicities of [Fe/H] $= -2.0, -1.0, 0.0$. These figures serve to illustrate not only the accuracy of the calibrated colors in transforming the various ZAMS models, but also the importance of the Strömgren m_1 index as a metallicity indicator. While the number of stars in the sample decreases for lower [Fe/H] values, all three trends appear to run almost parallel to each other with the higher metallicity stars displaced to larger m_1 values. The figure is extremely helpful in deriving an estimate of star's metallicity based solely on its position in either or both of these diagrams. While panel (a) would require prior knowledge of a star's effective temperature to obtain an

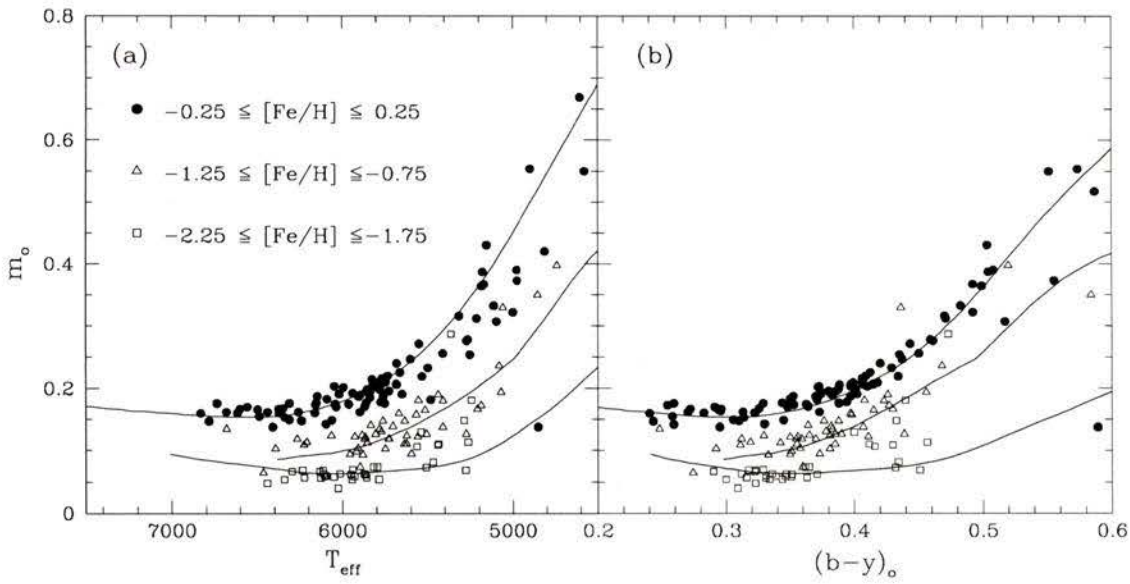

Figure 3.10: The locations of field dwarf stars in the [T_{eff}, m_o] and [$(b-y)_o$, m_o] planes according to their metallicities. The different symbols identify the indicated metallicity bins into which the field stars have been grouped. Solid lines represent the ZAMS models transformed using the calibrated Strömgren colors for [Fe/H] values of 0.0, −1.0, and −2.0.

[Fe/H] estimate, panel (*b*) is an entirely observational and the stars appear to define a tighter sequence.

3.2.2 Testing the Calibrated Colors Using Population II Subdwarf Standards

Extending these types of comparisons and tests to lower metallicities is somewhat more problematic owing to the fewer number of cool, metal-poor stars in the sample which could be used to probe the accuracy of the colors towards the redder limits of the main sequence and giant branch. To remedy this problem, a sample of metal-deficient, Population II field subdwarfs is selected from Table A.1 which have been

extensively studied in the literature. The goal of this process is to investigate if the calibrated *uvby* colors can correctly reproduce the observed Strömgren indices for these Population II stars provided accurate and consistent estimates of their effective temperature, surface gravity, and metallicity are available.

Given that the effective temperature is the most critical determinate of stellar color, Table 3.2 presents a comparison between the temperatures derived in a number of different studies for the sample of Population II subdwarfs considered here. Listed in the first column are the same IRFM temperatures from AAM96 which were adopted to calibrate the synthetic colors. The temperatures quoted by Gratton et al. (1996) and Clementini et al. (1999) were all calculated using an iterative procedure which attempts to fit the flux distribution of an ATLAS9 model atmosphere to the observed spectrum for a particular star (see § 3 of Gratton et al. 1996 for specifics). Effective temperatures from the Gratton et al. (2000) study were calculated from dereddened $(B-V)_o$ and $(b-y)_o$ colors using the color-T_{eff} transformations from Kurucz (1993). Finally, Axer et al. (1994) chose to calculate T_{eff} spectroscopically by fitting the profile wings of the first four Hydrogen Balmer lines.

While all of these studies rely on different methods of deriving T_{eff}, they appear to yield quite consistent results. In general, most of the effective temperatures derived from the IRFM by AAM96 show good agreement with those determined from the indicated sources to within $\pm\,100$ K. The most notable case of agreement is HD 19445 for which the estimates from the five different sources yield a mean T_{eff} of 6055 K with a deviation of only $\pm\,14$ K. There are, however, a few cases where the agreement is not as satisfactory. For instance, the IRFM temperatures for HD 134439 and HD 134440 are both $\approx$ 100-150 K cooler than those derived in other studies. While it is not immediately apparent why the temperatures estimates for these two stars are in slight disagreement, the Strömgren colors derived from models using the higher temperatures appear in better agreement with the actual photometry (see below).

In order to derive the synthetic Strömgren colors for these subdwarfs, accurate

Table 3.2: Comparison of the T_{eff}'s derived from the infrared flux method by Alonso et al. (1996a) with results from the indicated studies for selected Population II subdwarfs.

Star ID	T_{eff} (K)				
	Alonso et al. (1996a)	Gratton et al. (1996b)	Gratton et al. (2000)	Clementini et al. (1999)	Axer et al. (1994)
HD 19445	6050	6080	6047	6059	6040
HD 25329	4842	4849	4840	-	-
HD 64090	5441	5515	5530	5475	5499
HD 74000	6224	6341	-	-	6211
HD 84937	6330	6344	-	-	-
HD 103095	5029	5124	5152	5016	-
HD 132475	5788	-	5758	-	-
HD 134439	4974	-	5134	5106	-
HD 134440	4746	-	-	4879	-
HD 140283	5691	5763	-	-	5814
HD 188510	5564	5628	-	-	5500
HD 201891	5909	-	5991	5957	5797

estimates of a star's surface gravity and metallicity must supplement the effective temperature. The majority of $\log g$ estimates for this subdwarf sample were taken from the study of Nissen, Høg, & Schuster (1997) while [Fe/H], absolute magnitude, dereddened broadband color, and reddening values were obtained from Carretta et al. (2000). Table 3.3 presents these adopted parameters together with their dereddened photometry for the selected sample of subdwarfs.

Table 3.3: Fundamental parameters and *uvby* photometry for selected Population II subdwarfs. Estimates for $\log g$ are taken from Nissen, Høg, & Schuster (1997) while [Fe/H], absolute magnitude, broadband color, and reddening values are obtained from Carretta et al. (2000) unless otherwise noted. The Strömgren reddening value has been derived assuming $\mathrm{E}(b-y) = 0.734\mathrm{E}(B-V)$.

Star ID	$\log g$	[Fe/H]	$\mathrm{E}(b-y)$	M_V	$\sigma_{\mathrm{M_V}}$	$(B-V)_o$	$(b-y)_o$	m_o	c_o
HD 19445	4.44	-1.91	0.002	5.09	0.09	0.458	0.349	0.059	0.208
HD 25329	4.75	-1.69	0.000	7.17	0.04	0.864	0.529	0.304	0.143
HD 64090	4.59	-1.48	0.000	6.01	0.06	0.614	0.430	0.109	0.116
HD 74000[a]	4.13	-2.00	0.000	3.97	0.37	0.431	0.264	0.075	0.299
HD 84937	4.10	-2.07	0.007	3.71	0.18	0.382	0.295	0.056	0.367
HD 103095[b]	4.70	-1.24	0.000	6.61	0.02	0.752	0.484	0.222	0.155
HD 132475	3.87	-1.73	0.027	3.51	0.22	0.522	0.366	0.084	0.281
HD 134439	4.72	-1.30	0.005	6.70	0.08	0.767	0.482	0.217	0.162
HD 134440	4.73	-1.28	0.005	7.03	0.11	0.845	0.518	0.292	0.174
HD 140283	3.79	-2.40	0.018	3.32	0.12	0.463	0.361	0.046	0.289
HD 188510	4.55	-1.37	0.001	5.83	0.13	0.598	0.415	0.107	0.148
HD 201891	4.25	-0.97	0.003	4.61	0.08	0.514	0.355	0.105	0.263

[a] [Fe/H] taken from Fulbright 2000. Photometric parameters derived from *Hipparcos* data assuming $\mathrm{E}(B-V) = 0.0$.

[b] $\log g$ taken from Fulbright 2000.

Table 3.4 lists the results of a number of calculations that have been carried out in an attempt to match the observed, dereddened colors of the subdwarf sample. While the Strömgren color indices for each star have been derived from the calibrated *uvby* colors, the $(B-V)$ colors are calculated from the broadband C-T relations of VandenBerg (2001, in preparation). The first set of model colors uses the stellar parameters adopted by the AAM96 investigation while the second set considers the same IRFM temperature but with the surface gravity and metallicity estimates listed in Table 3.3. For the majority of stars the best agreement between the predicted and observed color indices occurs for the second set of calculations. However, a few stars still appear to show some differences, particularly in the m_o and c_o colors, regardless of which set of parameters is adopted. Possible reasons for such discrepancies are discussed on a star by star basis below.

Table 3.4: The *uvby* (and *BV*) colors derived from the calibrated Strömgren colors assuming various models adopting the indicated values of T_{eff}, $\log g$, and [Fe/H] for the sample of Population II subdwarfs.

Star ID	$(b-y)_o$	m_o	c_o	$(B-V)_o$	Comments
HD 19445	**0.349**	**0.059**	**0.208**	**0.458**	Intrinsic colors
(6050/4.25/-2.15)	0.342	0.055	0.250	0.444	Alonso et al. (1996a)
(6050/4.44/-1.91)	0.343	0.063	0.221	0.455	
HD 25329	**0.529**	**0.304**	**0.143**	**0.864**	Intrinsic colors
(4842/4.50/-1.64)	0.534	0.191	0.194	0.837	Alonso et al. (1996a)
(4842/4.75/-1.69)	0.538	0.192	0.186	0.848	
(4842/4.75/-1.69)	0.537	0.253	0.165	0.848	CNO enhanced (see text)
HD 64090	**0.430**	**0.109**	**0.116**	**0.614**	Intrinsic colors
(5441/4.50/-1.82)	0.433	0.084	0.169	0.618	Alonso et al. (1996a)
(5441/4.59/-1.48)	0.428	0.111	0.161	0.636	
HD 74000	**0.316**	**0.057**	**0.311**	**0.431**	Intrinsic colors
(6224/4.50/-2.00)	0.321	0.064	0.239	0.418	Alonso et al. (1996a)
(6224/4.13/-2.00)	0.316	0.063	0.308	0.411	
HD 84937	**0.295**	**0.056**	**0.367**	**0.382**	Intrinsic colors
(6330/4.50/-2.49)	0.312	0.050	0.271	0.392	Alonso et al. (1996a)
(6330/4.10/-2.07)	0.302	0.064	0.348	0.390	
HD 103095	**0.484**	**0.222**	**0.155**	**0.752**	Intrinsic colors
(5029/4.50/-1.35)	0.491	0.182	0.182	0.775	Alonso et al. (1996a)
(5029/4.70/-1.24)	0.491	0.205	0.173	0.784	
HD 132475	**0.366**	**0.084**	**0.281**	**0.522**	Intrinsic colors
(5788/4.00/-1.53)	0.371	0.074	0.262	0.517	Alonso et al. (1996a)
(5788/3.87/-1.73)	0.370	0.067	0.272	0.503	
(5788/3.87/-1.43)	0.369	0.077	0.289	0.518	[Fe/H] from Gratton et al. (2001)
HD 134439	**0.482**	**0.217**	**0.162**	**0.767**	Intrinsic colors
(4974/4.50/-1.52)	0.502	0.171	0.187	0.791	Alonso et al. (1996a)
(4974/4.72/-1.30)	0.501	0.210	0.176	0.803	
(5106/4.72/-1.30)	0.478	0.182	0.169	0.757	T_{eff} from Clementini et al. (1999)
(5106/4.72/-1.30)	0.484	0.200	0.174	0.757	$[\alpha/Fe] = 0.0$
HD 134440	**0.518**	**0.292**	**0.174**	**0.845**	Intrinsic colors
(4746/4.50/-1.57)	0.553	0.228	0.209	0.875	Alonso et al (1996a)
(4746/4.73/-1.28)	0.547	0.286	0.190	0.891	
(4879/4.73/-1.28)	0.519	0.242	0.181	0.839	T_{eff} from Clementini et al. (1999)
(4879/4.73/-1.28)	0.524	0.268	0.190	0.830	$[\alpha/Fe] = 0.0$
HD 140283	**0.361**	**0.046**	**0.289**	**0.463**	Intrinsic colors
(5691/4.00/-2.37)	0.388	0.051	0.230	0.508	Alonso et al. (1996a)
(5691/3.79/-2.40)	0.385	0.049	0.262	0.501	
(5814/3.79/-2.40)	0.368	0.047	0.284	0.475	T_{eff} from Axer et al. (1994)
HD 188510	**0.415**	**0.107**	**0.148**	**0.598**	Intrinsic colors
(5564/4.00/-1.80)	0.406	0.072	0.215	0.560	Alonso et al. (1996a)
(5564/4.55/-1.37)	0.408	0.109	0.176	0.601	
HD 201891	**0.355**	**0.105**	**0.263**	**0.514**	Intrinsic colors
(5909/4.50/-1.22)	0.358	0.091	0.228	0.517	Alonso et al. (1996a)
(5909/4.25/-0.97)	0.353	0.102	0.278	0.521	

- *HD 140283:* This well documented sub-giant is the most metal-deficient star in the subdwarf sample. The third model for HD 140283 listed in Table 3.4 considers the T_{eff} obtained from the Axer et al. (1994) study. It seems clear this particular model yields much better agreement for all indices due to the adoption of a higher temperature than what is predicted by the IRFM. Indeed, Ryan, Norris, & Beers (1999) have pointed out that the IRFM temperatures derived by AAM96 appear to show nonphysical trends at very low metallicities (i.e. [Fe/H]<-2.0), which could cast some doubt on temperatures derived for stars with extremely low abundances. Furthermore, recent investigations by Furhmann (1998) and Grundahl et al. (2000a) advocates adopting a slightly higher temperature of ≈ 5800 K for HD 140283 due to the effects of reddening in the determination of T_{eff}.

  While this may solve the problem for HD 140283, the question arises concerning the validity of the color calibrations used to correct the synthetic Strömgren colors. If the derived IRFM temperatures are systematically in error by a few hundred Kelvin for extremely metal-deficient field stars, this could in turn affect the size of the correction needed to put the model colors onto the observed system. However, the number of stars (particularly dwarfs) with [Fe/H]<-2.0 listed in Table A.1 totals just over 35 which is only a small fraction of the total sample on which the color calibrations are derived. Therefore, it seems unlikely that any possible errors in the IRFM temperatures could pose problems for the low metallicity synthetic colors.

- *HD 25329:* This cool subdwarf shows that largest discrepancy between the calculated and observed Strömgren indices, particularly for m_o which differs by more than 0.1 mag. It seems quite unlikely that errors in the adopted T_{eff} could be causing such mismatch given the good agreement between the $(b-y)$ and $(B-V)$ colors. In addition to the temperatures listed in Table 3.2,

Thévenin & Idiart (1999) and Taylor (1994) derive temperatures of 4846 K and 4893 K, respectively, for HD 25329 leading to an average T_{eff} of 4854 ± 20 K. Ruling out possible errors in temperature, it also seems improbable this star could have a surface gravity or metallicity which deviates significantly from the values used for this study. Moreover, even if the reddening is significantly larger than the $E(b-y) = 0.0$ adopted here, it would only serve to increase the observed value for m_o [since $m_o = m_1 + 0.347E(b-y)$]. To shed some light on this problem, Speisman (1992) comments that HD 25329 exhibits unusually strong CN absorption for a metal-poor subdwarf, and the abundance analysis of Carbon et al. (1987) yields [C/Fe] = +0.44 and [N/Fe] = +0.45. In addition, Meléndez & Barbuy (2001) report a slightly higher oxygen abundance than usually found in Population II field stars ([O/Fe] = +0.48). Recent papers have investigated the effect of enhancements in the CNO process elements on both the m_1 and c_1 index due to increased absorption by the CN and NH molecular bands at 4215Å and 3360Å, respectively (e.g., see Briley, Grundahl, & Anderson 1999, Grundahl et al. 2000, and Hilker 2000). Therefore, it seems reasonable to expect some disagreement between the observed and calculated m_o and c_o colors due to the unusually high abundances of C, N, and O in HD 25329. Since the synthetic colors derived in this work are all derived assuming scaled solar carbon and nitrogen abundances, the enhancement in CNO would affect both the line and continuum absorption due to the treatment of OH and CH bound-free absorption in the synthetic spectra calculations. To investigate the effects of such elemental enhancements on the Strömgren colors, a new model atmosphere and synthetic spectrum for HD 25329 is constructed assuming the same parameters as before (4842/4.75/-1.69) but with the abundances for C, N, and O enhanced by +0.44, +0.45, and +0.48, respectively. The resulting colors are derived using the methods described in the last chapter and calibrated using the relations listed in Table 3.1. From the results of this new model listed in

Table 3.4 there appears to be an increase in the model m_o colors by about 0.06 mag. While this increase is still not sufficient to match the observed m_o colors of HD 25329, it does serve to illustrate the effect of CNO enhancements on the Strömgren m_1 index.

- *HD 134439/134440:* These two neighboring stars are among the coolest subdwarfs in the sample. It appears from the model calculations that the $(b-y)$ colors are the most discrepant in both HD 134439 and 134440 if the IRFM temperatures of AAM96 are adopted. However, the comparisons given in Table 3.2 show these effective temperatures appear to be ≈ 130 K cooler than those of Gratton et al. (2000) and Clementini et al. (1999) for both stars. Furthermore, Prieto & Lambert (2000) quote a temperature of 5110 K for HD 134439, while Nissen, Høg, & Schuster (1997) give 5040 K and 4842 K for 134439 and 134440, respectively. Under these considerations, an additional model is given for both stars in Table 3.4 which adopts the $T_{\rm eff}$ estimates of Clementini et al. (1999). While the better agreement in the $(b-y)$ colors (and arguably $B-V$) appears to favor the higher temperatures for the subdwarf pair, the m_o colors are now mismatched. One possible explanation to this problem is that HD 134439/134440 are suffering from the same anomalous CNO abundances as HD 25329. However, a more likely explanation lies in the fact that both of these stars exhibit a near-solar abundance of the α process elements ($[\alpha/{\rm Fe}] = 0.0$) as opposed to $[\alpha/{\rm Fe}] = +0.3$ commonly found in most metal-poor subdwarfs. Indeed, King (1997) derived elemental abundances from high resolution and high S/N spectra for these two stars and discovered the pair exhibit little or no significant enhancement of the α elements ($[\alpha/{\rm Fe}] \approx 0.0$). In addition, Fulbright (2000) also confirms the pair has near-solar $[\alpha/{\rm Fe}]$ values. Given these facts, it is difficult to assess how the indices derived in Table 3.4 from the calibrated Strömgren colors would differ given an under-abundance of the α process ele-

ments. As mentioned in Chapter 2, the lowest metallicity synthetic colors were initially calculated assuming $[\alpha/\mathrm{Fe}] = +0.3$. Therefore, two additional models are computed for HD 134439/134440 assuming the same T_{eff}, $\log g$, and [Fe/H] but with $[\alpha/\mathrm{Fe}] = 0.0$. These two new models show that adoption of $[\alpha/\mathrm{Fe}] = 0.0$ does increase the calculated m_o colors and brings them into better agreement with the observed indices for each star. However, the fact that model m_o colors are still ≈ 0.02 mag too low or that the c_o colors now show a slightly worse agreement than before cannot be readily explained.

- *HD 64090, HD 103095, and HD 188510:* According to the models listed in Table 3.4, the only disagreement between the synthetic and observed colors for these stars lies in the c_o index. As was the case with HD 25329, a possible explanation is that these subdwarfs could have abundances for C, N, and/or O which differ significantly from other field dwarfs. Unlike HD 25329, however, the analysis of Carbon et al. (1987) reveals that all of these stars exhibit an *under*-abundance of nitrogen with respect to most other field subdwarfs ($[\mathrm{N/Fe}] = -0.3$, -1.0, and -0.7 for HD 64090, 103095, and 188510, respectively). From the previous discussion, lower nitrogen abundances would imply *less* absorption in the Strömgren u filter from the NH band at 3360 Å, leading to a *lower* value for the c_1 index than what is predicted by the models. However, it is not clear why such an under-abundance of nitrogen does not appear to change the m_o colors significantly due to the effects of the CN band in the v filter.

In conclusion, the calibrated *uvby* colors appear to provide a satisfactory match to the observed indices for most of the selected subdwarfs. Although a few of the stars exhibit some abundance anomalies which lead to a mismatch with the calculated colors, these problematic stars also serve to illustrate the obvious usefulness of the Strömgren m_1 and c_1 indices as indicators of abundance variations in cool stellar atmospheres. Note, however, that the explanations given above for the discrepancies

in the calculated/observed subdwarf colors are only suggestive. It is quite possible that errors in the photometry, the calibrated colors, the reddening estimates, and/or the basic stellar parameters are at the root of the problem, despite the fact these subdwarfs have been extensively studied.

3.2.3 Comparisons with Other Strömgren Color-Temperature Relations

The final section in this chapter investigates how the newly calibrated Strömgren colors compare against other *uvby* C-T relations available in the literature. For this purpose a number of color transformations are selected which have been derived both theoretically and empirically. While both methods have their advantages and disadvantages as discussed in Chapter 1, it is interesting to see how past C-T relations compare to the current set of colors which are calculated from synthetic models and calibrated against stars that have empirically determined parameters.

Figures 3.11 and 3.12 compare the newly calibrated *uvby* C-T relations against the previous MARCS-SSG results of VandenBerg & Bell (1985, hereafter VB85) and the latest grid of ATLAS9 model colors computed and discussed by Castelli et al. (1997, hereafter C97) for two representative [Fe/H] values. In each panel $\log g$ is plotted versus the indicated color and solid lines are used to represent the isotherms corresponding to the newly calibrated colors while the uncalibrated colors are shown as dotted lines. In addition, the overplotted filled circles give the C97 colors whereas open circles represent the VB85 data. Differences between the current non-calibrated colors and the VB85 colors can be attributed to improvements in the MARCS-SSG synthetic models over the years, while differences compared to the C97 colors are likely due to different treatments of the line blanketing and the use of two separate modeling programs in generating the synthetic Strömgren colors (ATLAS9 and MARCS-SSG).

At first glance, it is difficult to distinguish the differences between the VB85

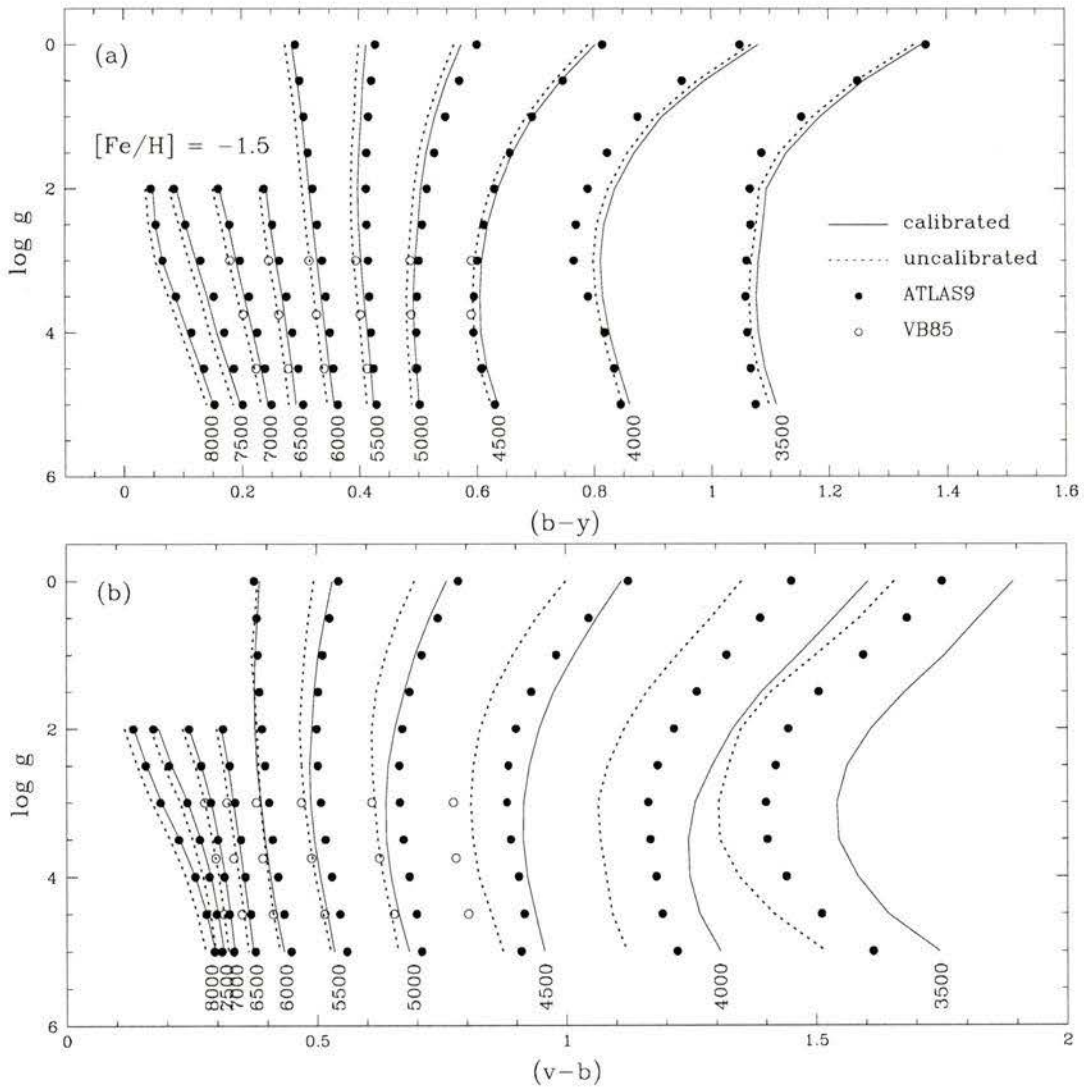

Figure 3.11: A comparison of various theoretical $(b-y)$ and $(v-b)$ C-T relations for [Fe/H] $= -1.5$. In both panels the calibrated colors are represented by solid lines while the uncalibrated colors are given by dotted lines. Overplotted in each panel are the colors based on the Kurucz ATLAS9 models (filled circles) computed by Castelli et al. (1997) and the previous MARCS-SSG colors (open circles) of VandenBerg & Bell (1985).

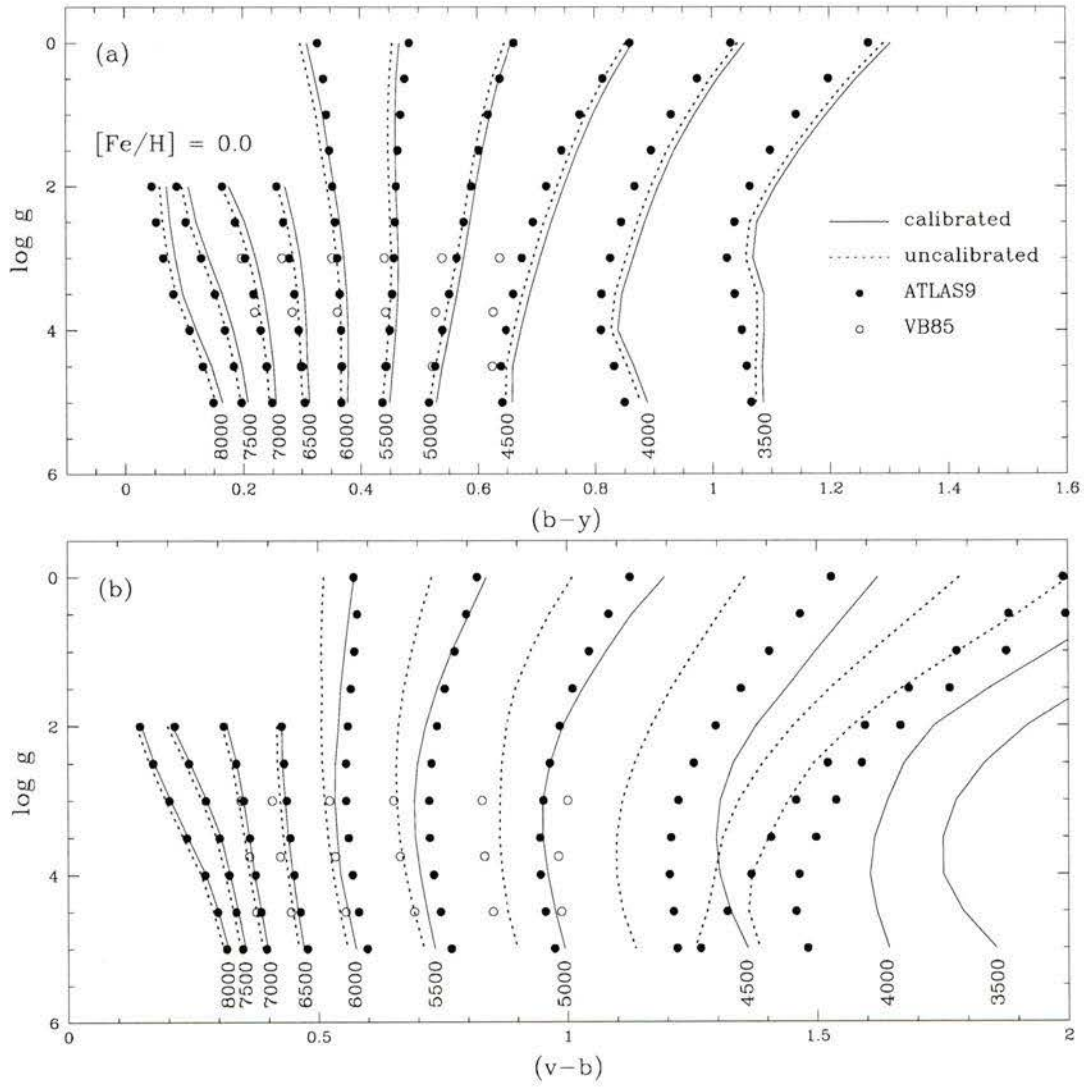

Figure 3.12: Same as the previous figure except for [Fe/H] = 0.0.

and non-calibrated colors for the lower metallicity case in Figure 3.11. It appears the agreement between the two is quite good for the $(b-y)$ colors, and arguably as good in the $(v-b)$ plane with the exception of the 4500 K isotherm for which the VB85 colors are slightly too blue. However, the same agreement does not hold true for the solar metallicity (Figure 3.12) C-T relations. While the correspondence is good for warmer temperatures (i.e. $T_{\rm eff} > 5500$ K), it appears the VB85 colors are systematically too blue compared to the uncalibrated colors. These discrepancies are likely due to the advancements in the stellar synthesis models, such as the inclusion of more detailed atomic and molecular line lists as well as improved low temperature opacities since the VB85 colors were calculated.

For the ATLAS9 colors, the differences between the $(b-y)$ C-T sets appear to be mainly a zero-point offset, likely due to the adoption of slightly different Vega-based normalizations for the synthetic indices. The $(v-b)$ colors are a little more difficult to explain given that the cooler ATLAS9 isotherms are systematically redder for $T_{\rm eff} < 6000$ K (in addition to an apparent zero-point difference) than the uncalibrated colors. In fact, the ATLAS9 $(v-b)$ colors appear to be more consistent with the current set of *calibrated* colors for cooler temperatures. This may be due to the ATLAS9 line lists being more detailed than those used in the SSG code. Despite this, the ATLAS9 colors are still too blue to equate with the newly calibrated colors and would not likely be able to accurately reproduce the colors of the field stars with cooler effective temperatures.

To further exemplify the comparison between the different theoretical *uvby* colors discussed so far, Figures 3.13 and 3.14 plot a 10 Gyr isochrone transformed to two Strömgren color-magnitude planes using both the current C-T relations (calibrated and uncalibrated) as well as those derived from the ATLAS9 models. It is important to note that the same bolometric corrections (namely those of Wood & Bessell) have been used to derive M_V in each plot. This ensures that any difference between the isochrones is due solely to variations in the color transformations. Also, the VB85

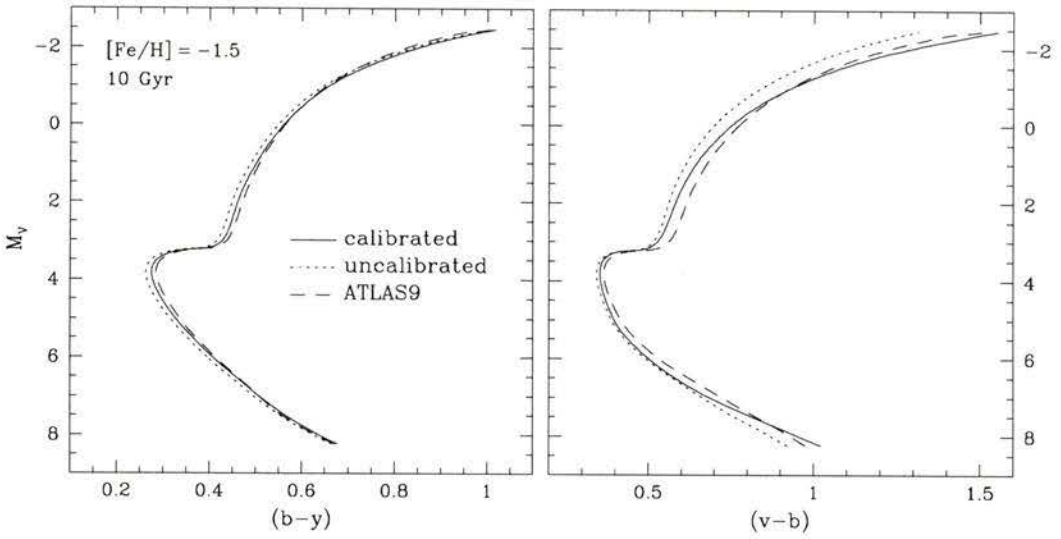

Figure 3.13: Comparisons of a 10 Gyr, [Fe/H] = −1.5 isochrone transformed to the indicated Strömgren color planes using the calibrated, uncalibrated, and ATLAS9 model colors.

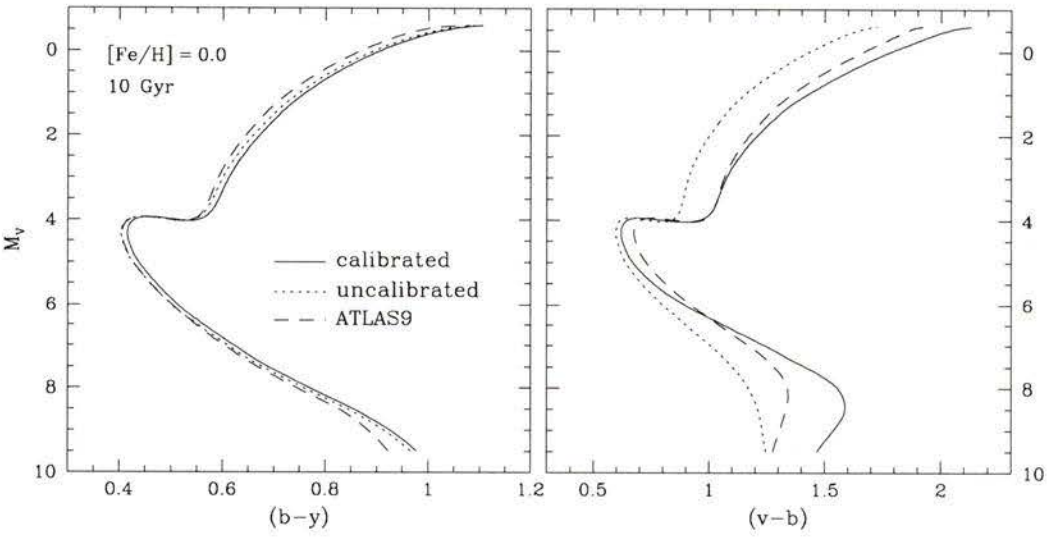

Figure 3.14: Same as previous figure except for a 10 Gyr isochrone with [Fe/H] = 0.0.

colors were not used for this comparison due to their limited coverage of parameter space. From these two figures, one can see that the differences in the C-T relations have quite large effects on the location and morphology of the isochrones, especially in the $[(v-b),\ M_V]$ plane. It is encouraging, however, that the $(b-y)$ isochrones for each metallicity case appear to follow roughly the same trend from the main sequence through the giant branch with only small color differences between them. As mentioned earlier, these color shifts are likely due to different zero-point standardizations between the ATLAS9 and calibrated MARCS-SSG C-T grids. While it does appear the ATLAS9 isochrones would better agree with the calibrated isochrone near the turnoff region if a negative color shift were applied, they are consistently too blue to match the calibrated model for the coolest temperatures.

Turning to comparisons involving empirically derived C-T relations, a number of recent calibrations of $T_{\rm eff}$ versus $(b-y)$ have been extracted from the literature which are briefly described in the following:

- Saxner & Hammerbäck (1985, hereafter SH85) presented one of the first empirical calibrations of $T_{\rm eff}$ versus $(b-y)$ based on stellar temperatures derived using the IR flux method of Blackwell & Shallis (1977). Their examination was based on a total of 30 main sequence stars ranging in temperature between 5800 and 7000 K whose colors fall within the range of $0.20< (b-y) <0.40$. While the stars used in their study covered a limited range in metallicity, an abundance term is included in the final calibration to account for possible metallicity variations.

- The IRFM temperatures for ≈ 75 stars (dwarfs and giants) used in the Gratton et al. (1996, hereafter GCC96) calibration were collected from the lists of Bell & Gustafsson (1989) and corrected to the same temperature scale as Blackwell & Lynas-Gray (1994). This large sample of stars covered a much wider range in both temperature and gravity than the aforementioned SH85 study, and their final dwarf calibration can be reasonably applied to stars with $(b-y)$ colors

between 0.06 and 0.79.

- The $(b-y)$-T_{eff} calibration of Alonso et al. (1996b, hereafter AAM96b) makes use of the same IRFM temperatures used to calibrate the synthetic *uvby* colors at the beginning of this chapter. The sample of approximately 500 stars is by far the largest with well-determined temperatures to date and includes dwarfs and subgiants with spectral types F0 to K5 covering a wide range in metal content ($+0.5 \leq$ [Fe/H] ≤ -3.0). To account for the effects of differing metal abundances and gravity in their sample stars, the final temperature calibrations are a function of not only $(b-y)$, but also [Fe/H] and c_1.

Figure 3.15 compares the empirical T_{eff}-$(b-y)$ calibrations derived in the various studies mentioned above together with the relationship between $(b-y)$ and T_{eff} predicted by the calibrated Strömgren colors for a representative $\log g = 4.5$ appropriate for main sequence dwarf stars. For those calibrations which include a metallicity term (SH85 and AAM96b), all of the curves plotted in the figure assume a solar metallicity ([Fe/H] $= 0.0$). Also, the original calibration of SH85 has been extended from its original calibration limit of $(b-y) = 0.45$ to $(b-y) = 0.6$ to illustrate its limited validity for cooler temperatures. It is quite reassuring that all three empirical calibrations appear to agree well in the range $0.2 < (b-y) < 0.5$ which illustrates the consistency of the IRFM in predicting stellar temperatures. In addition, their correspondence with the C-T relations derived from the calibrated colors serves to prove that the synthetic Strömgren colors can accurately relate stellar color and temperature for $(b-y)$. Indeed, the calibrated C-T relation together with the calibrations of GCC96 and AAM96b are in superb agreement over a broad temperature and color range. To further illustrate this point, a solar color of $(b-y) = 0.412$ has been derived from the calibrated colors assuming $T_{eff} = 5770$, $\log g = 4.44$, and [Fe/H] $= 0.0$. Applying the same solar temperature to the relations of SH85, GCC96, and AAM96b yields $(b-y)_\odot = 0.407$, 0.401, and 0.414, respectively.

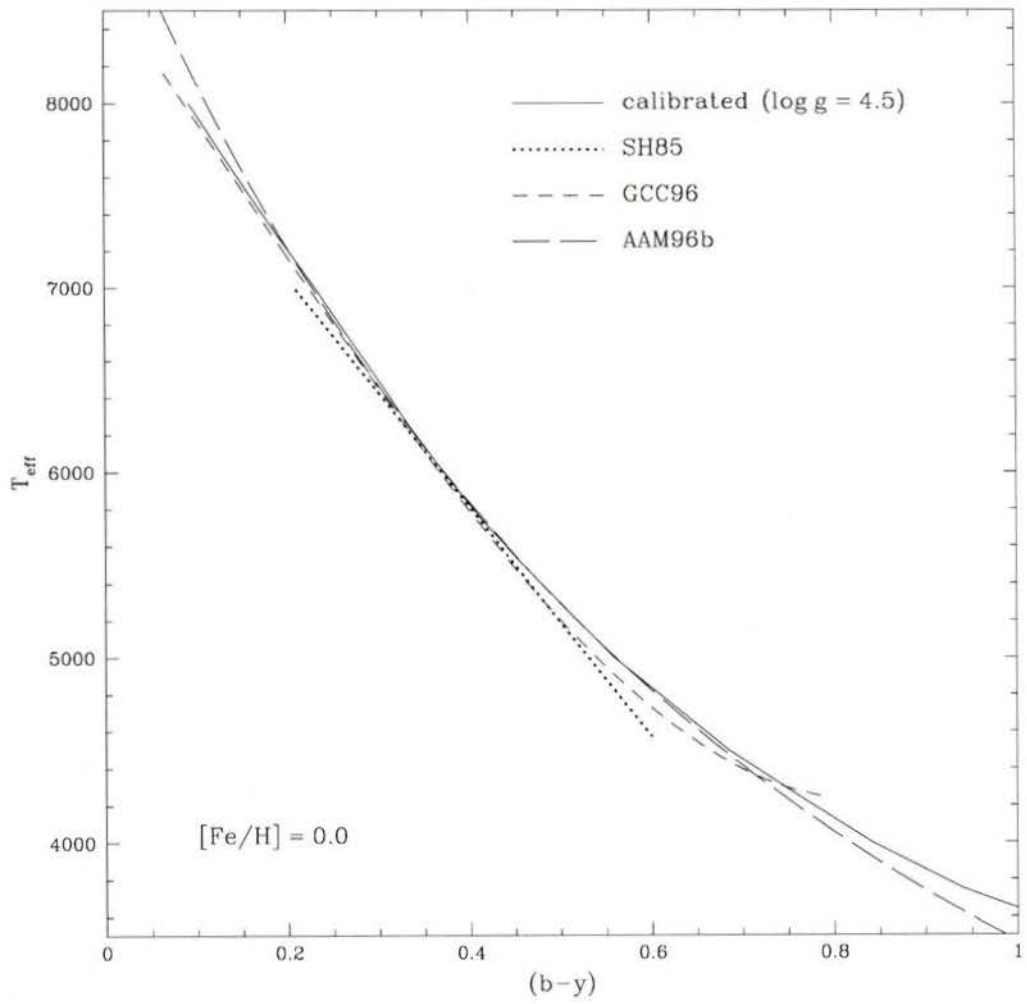

Figure 3.15: A comparison of empirical C-T calibrations from the indicated studies with the relationship between $(b-y)$ and T_{eff} predicted by the calibrated Strömgren colors for $\log g = 4.5$.

In summary, this chapter has discussed the derivation of the color calibrations needed to put the synthetic *uvby* colors onto the observational systems. Furthermore, the accuracy of newly calibrated colors was put to the test by comparing them with both a large sample of field stars, as well as a selected group of well-observed Population II subdwarfs. While the tests attempt to cover a number of observational regimes with stars that define a wide range in effective temperature, gravity, and metallicity, there are still a number of areas in which the calibrated colors remain untested. For instance, no mention was made as to the validity of the colors for more metal-poor giant stars for two reasons. First, very few metal-poor field giants have been as extensively studied as the dwarf and subdwarf sample presented here. Second, and more importantly, the effects of CN variations seen in a few subdwarfs are more common and profound among RGB stars in globular clusters (Grundahl et al. 2000b) and in the field (Hilker 2000) due to evolutionary effects. Therefore, deriving an adequate sample of metal deficient giants to test the colors against would require some prior knowledge of their chemical abundances (particularly carbon and nitrogen) in order to yield accurate results. Rather than resort to this type of analysis, the next chapter will continue to test the calibrated colors by comparing model isochrones to the CMDs of a number of metal-poor globular clusters and metal-rich open clusters. These clusters serve as perfect laboratories against which to test the Strömgren indices since all of the member stars have the same distances, reddenings, ages, and metallicities. Thus, errors due to star-to-star differences in these properties, which were inherent with the field stars, are reduced to a minimum with cluster stars. In addition, the next chapter will compare the isochrone fits to cluster CMDs in the Strömgren system with those in the broadband $UBVRI$ system in order to check the consistency of the models in two different photometric systems.

Chapter 4

Examining Star Clusters With Strömgren Photometry

Star clusters serve as ideal testing grounds in which to study the theories of stellar structure and evolution because their members are believed to have all formed at approximately the same time from the same molecular cloud. As a result, individual clusters have essentially the same age, distance, and chemical composition. These stellar populations can provide valuable insight into the structure and evolution of the galaxy as a whole. For instance, a simple correlation between cluster ages, metallicities, velocities, and spatial locations leads to the conclusion that the galaxy is composed of two distinct stellar populations. The extremely metal-poor, populous globular clusters (GCs), which are among some of the oldest known objects in the universe, represent one population, while the younger, metal-rich galactic open clusters (OCs) comprise the other.

Within the past two decades a large amount of high quality photometric data for a significant number of GCs and OCs has accumulated in the literature due in part to the use of large format CCD detectors in observations. This type of photometric accuracy has resulted in cluster color-magnitude diagrams (CMDs) which

exhibit an extremely well defined sequence of stars in different stages of evolution ranging from the main sequence (MS) through the red giant branch (RGB). As a result, the technique of isochrone fitting discussed earlier has greatly benefitted from the increased photometric precision by yielding more reliable age estimates for these clusters. Ideally, the best way to determine a cluster's age (once the distance, reddening, and metallicity of the clusters has been constrained in some way) is to assess which isochrone provides the best fit to the CMD in the vicinity of the turnoff (TO). This TO point, defined as the location where stars exhaust their core hydrogen fuel and begin to evolve away from the main sequence, is the most sensitive indicator of cluster age owing to the fact that the older the cluster, the redder and less luminous the TO point. While this method has been widely applied to a large sample of clusters with broadband ($UBVRI$) photometric data (see, e.g., VandenBerg 2000 and Salaris & Weiss 1997 for recent discussions), the interpretation of CMDs in the Strömgren filter system has been rarely discussed in years past due to the fact that accurate *uvby* photometric data is largely unavailable for a sufficient number of star clusters. Moreover, any interpretation of existing cluster photometry using theoretical stellar models has suffered from the lack of modern and precise color-temperature (C-T) relations for the *uvby* system.

This chapter sets forth to remedy these problems and also illustrate the viability of the Strömgren photometric system as an alternative to the broadband system for cluster studies from two fronts. First, the accuracy of the synthetic Strömgren C-T relations calibrated in the previous chapter are further tested by fitting isochrones to the *uvby* CMDs for a selected sample of clusters. Indeed, the reliability of the calibrated *uvby* colors for near-solar abundances has already been demonstrated for the case of the open cluster M 67 (see Figure 3.7). In addition to M 67, the current study makes use of *uvby* data for a number of other OCs and metal-poor GCs to both further constrain the accuracy of the model colors for solar metallicities, as well as to extend the tests to lower abundances. Second, and more importantly, broadband

data for these clusters are collected from the literature to assess whether the same isochrone fits the cluster CMDs independently of the color [i.e. $(b-y)$ or $(B-V)$] that is employed[1].

In the discussion which follows, a few general requirements should be kept in mind when inspecting the isochrone fits to the cluster CMDs. First, for a given cluster, the fits on different Strömgren color planes should be of the same quality. Next, little or no ad hoc color shifts should be necessary to adequately match the data once the appropriate reddening for the cluster is adopted. Finally, estimates for quantities such as age and distance should be totally independent of which color is used for the isochrone fit. Adhering to these basic guidelines not only assures that a "good" isochrone fit to the data has been achieved, but also reinforces the validity of the Strömgren C-T relations used to transform the isochrone.

4.1 Open Clusters

Open clusters serve as excellent tracers of the structure and chemical evolution of the galactic disk due to their wide distribution in age and metallicity. While photometric observations of OCs in the four-color system have received some moderate attention in literature, the amount of high quality *uvby* data currently available is still quite small when compared to broadband observations. For this reason, a recent observing program aimed at obtaining *uvby* photometry for two OCs was performed in conjunction with the present study. Including these recent observations together with data for other OCs in the present sample provides a variety of clusters covering a wide range in age against which the accuracy of the calibrated Strömgren colors can be further tested for metallicities near solar.

[1]It should be mentioned that throughout this chapter comparisons involving isochrones fitted to various broadband CMDs are transformed to the observed plane using the semi-empirical C-T relations presented by VandenBerg (2001, in preparation) and briefly described in VandenBerg (2000).

4.1.1 The Hyades

The Hyades is perhaps the most documented open cluster and has served as an important "standard" cluster against which other stellar populations have been compared for many years as well as a fundamental constraint on the extragalactic distance scale. Furthermore, with a well established metallicity of [Fe/H]$\approx$+0.12 (Cayrel et al.1985, Boesgaard 1989, and Boesgaard & Friel 1990) it is the ideal test for stellar models and the synthetic Strömgren colors for metallicities above solar. In a recent study Perryman et al. (1998) presented the *Hipparcos* view of the Hyades in which they investigated the dynamical properties of the cluster as well as its HR diagram and age. More importantly, however, their examination of the three-dimensional spatial and velocity distribution of member stars lead to a precise estimate of the distance to the Hyades (D = 46.24 $\pm$ 0.27 pc). Even more recently de Bruijne, Hoogerwerf, & de Zeeuw (2001, hereafter BHZ) derived secular parallaxes from *Hipparcos* proper motions in order to isolate a set of 88 "high-fidelity" cluster members which define a tight main sequence in the $[(B-V), M_V]$ plane.

The Hyades cluster is one of the few OCs which has a received a considerable amount of attention in the Strömgren system. The extensive survey of Crawford & Perry (1966) reported $uvbyH\beta$ photometry for 132 member stars down to V$\approx$8 mag. In addition, Eggen (1982) and Reglero et al. (1992) obtained observations for a combined total of 100 stars which extended the cluster data down to V$\approx$11. Figure 4.1 presents a number of *uvby* CMDs for the Hyades using a total of 67 stars from the "high-fidelity" sample of BHZ which have available Strömgren photometry. Overplotted in each panel of the figure is a ZAMS model (VandenBerg, private communication) corresponding to the Hyades metallicity of [Fe/H] = +0.12. Overall, the ZAMS shows exceptional agreement for the majority of stars lying on the main sequence. The few stars showing the largest deviation from the ZAMS with $M_V \leq 3$ are likely slightly evolved. In addition to these CMDs, Figure 4.2 illustrates the accu-

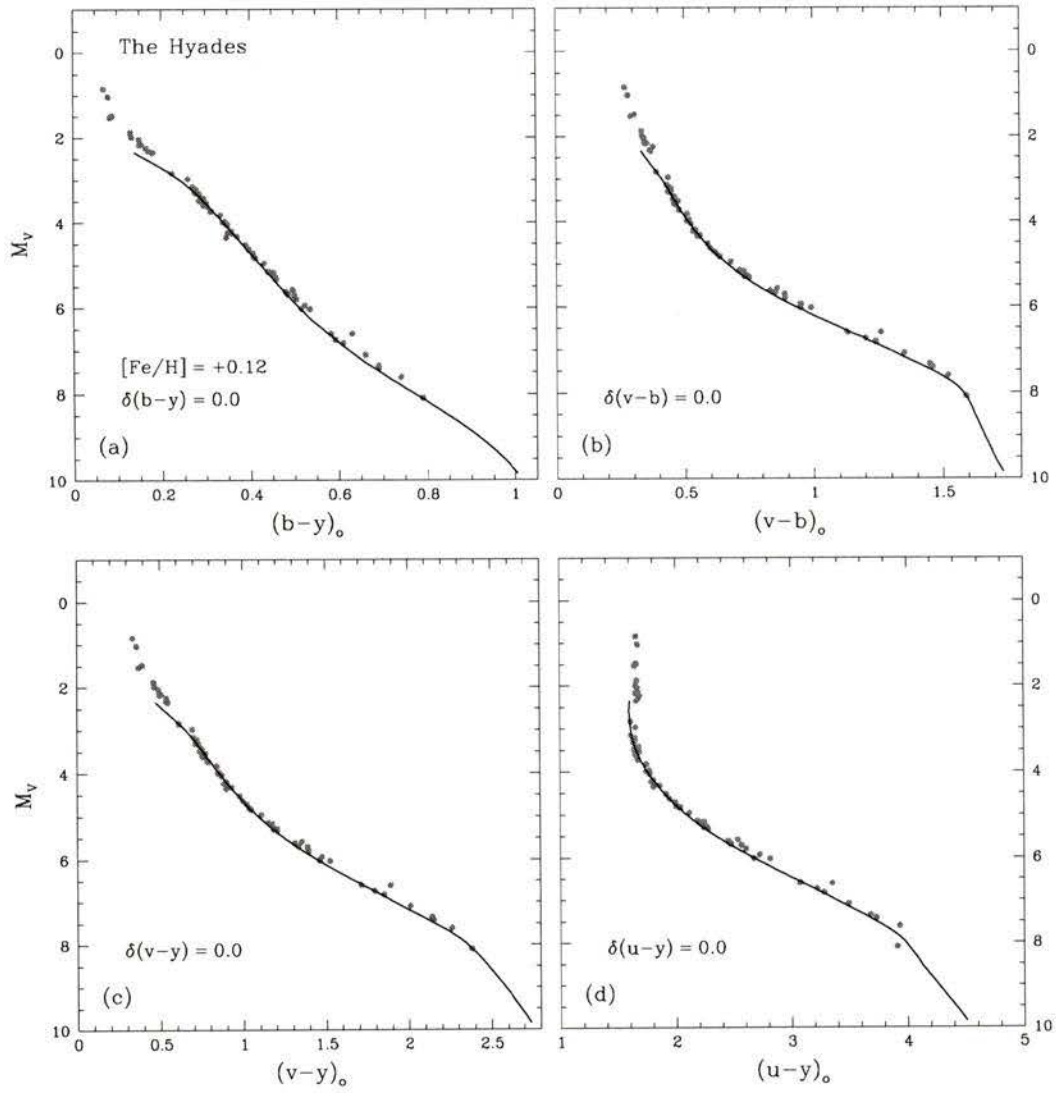

Figure 4.1: Fits of a ZAMS model having a metallicity of [Fe/H] = +0.12 to the 67 "high-fidelity" members of the Hyades open cluster. Absolute magnitudes for each star have been derived from the secular parallaxes determined by de Bruijne, Hoogerwerf, & de Zeeuw (2001). No reddening corrections have been applied to the photometric data.

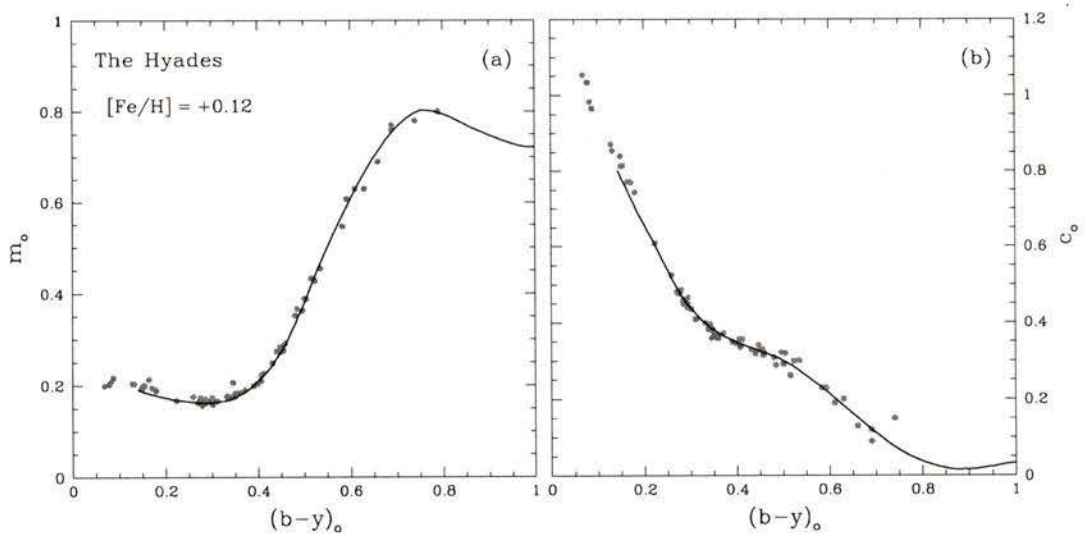

Figure 4.2: Color-color plots of $(b-y)_o$ vs. m_o (**a**) and $(b-y)_o$ vs. c_o (**b**) overplotted with the same [Fe/H] = +0.12 ZAMS from previous figure.

racy of the calibrated colors in matching the ZAMS to the data on various Strömgren color-color diagrams. Overall, the ZAMS fits in both figures are exceptionally good, and the use of high quality Hyades members from BHZ ensures that only single stars lying on or near the main sequence are considered in the plots (i.e., all binaries and anomalous stars are excluded).

4.1.2 M 67

M 67 has long been an important cluster for calibrating solar metallicity stellar models. Its moderately old age combined with its rather rich population also provides an opportunity to investigate to the evolution of solar like stars near the end of the main sequence phase. Spectral abundance analyses have constrained its metallicity to be just slightly less than solar ([Fe/H] = −0.04; Montgomery, Marschall, & Janes 1993). In the last chapter the accuracy of the calibrated Strömgren colors were illustrated by fitting a 4 Gyr isochrone with [Fe/H] = −0.04 to the *uvby* CMDs of M 67.

Assuming a distance modulus of $(m-M)_V = 9.60$ and a reddening of $E(b-y) = 0.029$ (Schlegel et al. 1998), it appears from Figure 4.3 that the isochrone matches the data quite well for all colors. In addition, identical fits using the same isochrone are obtained for the BV and VI data from Montgomery et al. (1993) in Figure 4.4.

4.1.3 NGC 6819 and NGC 188

In an effort to increase the amount of Strömgren data available for star clusters, observations of the two prominent open clusters NGC 188 and NGC 6819 were obtained by the author in the *uvby* system. Both of these OCs together with their counterpart M 67 serve as ideal clusters in which to test the calibrated *uvby* colors for solar metallicities due to their range in ages but very similar chemical compositions. The details of the observation process and reduction of the photometric data are left to Appendix C while the current discussion will precede with the presentation of the *uvby* CMDs of NGC 188 and NGC 6819.

Figure 4.5 exhibits various *uvby* CMDs for NGC 6819 down to V≈19.5. While the cluster suffers from significant field star contamination in its CMDs, a tight, well-defined main sequence and turnoff as well as a noticeable population of clump giant stars are easily seen despite the clutter. In addition, the preferred isochrone with an age of 2.5 Gyr is overplotted in each panel. As with M 67 and the Hyades, the fits of the isochrone to the CMDs are exceptionally good with little or no color shifts necessary to adequately match the data. The metallicity of NGC 6819 is fairly well constrained with recent estimates hovering around a near solar value. Recent spectroscopic examinations have yielded $[Fe/H] = +0.05 \pm 0.11$ (Friel & Janes 1993) and $+0.09 \pm 0.03$ (Bragaglia et al. 2001). However, it is important to note that the Friel & Janes metal abundance is highly dependent on the cluster's reddening value (which they adopted to be $E(B-V) = 0.280$) due to the use of a photometrically based T_{eff} scale in their analysis. The Bragaglia et al. value, on the other hand, is

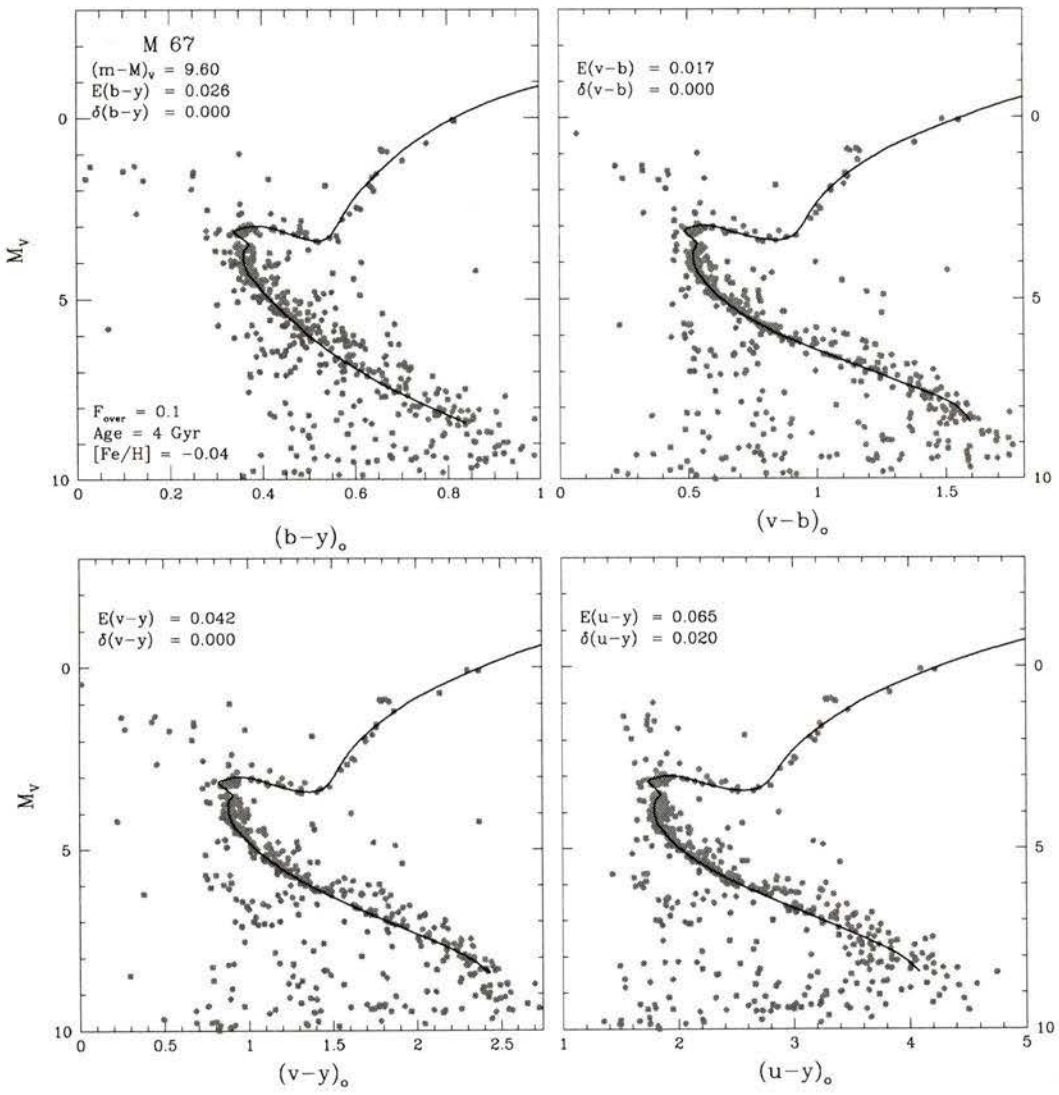

Figure 4.3: Fits of a 4 Gyr isochrone for the indicated parameters to the various *uvby* CMDs of M 67: note the isochrones have been shifted in color by the indicated amounts to provide the best match to the photometric data. The *uvby* data has been provided by F. Grundahl.

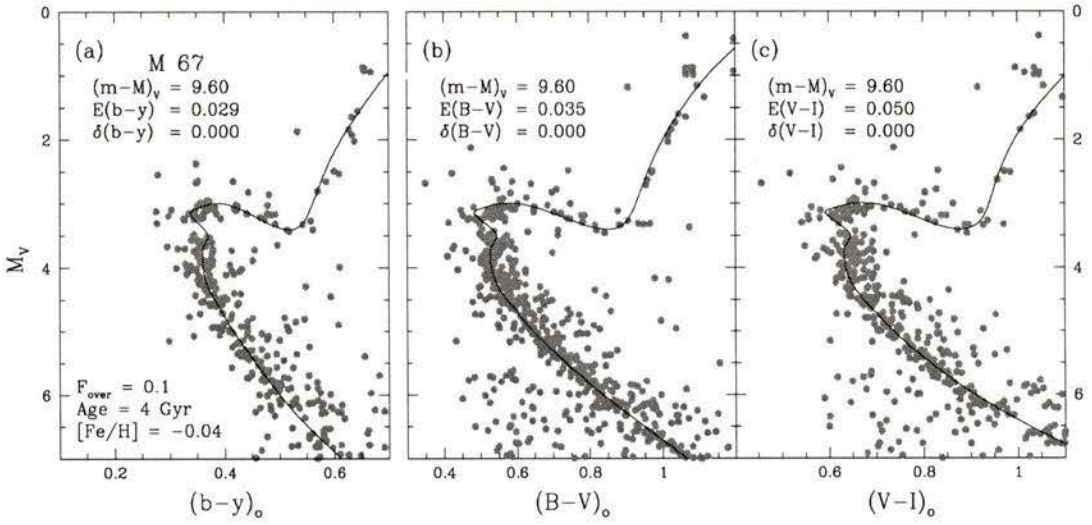

Figure 4.4: Fits of the same 4 Gyr isochrone from the previous figure to the indicated Strömgren and broadband CMDs. The BV and VI photometric data are taken from Montgomery et al. (1993).

independent of the assumed reddening, and they used their spectra to derive $\mathrm{E}(B-V) = 0.140 \pm 0.04$. While other quoted values for the reddening range as low as $\mathrm{E}(B-V) = 0.1$ (Kalirai et al. 2001) up to 0.3 (Lindoff 1972), the recent reddening maps of Schlegel et al. (1998) give 0.204. Given this evidence, the NGC 6819 CMDs shown in Figure 4.5 are fit with a solar metallicity isochrone with the photometry being corrected for reddening using a value of $\mathrm{E}(B-V) = 0.145$. The adoption of these parameters appears to yield an adequate fit to the data without any significant color shifts being required and gives a cluster age of 2.5 Gyr. Figure 4.6 shows how the fit of the same isochrone on the $[(v-y)_o, \mathrm{M}_V]$ CMD compares with the fit to the $(B-V)$ data of Rosvick & VandenBerg (1998). In each panel of this figure, the same isochrone appears to give similar interpretations of the photometric data when identical cluster parameters are assumed.

NGC 188 has been the subject of much study in the past because it is one of the oldest known open clusters. Figure 4.7 presents the Strömgren CMDs for NGC 188

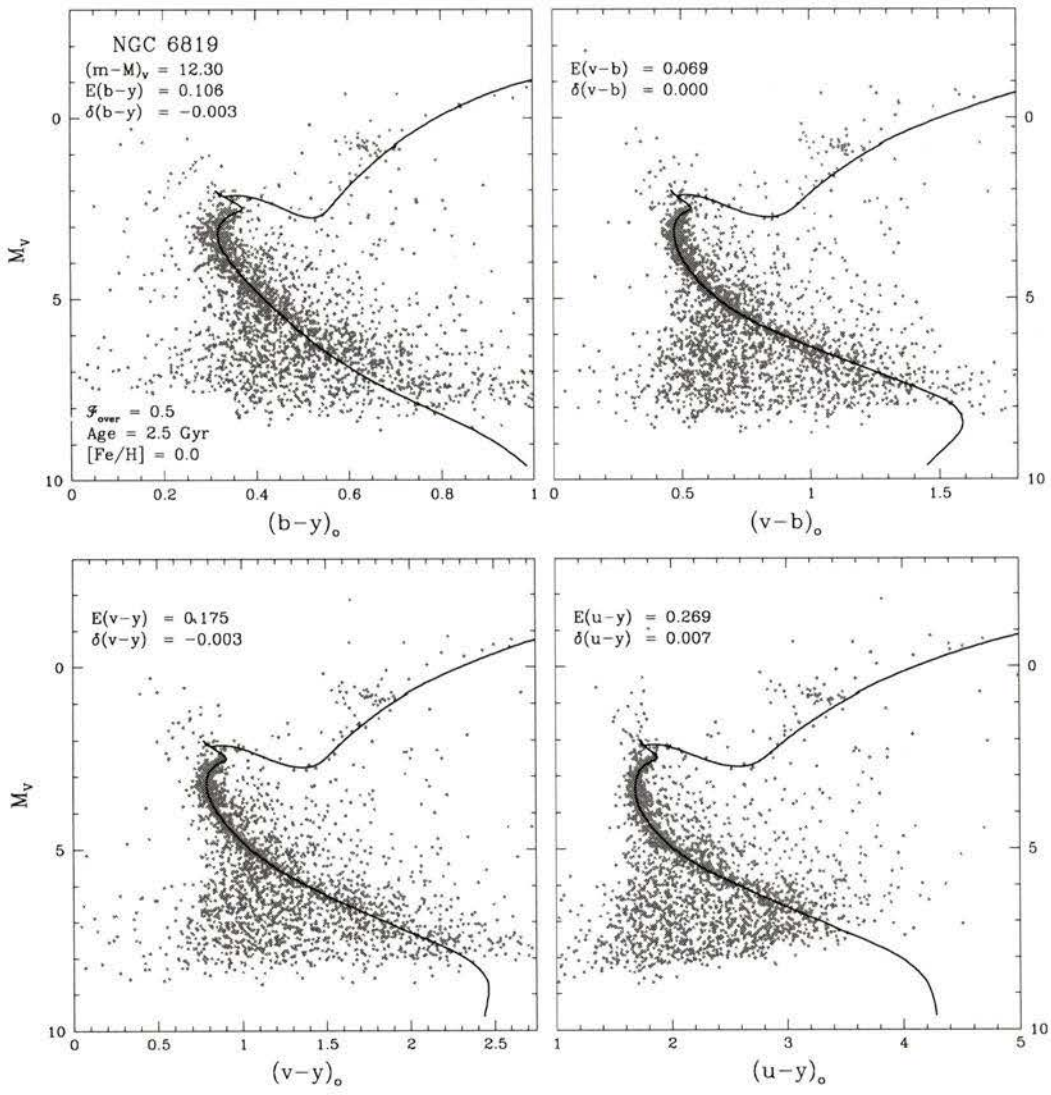

Figure 4.5: Fits of a 2.5 Gyr isochrone for the indicated parameters to the various *uvby* CMDs of NGC 6819.

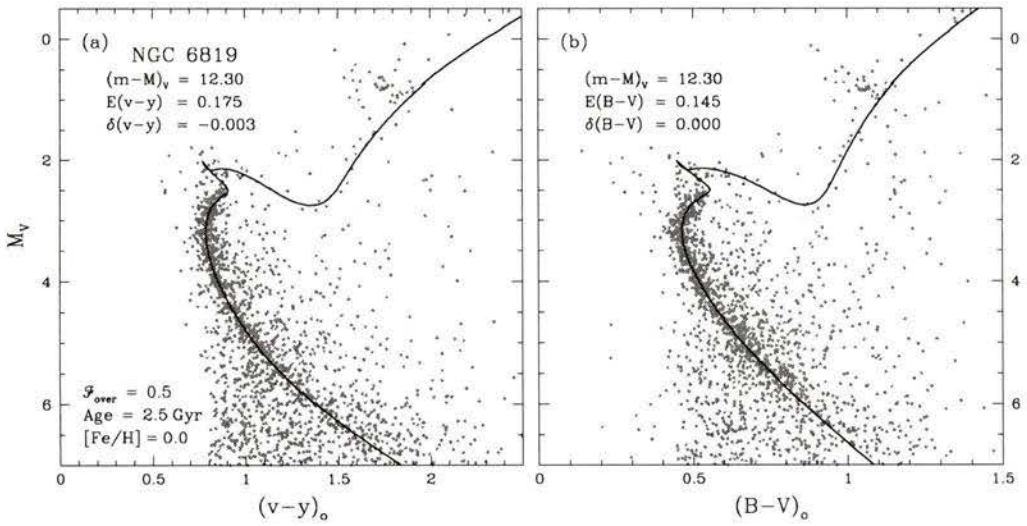

Figure 4.6: Fits of the same 2.5 Gyr isochrone from the previous figure to the indicated Strömgren and broadband CMDs. The BV photometric data are taken from the study of Rosvick & VandenBerg (1998).

fitted with a 7 Gyr, $[\mathrm{Fe/H}] = -0.04$ isochrone. The metallicity of the cluster is comparable to that of the aforementioned NGC 6819 and M 67 with modern estimates of $[\mathrm{Fe/H}] = 0.02 \pm 0.11$ (Caputo et al. 1990), -0.12 ± 0.16 (Hobbs et al 1990), and -0.02 (Twarog & Anthony-Twarog 1989). Furthermore, the fact that NGC 188 is considerably older than the OCs previously discussed is apparent by the smooth distribution of stars at the cluster turnoff and well populated subgiant and red giant branches. Again, the 7 Gyr isochrone appears to match the data quite well on all color-magnitude planes from the MS through the RGB. In a recent work, Sarajedini et al. (1999) published their high-precision $UBVRI$ photometry for NGC 188 and used it to derive the cluster's reddening, distance, and age. Their $[(B-V), \mathrm{M}_V]$ CMD is plotted in the right panel of Figure 4.8 as a comparison against the Strömgren equivalent in the left panel. Both CMDs are again fitted with the same 7 Gyr isochrone used in Figure 4.7 assuming the same cluster parameters. A Schlegel et al. reddening of $\mathrm{E}(B-V) = 0.087$ has been used to correct both sets of data along with a distance

modulus of $(m - M)_V = 11.40$. These values correspond well with the reddening and distance modulus of 0.09 ± 0.02 and 11.44 ± 0.08, respectively, determined by Sarajedini et al. from their comparison of the cluster data against the M 67 photometry of Montgomery et al. (1993). Furthermore, their investigation also led to a derived age for NGC 188 of 7.0 ± 0.5 Gyr, in precise agreement with the age suggested from isochrone fits to the *uvby* data presented here.

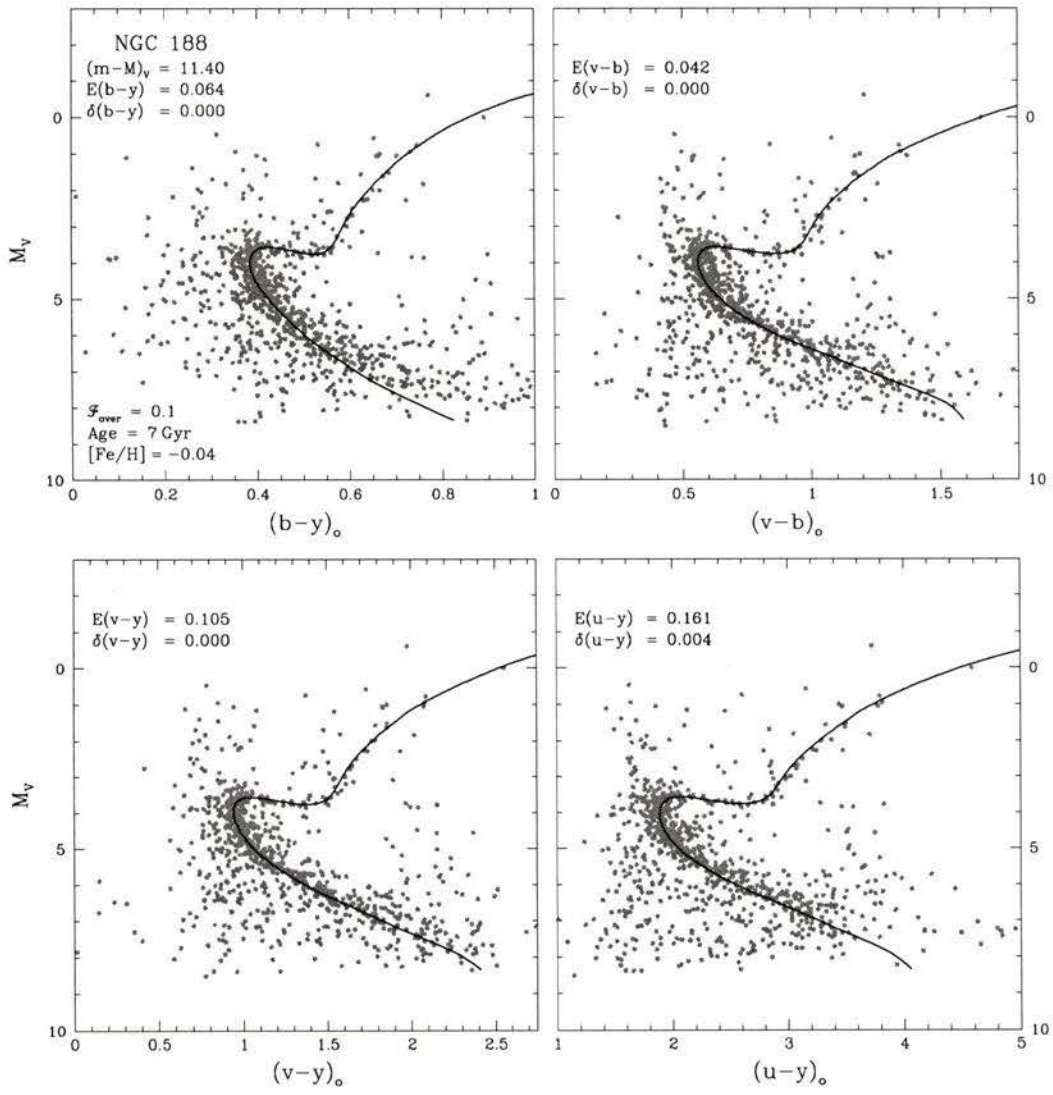

Figure 4.7: Fits of a 7 Gyr isochrone for the indicated parameters to the various *uvby* CMDs of NGC 188.

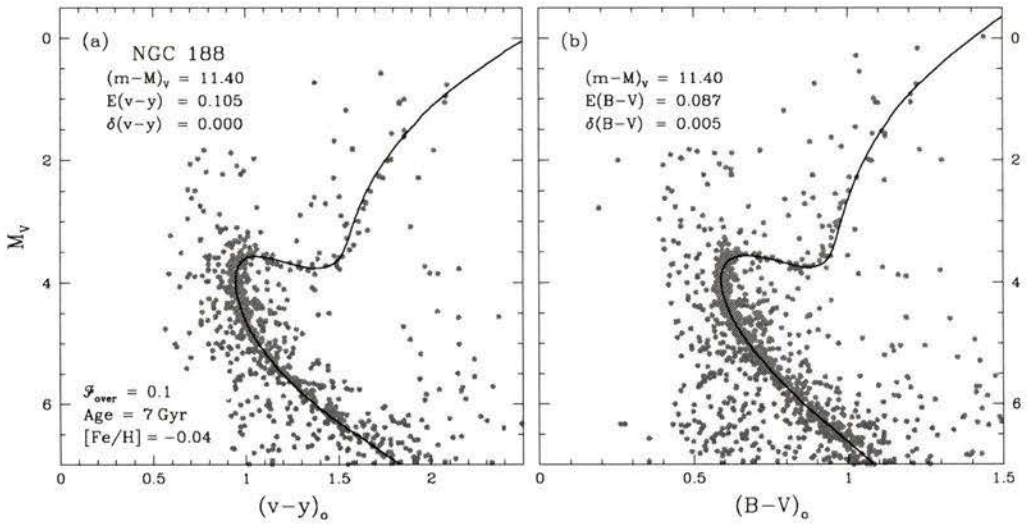

Figure 4.8: Fits of the same 7 Gyr isochrone from the previous figure to the indicated Strömgren and broadband CMDs. The BV photometric data are taken from the study of Sarajedini et al. (1999).

4.2 Globular Clusters

Globular clusters have long been considered to be the oldest known objects in the Milky Way, and for this reason there is a great interest in deriving the absolute ages of these systems in order to constrain the age of both the galaxy and the universe. With the availability of precise and well calibrated photometry mentioned at the beginning of this chapter, the problems of determining accurate GC ages no longer lie in the lack of accurate photometric data, but rather in determining reliable values for the basic parameters which enter into the derivation of a cluster's age, namely its distance, reddening, and metallicity. One common impediment in age determinations lies in establishing an appropriate cluster distance scale. For example, recent studies involving fits of local subdwarfs with accurate *Hipparcos* parallaxes to GC fiducials have favored ages of $\lesssim 12$ Gyr for the oldest clusters (Reid 1997 and Gratton et al. 1997). Ages from RR Lyrae studies, on the other hand, seem to imply ages $\gtrsim 16$ Gyr

(Layden et al. 1996, Fernley et al. 1998, and Gratton 1998). Given the obvious lack of agreement in adopted distance scales and derived ages between various studies, Strömgren photometry can offer a viable alternative to estimating cluster ages by circumventing the distance problem. Recently, Grundahl et al. (2000a) investigated the possibility of deriving a distance-independent age for the globular cluster M 92. While their analysis yielded an intermediate age for ≈ 14.5 Gyr for the cluster based on isochrone fits to the dereddened $[(v-y)_o,\ c_1]$ diagram, these resulting fits (see their Figure 1) showed an obvious lack of agreement between the isochrones and the cluster photometry in the region of the RGB. Indeed, the confidence in ages derived from theoretical isochrones is higher if the isochrone is able to reproduce the complete trend defined by the cluster photometry from the lower main sequence to the tip of the RGB. Therefore, reliable *uvby* colors are required to transform the isochrones before any definite conclusion can be made regarding cluster ages.

Despite the potentials Strömgren photometry holds for deriving distance independent ages for GCs, no attempt will be made here to reach any definite conclusions regarding cluster age or distance. Rather, the main goal of this section is to assess the consistency of the Strömgren C-T relations with those adopted by VandenBerg (2000) on various broadband CMDs. For such a purpose, a number of prominent GCs spanning a wide metallicity range is employed which have precise *uvby* and *BVI* photometry.

Before continuing with the present discussion, a few things should be noted concerning the isochrones and photometric data used here. First, the isochrones employed throughout this section have been derived from the VandenBerg et al. (2000) evolutionary tracks using the interpolation techniques described by Bergbusch & VandenBerg (2001). These models have been computed for 17 [Fe/H] values ranging from -2.31 to -0.30 employing the most up-to-date physics and opacity data available and account for enhancements in α element abundances by assuming $[\alpha/\mathrm{Fe}] = 0.0$, $+0.3$, and $+0.6$ for each metallicity value. Cluster metallicity estimates are taken from Zinn

& West (1984, hereafter ZW) while reddening values are derived from the reddening maps of Schlegel et al. (1998, hereafter SFD) unless otherwise noted. In addition, a value of $[\alpha/\mathrm{Fe}] = +0.3$ is generally adopted for all the GCs presented here (Carney 1996). Regarding isochrones fits to the photometric data, the same basic requirements which were adhered to in the previous section for OCs are also adopted here to the GC CMDs. Finally, the cluster CCD photometry has been graciously provided by F. Grundahl as part of his extensive and unprecedented *uvby* photometric survey of a large sample of globular and open clusters (see Grundahl et al. 1998, 1999, 2000a, and 2000b for details regarding the observational procedures and photometric reductions as well as in-depth investigations of the cluster properties, including distance and age).

4.2.1 M 92

The globular cluster M 92 serves as a representative of the oldest and most metal-poor clusters in the present sample. The ZW metallicity scale provides a value of $[\mathrm{Fe/H}] = -2.24$ for the cluster, whereas Sneden et al (1991) and Carretta & Gratton (1997) have derived -2.25 and -2.16, respectively, on the basis of high-resolution spectroscopy of cluster giants. In addition, the reddening of the cluster is similarly well constrained, with the SFD reddening maps giving $\mathrm{E}(B-V) = 0.023$. Figure 4.9 presents the observed *uvby* CMDs for M 92 along with the corresponding best fitting 16 Gyr isochrone transformed to each indicated color (note that this age estimate is reduced by 10 - 12 % when diffusive processes are taken into account - see VandenBerg et al. 2001, in preparation). For the purpose of the fit, an isochrone corresponding to $[\mathrm{Fe/H}] = -2.31$ is preferred based on the metallicity estimates mentioned above.

Overall, the isochrone fits to the M 92 CMDs appear to agree remarkably well with each other when a distance modulus of $(m-M)_V = 14.55$ and the SFD reddenings are adopted. The only mentionable discrepancy is the moderately large color shift

required to match the data on the $[(u-y),\ M_V]$ plane. Concerning this matter, Grundahl et al. (2000a) have noted that their u magnitudes for M 92 could suffer from a zero point problem as large as 0.04 mag, which might explain the reason for such a needed shift in color. Regardless of the cause, the validity of the calibrated Strömgren colors for extremely low metallicities is confirmed in all four panels of Figure 4.9 by the fact that the isochrone matches all components of the CMDs from the MS to the RGB.

While Figure 4.9 compared isochrone fits on various Strömgren color planes, Figure 4.10 presents a similar comparison between a $(b-y)$ CMD and its broadband equivalents. The BV fiducial sequence plotted in panel (b) has been taken from Stetson & Harris (1988) while the VI data in panel (c) comes from the study of Johnson & Bolte (1998). In each panel a number of isochrones are plotted ranging in age from 8 to 18 Gyr in steps of 2 Gyr and corresponding to the same metallicity considered above. In addition, the same SFD reddening is adopted to correct the photometry for each case. The only parameter which is notably different between this figure and the previous one is the slightly larger distance modulus of 14.59 adopted on the basis of fits to all three color planes which suggests there are slight differences in the V magnitude scales in these investigations. From inspection of this figure, it is immediately evident that the same 16 Gyr, $[\mathrm{Fe/H}] = -2.31$ isochrone yields the same basic interpretation of the data regardless of which photometric color is adopted. Not only does this lend reassurance to the accuracy of the calibrated Strömgren colors, but also for the T_{eff} scale predicted by the isochrones.

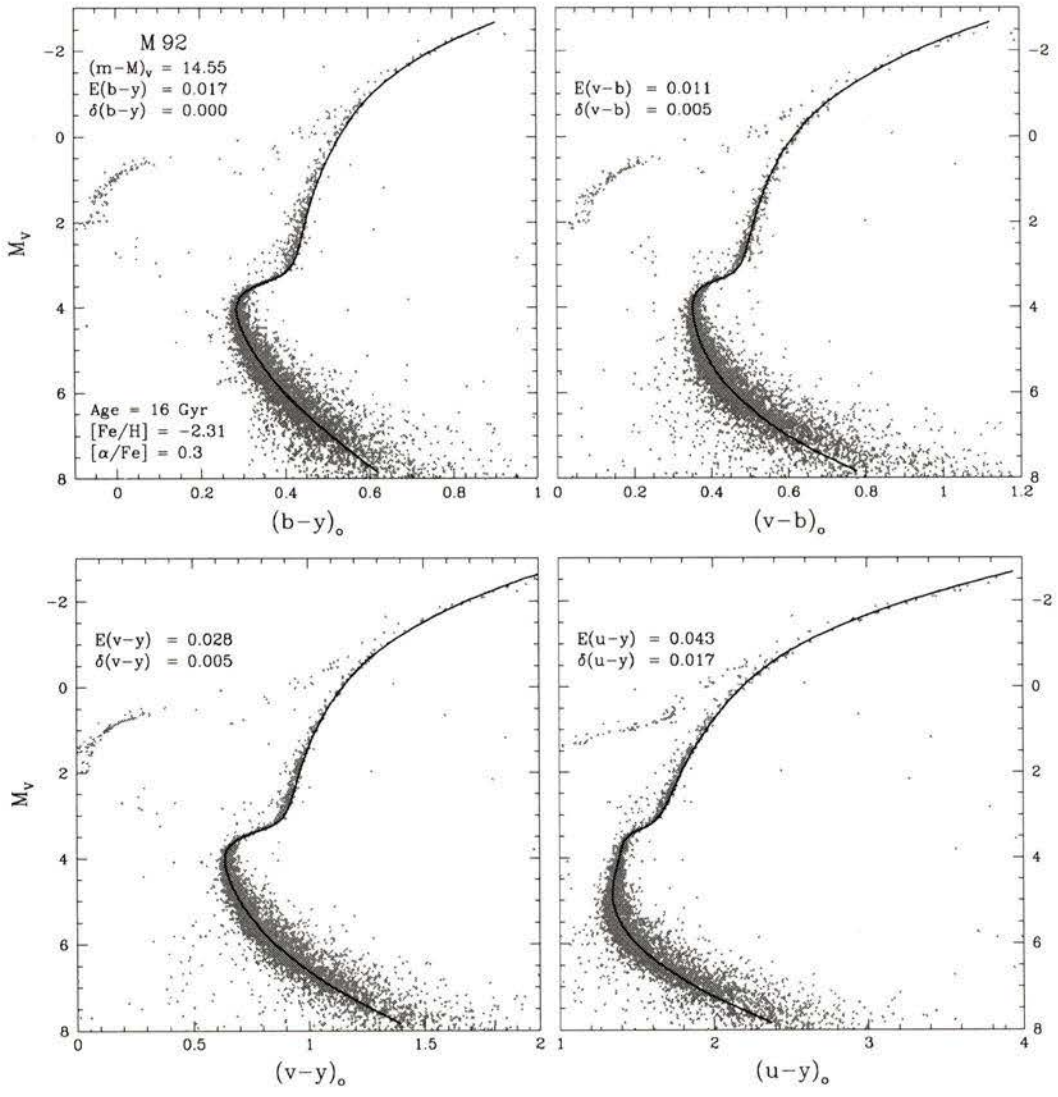

Figure 4.9: Fits of a 16 Gyr isochrone for the indicated parameters to the various *uvby* CMDs of M 92.

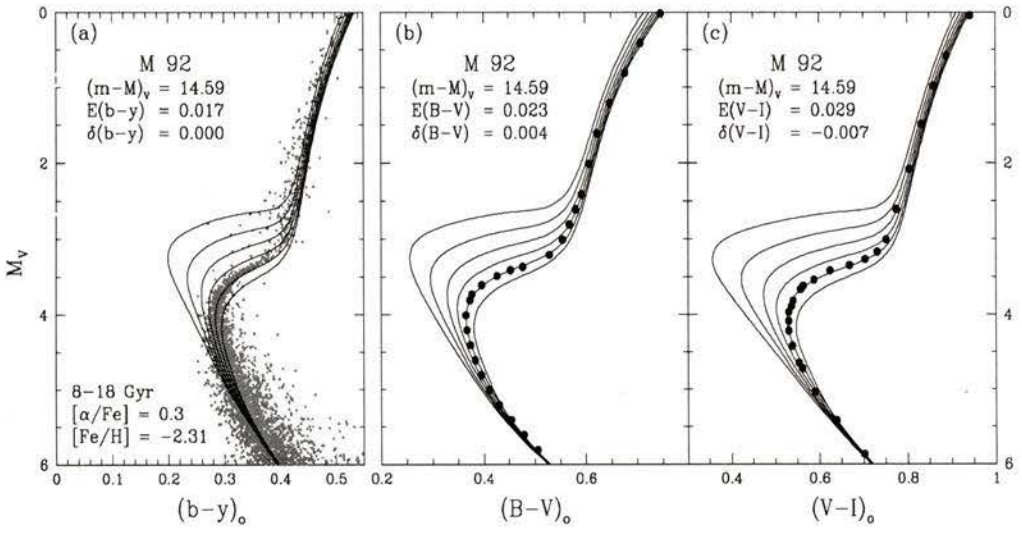

Figure 4.10: Fits of isochrones to the indicated Strömgren and broadband CMDs for M 92. The BV fiducial sequence is taken from Stetson & Harris (1988) whereas the VI fiducial is from the study of Johnson & Bolte (1998).

4.2.2 M 13 and NGC 288

M 13 and NGC 288 are chosen as the best examples of two intermediate metallicity globular clusters with ZW [Fe/H] values of −1.65 and −1.40, respectively. As with M 92, Figures 4.11 and 4.12 illustrate the superb quality of the isochrone fits among various Strömgren CMDs for both clusters. For each case, the isochrone adopted for each cluster has a metallicity which closely corresponds to the ZW values mentioned above, and the distance moduli are tentatively estimated based on the agreement of fits on different color planes. Moreover, it appears M 13 is best fit with a 16 Gyr isochrone, while NGC 288 tends to favor a slightly younger age of 14 Gyr. The only possible problem worth noting is the rather large color shifts required to match to data for NGC 288 for the majority of colors presented in Figure 4.12. While the discrepancies in the $(u-y)$ plane for both NGC 288 and M 13 could be attributed to the same reason mentioned above for M 92, it is rather surprising such large shifts in

color are needed for the $(v-b)$ and $(v-y)$ colors. One possible explanation lies in the fact that NGC 288 could be slightly more metal-rich than quoted by ZW. Indeed, fits to the broadband CMDs for NGC 288 (see, e.g., Figure 28b of VandenBerg 2000b) indicate that a $[\mathrm{Fe/H}] = -1.31$ isochrone can provide an adequate fit to the cluster fiducial if a SFD reddening is assumed.

Turning to Figures 4.13 and 4.14 for the comparisons of *uvby* and broadband CMDs, it is quite evident that the results yield excellent consistency between to the fits for both clusters. However, it is not clear why such a large, negative color shift is required to match the VI fiducial for M 13.

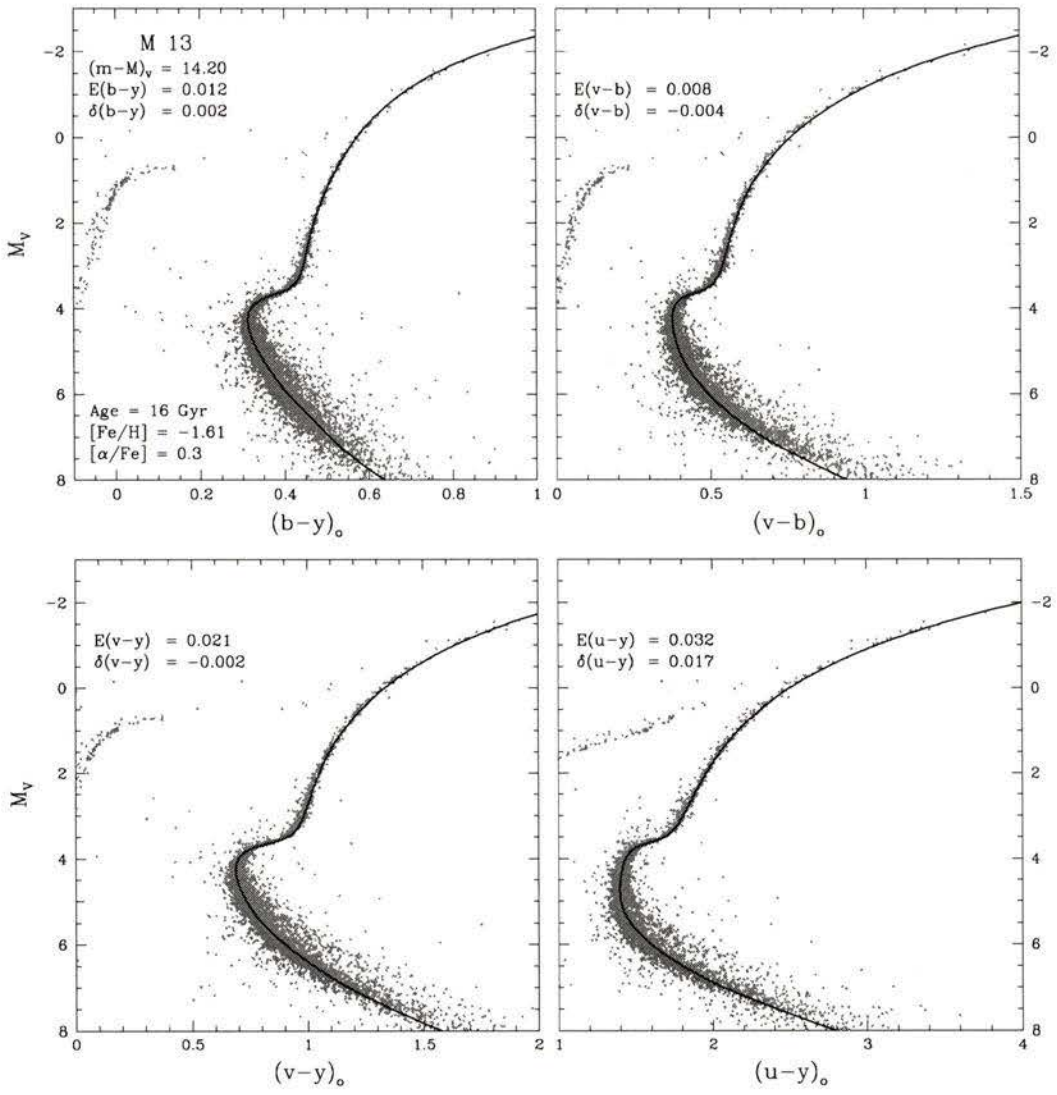

Figure 4.11: Fits of a 16 Gyr isochrone for the indicated parameters to the various *uvby* CMDs of M 13.

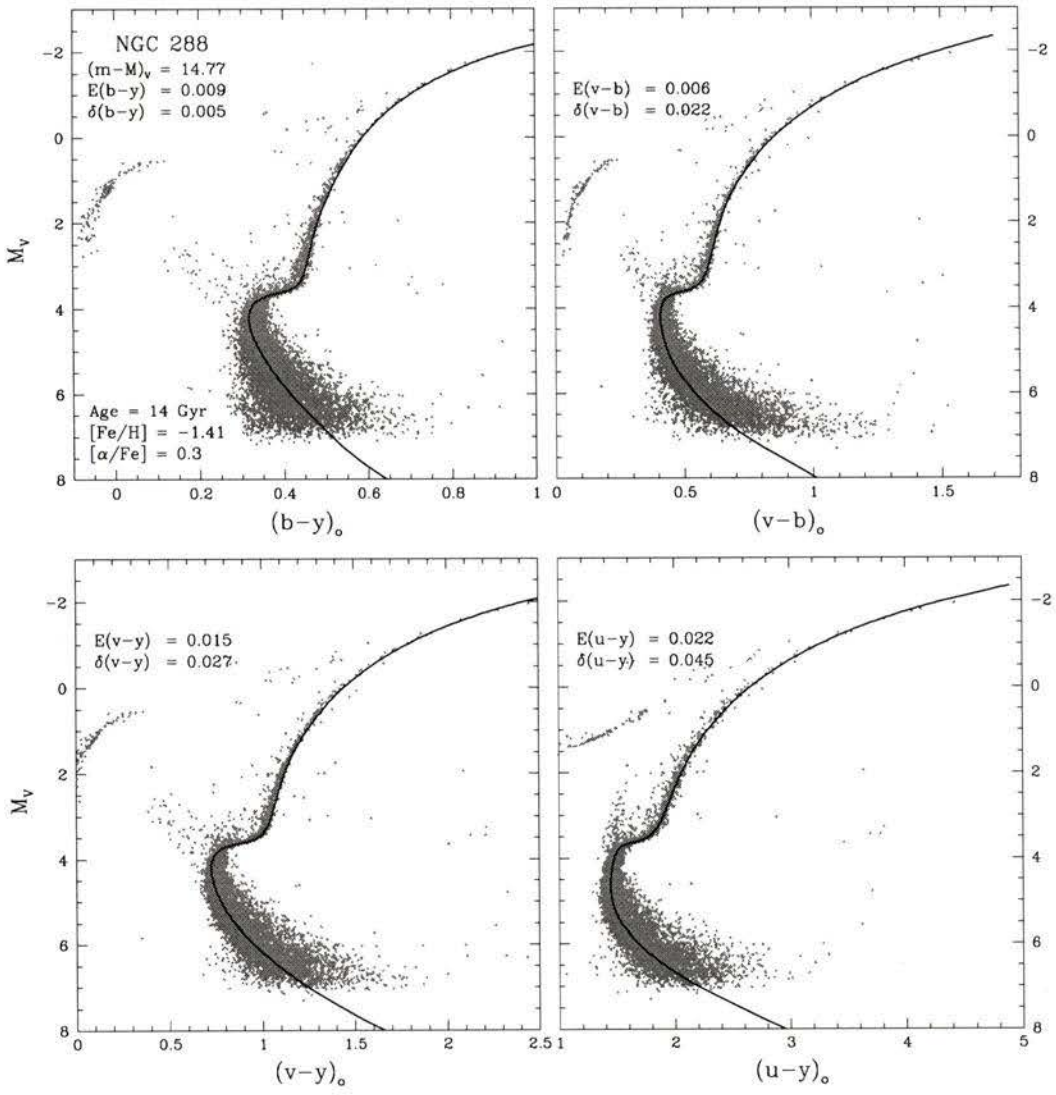

Figure 4.12: Fits of a 14 Gyr isochrone for the indicated parameters to the various *uvby* CMDs of NGC 288.

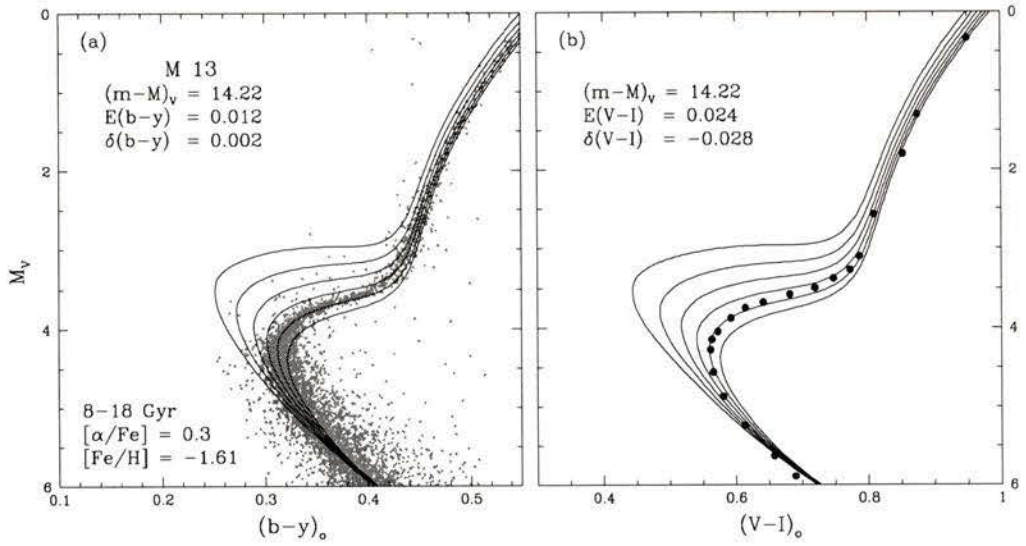

Figure 4.13: Fits of isochrones to the indicated Strömgren and broadband CMDs for M 13. The VI fiducial sequence is taken from Johnson & Bolte (1998).

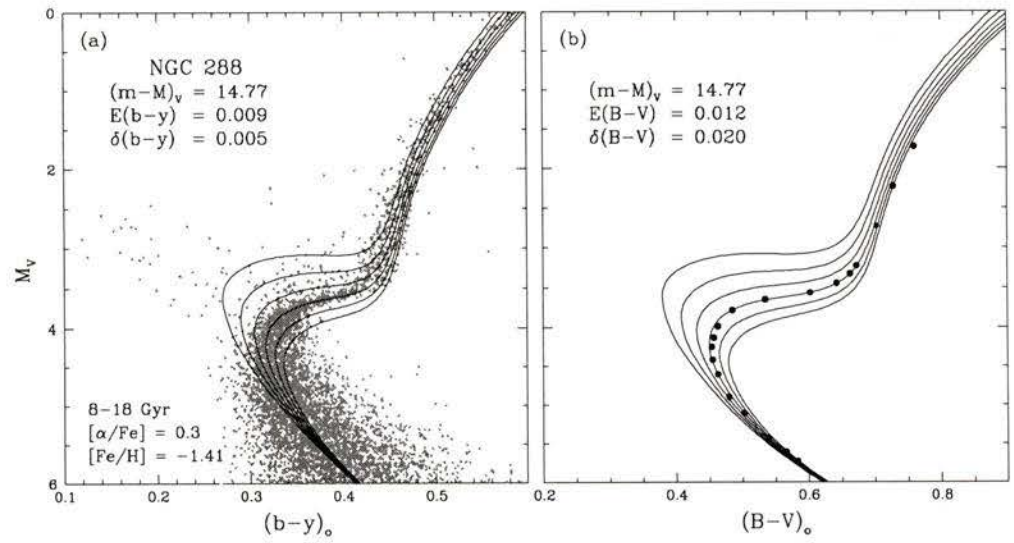

Figure 4.14: Fits of isochrones to the indicated Strömgren and broadband CMDs for NGC 288. The BV fiducial sequence is derived from the photometry of Bolte (1992).

4.2.3 NGC 104

The final GC to be investigated is NGC 104 (47 Tucanae), and with current metallicity estimates for the cluster hovering around [Fe/H]≈ -0.7, it is one of the most metal-rich GCs known. Figure 4.15 further indicates that it is also the youngest among the GCs discussed here with an age of 13 Gyr. While this age as well as the adopted distance modulus differ by ≈ 1 Gyr and ≈ 0.1 mag, respectively, from those adopted by VandenBerg (2000), they do agree quite well with the recent values of $(m-M)_V = 13.27 \pm 0.14$ and 13 ± 2.5 Gyr obtained from comparisons of white dwarfs within the cluster to their counterparts in the field (Zoccali et al. 2001). One other point concerning the $(u-y)$ fit in Figure 4.15 should be noted, specifically, the rather large color shift which has plagued the same colors for previous clusters is not needed here for NGC 104. Why a moderately large color shift was needed before and not now is not immediately clear.

For the purposes of comparing Strömgren and broadband data fits, Figure 4.16 employs the BV and VI data of Kaluzny et al. (1997, 1998). However, one immediate problem is apparent is panels (b) and (c) of the figure. In particular, rather large color offsets are required to fit the broadband data. The explanation for this discrepancy could lie in the fact 47 Tuc might be slightly more metal-poor than the ZW estimate used here. Indeed, VandenBerg (2000) has obtained more agreeable fits using the [Fe/H] $= -0.83$ grid of isochrones to the composite BV fiducial of Hesser et al. (1987).

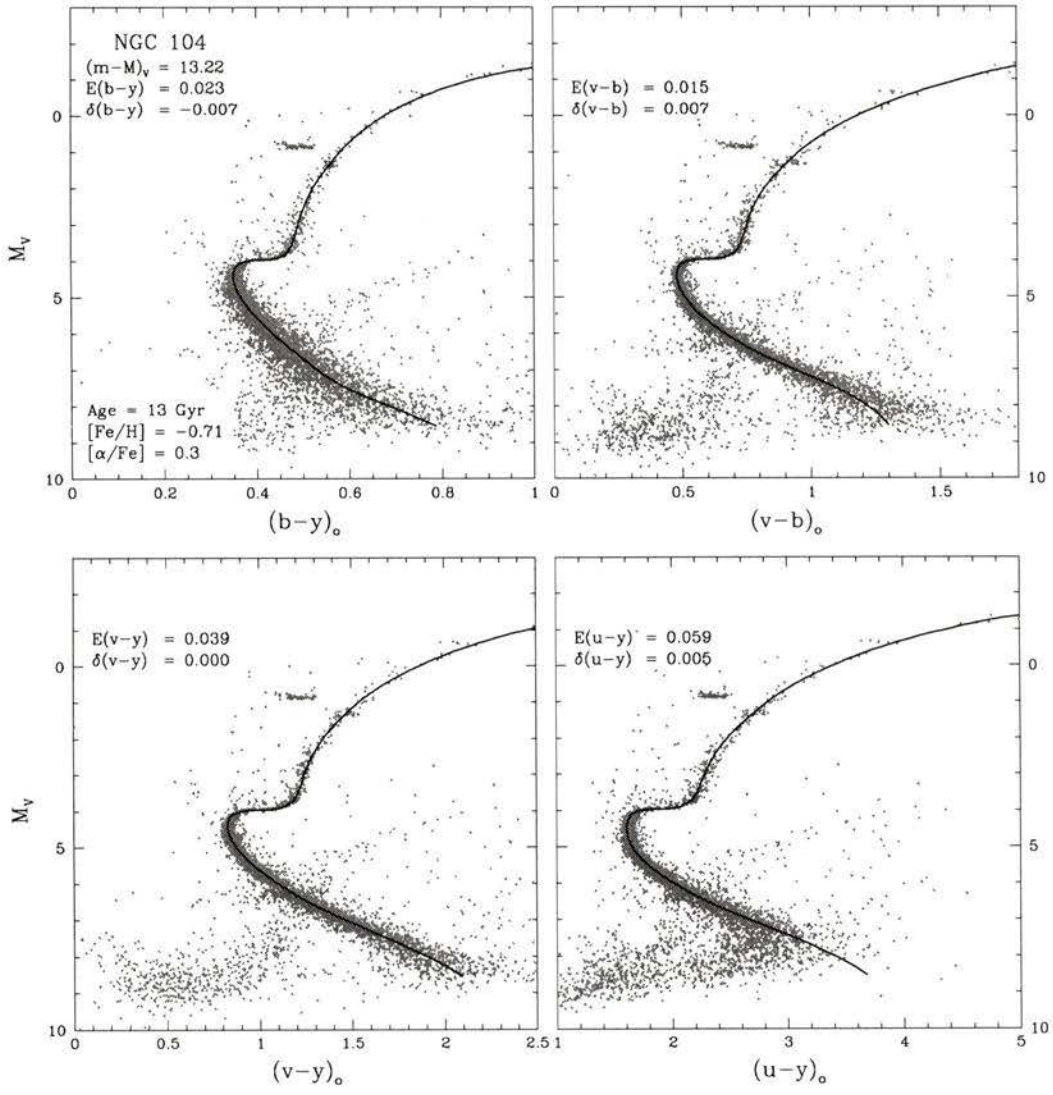

Figure 4.15: Fits of a 13 Gyr isochrone for the indicated parameters to the various *uvby* CMDs of NGC 104.

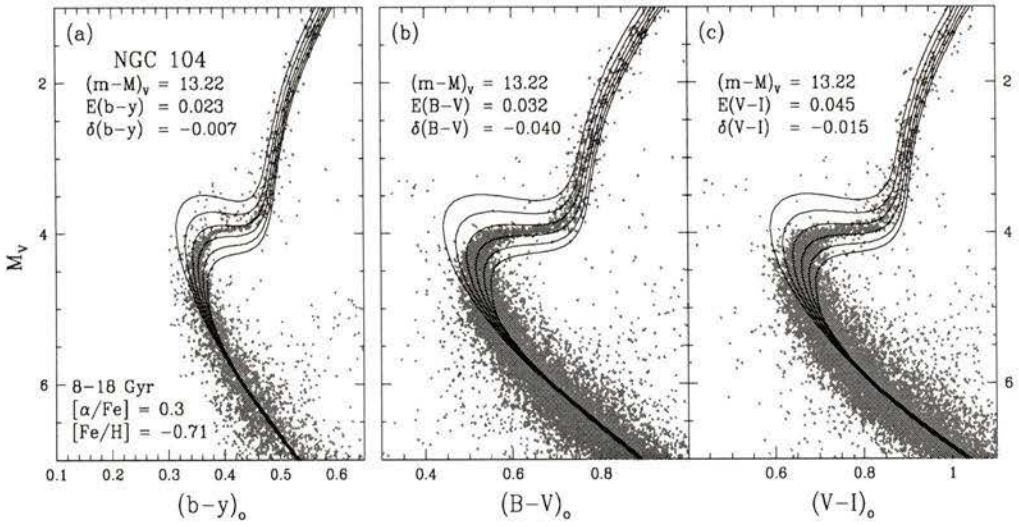

Figure 4.16: Fits of isochrones to the indicated Strömgren and broadband CMDs for NGC 104. The BV and VI photometric data are taken from the studies of Kaluzny et al. (1997, 1998).

Chapter 5

Conclusions

Owing to the superb quality of the isochrone fits to the various open and globular cluster *uvby* CMDs presented in the previous chapter, it is quite apparent that the color calibrations derived from the field star sample have adequately placed the synthetic Strömgren colors onto the same system as the observational data. Indeed, additional tests involving *uvby* photometry for other clusters from the observational surveys of F. Grundahl (e.g. M 3, NGC 362, NGC 1851, M 71, and NGC 6791), which are not discussed in the present work, likewise yield the same excellent agreement between the appropriate isochrone and cluster CMDs from the main sequence through the red giant branch. Equally important is the fact that these newly calibrated Strömgren C-T relations are able to provide similar interpretations of the *uvby* photometric data when compared to isochrone fits involving the same clusters observed in the broadband ($UBVRI$) system.

Although this work has attempted to assess the validity of the Strömgren colors by testing them against both the field stars used to calibrate them as well as a number of star clusters with new and accurate *uvby* photometry, this type of study could undoubtedly benefit from additional observational data, particularly for clusters. Apart from the cluster survey of F. Grundahl, a variety of very recent works

have reported precise CCD *uvby* photometry for other clusters such as NGC 6397, M 22, M 55, NGC 5139, and IC 4651 (see Anthony-Twarog & Twarog 2000, Richter et al. 1999, Hilker & Richtler 2000, and Meibom 2000) and have greatly increased the amount of *uvby* data currently available. Regardless of this fact, however, the quantity of cluster data in the broadband system still far outweighs that in the Strömgren system. More *uvby* data would in turn mean more opportunities to constrain the accuracy of the calibrated colors and to investigate consistencies between the two photometric systems in interpreting clusters CMDs.

While currently available synthetic Strömgren C-T relations are reasonably successful in reproducing the colors of warmer stars (i.e. $T_{eff} > 8000K$; see discussions by Relyea & Kurucz 1978 and Castelli 1991), it is nevertheless important to also test the colors outside of the temperature range considered here. One feasible way of doing this involves transforming Zero Age Horizontal Branch (ZAHB) models to the observations and comparing them to the actual distribution of horizontal branch stars in a cluster CMD. Although the results of such investigations are not discussed in the present work, the warmer colors do in fact yield good fits of the ZAHB models to horizontal branches of the same GC sample used in the last chapter.

Apart from providing the reliable means by which to transform theoretical stellar models to the observational plane so they may be readily compared to *uvby* photometric data, there are a number of other areas where these new Strömgren C-T relations can prove useful in cluster studies, some of which are discussed briefly in the following:

- *Distance independent GC ages.* The newly calibrated C-T relations can be used to derive more reliable, distance-independent ages for globular clusters using techniques akin to those described in Grundahl et al. (2000a) for M 92. This would prove most helpful not only in resolving the distance scale controversy briefly discussed in the previous chapter, but also in constraining the age of the

oldest globular clusters which can ultimately place a lower limit on the age of the universe.

- *Cluster $[Fe/H]$ estimates from GC red giant stars.* A number of studies have demonstrated the usefulness of Strömgren m_1 index in providing independent [Fe/H] estimates for red giant stars in globular clusters. However, a recent examination by Anthony-Twarog & Twarog (2000) illustrates that the isometallicity relations for red giants determined from the previous work of Anthony-Twarog & Twarog (1994), Grebel & Richtler (1992), and Hilker (2000) are not in good agreement with each other despite being derived from comparable samples of metal poor stars. Here, the Strömgren C-T relations offer the ability to provide a new and accurate metallicity calibration for GC red giants based on the fact these colors have already been calibrated against a sample of metal poor field giants stars and have also proven to provide excellent agreement to the red giant branches of globular clusters covering a wide range in metallicity.

- *Abundance variations in GC giant stars.* From the analysis of Grundahl et al. (1998, 2000b) it is apparent that the significant spread in c_1 colors seen among GC red giant stars could be due to variations in the abundances of C, N, O, Mg, and Al perhaps caused by deep mixing during post main sequence evolution. While the current set of C-T relations are computed and calibrated on the assumption of scaled solar abundances with only a +0.3 dex enhancements to the α process elements, it is unlikely they would be unable to adequately reproduce the colors of RGB stars with significant elemental anomalies. However, a new set of synthetic colors for cool RGB stars could be calculated on the basis of model spectra which account for various mixes and abundance differences among certain elements and then placed onto the observed system using the calibrations derived in this work. The resulting colors could likely provide a means by which to photometrically constrain which elements and to what

extend their abundances have been enhanced in RGB stars as well as isolate certain stars which might deserve further detailed spectroscopic analysis.

In addition to these possibilities, the new Strömgren C-T relations can also prove useful in applications to stars outside of the cluster environment. For instance, the calibrated grids would allow accurate estimates for a star's temperature, gravity, and metallicity to be obtained solely from the knowledge of its colors indices. By combining such information for a large sample of field stars with the parallax and proper motion data from the *Hipparcos* could prove useful in investigating the spatial distribution and kinematics of stars with different metallicities in the solar neighborhood.

In closing, the promise that the Strömgren photometric system holds for increasing our understanding of stellar populations is undeniable. From its ability to provide precise estimates of T_{eff}, $\log g$, and [Fe/H] on a star-by-star basis, to its numerous applications to cluster studies, *uvby* photometry has proven itself as a powerful and accurate tool for observers and theorists. Given these facts, as well as the discussions and results presented here, it is anticipated that the Strömgren photometric system will gain increased recognition as a viable alternative to the $UBVRI$ system for the examination of individual stars and stellar populations.

Appendix A

The Field Star Sample

The following pages list the field stars used to calibrate the synthetic Strömgren colors. The final column denotes the source of the $T_{\rm eff}$, $\log g$, and [Fe/H] information: 1=Houdashelt et al (2000b), 2=Alonso et al. (1996a), and 3=Alonso et al. (1999). The *uvby* photometry for each star has been taken from the catalog of Hauck & Mermilliod (1998) while the parallaxes and broadband photometry are from the *Hipparcos* catalog of Perryman et al. (1997). Photometric colors have been dereddened by the $E(b-y)$ values listed in the table. Histograms showing the number distribution of the field stars in terms of effective temperature and metallicity are shown in Figure A.1.

Table A.1:

Star ID	HIC	T_{eff}	log g	[Fe/H]	E$(b-y)$	π	V	M_V	$(B-V)_o$	$(b-y)_o$	m_o	c_o	Source
HD 224817	80	5859	4.50	-0.59	0.000	15.59	8.407	4.364	0.566	0.372	0.143	0.309	2
HD 20	434	5351	2.00	-1.66	0.006	1.40	9.053	-0.229	0.684	0.428	0.094	0.473	3
HD 693	910	6148	4.14	-0.45	0.002	52.94	4.907	3.509	0.484	0.326	0.131	0.404	1
SAO 166160	1298	5265	2.00	-1.12	0.011	0.86	9.589	-0.748	0.695	0.449	0.133	0.461	3
G 030-056	1301	5784	4.50	-0.85	0.000	8.67	9.747	4.430	0.569	0.383	0.135	0.284	2
HD 1343	1402	7101	4.00	0.00	0.000	20.47	6.457	3.016	0.386	0.259	0.142	0.509	2
HD 1368	1437	5834	4.50	-0.91	0.000	16.24	8.868	4.933	0.542	0.364	0.141	0.292	2
HD 1461	1499	5683	4.00	0.20	0.000	42.67	6.468	4.621	0.674	0.420	0.240	0.362	2
G 130-065	1785	6126	4.50	-2.18	0.000	1.37	9.260	-0.056	1.250	0.331	0.056	0.260	2
HD 1835	1803	5735	4.50	0.14	0.000	49.05	6.390	4.843	0.659	0.409	0.220	0.348	3
HD 2151	2021	5860	4.15	-0.20	0.001	133.78	2.813	3.452	0.616	0.386	0.196	0.358	1
HD 2628	2355	6979	3.00	0.00	0.000	17.62	5.200	1.430	0.271	0.169	0.166	0.870	3
HD 2665	2413	4990	2.40	-1.92	0.048	2.11	7.739	-0.659	0.682	0.501	0.095	0.349	3
HD 2925	2573	4792	2.50	-0.50	0.000	7.32	6.857	1.163	0.921	0.577	0.276	0.475	3
HD 3008	2618	4047	1.50	-1.85	0.011	2.88	9.455	1.787	1.254	0.840	0.300	0.725	3
HD 3179	2727	5233	2.00	-0.92	0.007	2.96	9.766	2.106	0.725	0.445	0.145	0.451	3
HD 3443	2941	5255	4.00	-0.16	0.000	64.38	5.580	4.614	0.715	0.435	0.254	0.287	2
HD 3567	3026	5858	4.50	-1.34	0.000	9.57	9.250	4.155	0.465	0.328	0.089	0.330	2
HD 3546	3031	4914	2.40	-0.70	0.000	19.34	4.353	0.772	0.871	0.553	0.241	0.453	3
HD 3628	3086	5651	4.00	0.00	0.000	21.79	7.338	4.031	0.633	0.402	0.191	0.338	2
BD+71 0031	3430	6026	4.50	-1.91	0.000	6.04	10.200	4.105	0.401	0.309	0.040	0.360	2
HD 4307	3559	5753	4.00	-0.13	0.000	31.39	6.154	3.634	0.603	0.388	0.176	0.349	2
G 033-009	3564	5500	5.00	-1.35	0.022	2.07	10.584	2.180	0.574	0.389	0.110	0.278	2
HD 4614	3821	5839	4.40	0.00	0.001	167.99	3.400	4.586	0.586	0.371	0.185	0.275	1
HD 4744	3884	4553	2.00	-1.28	0.033	5.91	7.619	1.458	1.019	0.615	0.308	0.455	3
HD 5015	4151	6042	4.09	-0.04	0.003	53.85	4.797	3.456	0.536	0.346	0.175	0.422	1
BD-20 0170	4458	5091	2.00	-1.90	0.014	1.05	10.287	0.356	0.734	0.481	0.131	0.429	3
HD 5916	4771	4944	2.00	-0.80	0.022	6.50	6.862	0.925	0.867	0.543	0.268	0.372	3
HD 6461	5104	5068	2.30	-0.93	0.020	1.89	7.661	-0.968	0.757	0.480	0.206	0.429	3
HD 6497	5240	4412	2.40	-0.40	0.000	10.26	6.412	1.466	1.188	0.732	0.548	0.419	3
HD 6582	5336	5315	4.00	-0.67	0.000	132.40	5.154	5.779	0.704	0.437	0.205	0.213	2
HD 6755	5445	5008	4.00	-1.71	0.000	7.74	7.731	2.164	0.701	0.487	0.108	0.306	2
HD 6833	5458	4402	1.50	-0.91	0.048	4.35	6.765	-0.058	1.075	0.705	0.311	0.476	3
HD 6961	5542	7787	2.00	0.00	0.000	23.73	4.325	1.216	0.170	0.088	0.213	0.998	3
HD 7424	5775	5625	4.00	-0.54	0.015	8.64	10.122	4.783	0.650	0.391	0.167	0.303	3
HD 8724	6710	4535	1.50	-1.60	0.029	3.04	8.328	0.714	0.920	0.657	0.159	0.440	3
HD 9051	6894	4836	2.00	-1.50	0.007	0.58	8.944	-2.253	0.810	0.532	0.161	0.386	3
HD 9562	7276	5783	3.84	0.09	0.000	33.71	5.760	3.389	0.639	0.399	0.209	0.405	3
HD 9826	7513	6154	4.22	0.00	0.002	74.25	4.093	3.453	0.533	0.344	0.177	0.414	1
HD 9927	7607	4425	2.10	0.12	0.012	18.76	3.570	-0.044	1.259	0.753	0.657	0.399	1
HD 10380	7884	4114	1.50	-0.30	0.000	8.86	4.433	-0.813	1.347	0.830	0.672	0.404	3
HD 10307	7918	5856	4.33	-0.11	0.001	79.09	4.961	4.451	0.616	0.388	0.199	0.348	1
HD 10476	7981	5172	4.00	-0.20	0.000	133.91	5.241	5.874	0.836	0.492	0.367	0.296	2
HD 10700	8102	5388	4.00	-0.46	0.000	274.17	3.496	5.680	0.727	0.443	0.253	0.244	2
G 245-032	8314	6231	4.46	-1.65	0.000	6.46	9.950	3.991	0.417	0.309	0.087	0.263	2
HD 12929	9884	4499	2.50	-0.25	0.006	49.48	2.010	0.482	1.143	0.692	0.531	0.386	1
G 072-060	9982	5638	4.50	-1.22	0.000	3.84	10.296	3.202	0.580	0.385	0.111	0.276	2
HD 13783	10629	5501	4.00	-0.55	0.000	25.82	8.311	5.360	0.674	0.420	0.200	0.241	2
HD 13974	10644	5591	4.00	-0.33	0.000	92.20	4.863	4.664	0.607	0.390	0.186	0.259	2
HD 14214	10723	5906	4.05	-0.01	0.000	40.04	5.601	3.612	0.588	0.370	0.187	0.405	3
BD-22 0395	11023	4815	1.75	-2.00	0.000	4.25	10.532	3.662	0.801	0.553	0.110	0.483	3
HD 15596	11698	4815	2.10	-0.43	0.018	10.40	6.234	1.295	0.883	0.562	0.259	0.429	3
BD-17 0484	11729	6234	4.50	-2.03	0.007	5.41	10.491	4.126	0.443	0.318	0.069	0.331	2
HD 15798	11783	6409	3.99	-0.19	0.003	38.73	4.783	2.680	0.450	0.295	0.138	0.482	1
HD 16031	11952	6114	4.00	-2.09	0.000	8.67	9.787	4.460	0.437	0.323	0.069	0.302	2
G 073-067	11983	4756	4.50	-0.41	0.000	24.80	9.788	6.782	0.906	0.534	0.437	0.233	2
G 075-031	12294	5881	4.50	-1.21	0.000	6.67	10.521	4.631	0.474	0.333	0.093	0.330	2
G 076-021	12529	5931	4.50	-2.15	0.000	5.22	10.166	3.758	0.513	0.346	0.059	0.243	2
G 004-036	12710	6100	4.50	-1.69	0.037	4.16	11.451	4.565	0.476	0.335	0.063	0.224	2
HD 16895	12777	6373	4.33	0.16	0.003	89.03	4.105	3.848	0.510	0.322	0.161	0.391	1
G 004-037	12807	6337	4.50	-3.31	0.051	8.64	11.422	6.093	0.400	0.312	0.049	0.295	2

Star ID	HIC	T_{eff}	log g	[Fe/H]	E$(b-y)$	π	V	M_V	$(B-V)_o$	$(b-y)_o$	m_o	c_o	Source
HD 17206	12843	6350	4.35	0.14	0.002	71.56	4.500	3.743	0.478	0.326	0.168	0.405	1
BD-10 0548	12978	4902	2.00	-1.07	0.000	1.95	10.412	1.860	0.774	0.513	0.129	0.315	3
G 036-050	14259	5437	4.50	-1.90	0.037	9.39	12.044	6.883	0.606	0.411	0.111	0.132	2
HD 19445	14594	6050	4.25	-2.15	0.000	25.85	8.056	5.102	0.486	0.351	0.058	0.208	2
HD 19373	14632	5994	4.19	0.02	0.005	94.93	4.050	3.937	0.588	0.372	0.202	0.377	1
HD 19476	14668	4879	3.10	0.10	0.000	29.05	3.798	1.106	0.980	0.605	0.414	0.406	3
G 076-068	14992	4549	4.50	-0.63	0.000	15.89	9.832	5.856	0.940	0.552	0.369	0.226	2
G 005-035	15904	5641	4.50	-1.70	0.000	12.65	10.755	6.270	0.571	0.395	0.087	0.158	2
G 005-036	16072	5968	4.50	-1.66	0.059	6.99	10.795	5.032	0.464	0.336	0.089	0.264	2
HD 21543	16169	5568	4.50	-0.55	0.000	21.98	8.229	4.940	0.619	0.400	0.164	0.284	2
G 038-001	16209	4051	5.00	0.00	0.000	35.30	11.060	8.839	1.314	0.822	0.615	-0.038	2
HD 21581	16214	4870	2.00	-1.70	0.033	4.27	8.721	1.852	0.741	0.527	0.140	0.333	3
G 246-038	16404	5279	4.50	-2.94	0.000	17.58	9.939	6.135	0.667	0.451	0.089	0.122	2
HD 22049	16537	5156	4.61	0.05	0.001	310.75	3.718	6.182	0.880	0.503	0.430	0.263	1
HD 22484	16852	5963	4.18	-0.12	0.004	72.89	4.291	3.603	0.569	0.363	0.175	0.375	1
HD 22879	17147	5798	4.00	-0.71	0.000	41.07	6.693	4.748	0.554	0.365	0.126	0.272	2
HD 22918	17183	4781	2.00	0.11	0.000	22.28	6.955	3.700	0.954	0.582	0.334	0.494	3
HD 23249	17378	4976	3.95	0.05	0.003	110.58	3.537	3.738	0.911	0.555	0.373	0.392	1
HD 23841	17792	4273	1.30	-0.90	0.040	4.61	6.686	-0.001	1.145	0.727	0.463	0.490	3
HD 24289	18082	5866	4.50	-2.07	0.037	4.91	9.977	3.425	0.482	0.351	0.062	0.280	2
HD 25329	18915	4842	4.50	-1.64	0.029	54.14	8.490	7.178	0.823	0.500	0.314	0.136	2
HD 25532	18995	5396	2.00	-1.23	0.051	4.39	8.210	1.412	0.587	0.431	0.110	0.498	3
HD 26297	19378	4322	1.20	-1.64	0.001	1.28	7.484	-2.004	1.087	0.736	0.239	0.609	3
BD+06 0648	19701	4186	0.80	-1.94	0.073	2.58	9.074	1.148	1.182	0.790	0.226	0.577	3
HD 26846	19777	4577	2.70	0.20	0.015	15.80	4.871	0.863	1.136	0.691	0.582	0.405	3
HD 26767	19786	5749	4.50	0.10	0.000	22.19	8.036	4.781	0.640	0.406	0.210	0.354	2
HD 284248	19797	6034	4.50	-1.61	0.000	12.84	9.234	4.773	0.362	0.322	0.071	0.292	2
HD 26965	19849	5114	4.65	-0.21	0.001	198.24	4.415	5.916	0.818	0.483	0.333	0.301	1
HD 26911	19877	6736	4.00	0.10	0.000	22.51	6.305	3.072	0.400	0.259	0.176	0.525	2
HD 27561	20357	6681	4.00	0.10	0.000	19.46	6.602	3.046	0.412	0.270	0.162	0.480	2
HD 27848	20567	6498	4.00	0.10	0.000	18.74	6.973	3.324	0.450	0.294	0.166	0.450	2
HD 28305	20889	4896	2.50	0.16	0.080	21.04	3.532	0.145	0.905	0.535	0.480	0.396	1
HD 28462	20978	5180	4.50	0.10	0.000	24.71	9.075	6.044	0.865	0.504	0.387	0.317	2
HD 28635	21112	6091	4.00	0.10	0.000	19.46	7.768	4.226	0.540	0.350	0.183	0.372	2
HD 28992	21317	5816	4.50	0.10	0.000	23.19	7.916	4.727	0.631	0.397	0.203	0.347	2
HD 29139	21421	3943	1.25	-0.10	0.022	50.09	0.900	-0.631	1.508	0.933	0.822	0.368	1
HD 29310	21543	5722	2.00	0.10	0.007	23.54	7.542	4.389	0.587	0.378	0.213	0.339	3
HD 29574	21648	4020	1.50	-1.79	0.036	0.66	8.370	-2.572	1.255	0.917	0.238	0.738	3
HD 30562	22336	5822	4.00	0.13	0.000	37.73	5.772	3.653	0.631	0.397	0.206	0.420	2
HD 30652	22449	6373	4.35	0.04	0.002	124.60	3.184	3.668	0.481	0.296	0.164	0.414	1
G 084-029	23344	6110	4.50	-2.01	0.000	7.80	9.796	4.250	0.413	0.312	0.063	0.365	2
HD 277559	23688	6226	4.50	-1.05	0.000	8.32	9.640	4.251	0.441	0.311	0.109	0.317	2
HD 241253	24030	5853	4.50	-1.19	0.015	10.29	9.723	4.772	0.500	0.342	0.113	0.237	2
HD 34334	24727	4193	2.15	-0.35	0.000	13.92	4.542	0.258	1.252	0.785	0.540	0.377	3
HD 34411	24813	5819	4.19	0.00	0.001	79.08	4.689	4.180	0.628	0.389	0.206	0.364	1
HD 35620	25541	4185	1.60	-0.18	0.015	8.14	5.068	-0.367	1.380	0.855	0.775	0.235	3
HD 36395	25878	3737	5.00	-1.50	0.000	175.72	7.928	9.194	1.474	0.917	0.531	0.167	2
HD 37160	26366	4719	2.17	-0.54	0.011	28.10	4.088	1.334	0.936	0.580	0.318	0.416	1
HD 37394	26779	5185	4.00	-0.20	0.000	81.69	6.200	5.771	0.840	0.499	0.364	0.315	2
HD 38393	27072	6259	4.22	-0.16	0.001	111.49	3.596	3.826	0.480	0.313	0.162	0.392	1
HD 38751	27468	4833	2.50	-0.06	0.022	6.25	4.874	-1.141	0.991	0.618	0.431	0.341	3
HD 39425	27628	4519	2.30	0.00	0.003	37.94	3.120	1.015	1.142	0.698	0.596	0.384	1
HD 39364	27654	4599	2.75	-0.62	0.000	29.05	3.797	1.076	0.984	0.610	0.310	0.440	3
HD 39003	27673	4604	2.25	-0.10	0.000	15.17	3.970	-0.125	1.132	0.692	0.513	0.351	3
HD 39587	27913	5839	4.41	-0.09	0.003	115.43	4.396	4.702	0.590	0.374	0.194	0.311	1
HD 39853	27938	3881	0.80	-0.43	0.037	4.37	5.610	-1.178	1.473	0.924	0.698	0.515	3
HD 40136	28103	7013	4.00	0.06	0.000	66.47	3.700	2.823	0.337	0.218	0.162	0.622	2
HD 250792	28671	5319	4.50	-1.26	0.000	14.86	9.346	5.140	0.646	0.401	0.166	0.143	2
G 102-047	28887	5353	4.50	-1.74	0.037	1.80	10.327	1.586	0.626	0.415	0.121	0.229	2
HD 42581	29295	3814	5.00	0.00	0.000	173.19	8.129	9.343	1.487	0.918	0.521	0.177	2
G 098-056	29662	5376	4.50	-1.32	0.000	5.16	11.316	4.903	0.654	0.421	0.150	0.171	2
HD 43039	29696	4664	2.50	-0.31	0.000	19.31	4.327	0.749	1.021	0.631	0.373	0.442	3
G 098-058	29759	5510	4.50	-1.86	0.000	5.78	8.905	2.730	0.611	0.432	0.073	0.222	2

Star ID	HIC	T_{eff}	log g	[Fe/H]	E$(b-y)$	π	V	M_V	$(B-V)_o$	$(b-y)_o$	m_o	c_o	Source
HD 44007	29992	4851	2.15	-1.63	0.037	5.17	8.060	1.617	0.779	0.522	0.150	0.356	3
G 101-033	30018	5284	4.50	-0.37	0.000	16.96	10.197	6.367	0.737	0.457	0.259	0.263	2
G 101-034	30098	5289	4.50	-1.83	0.073	0.68	10.730	-0.097	0.646	0.433	0.148	0.211	2
HD 45282	30668	5264	3.30	-1.40	0.015	7.34	8.028	2.328	0.683	0.436	0.113	0.274	3
HD 291763	31085	4855	4.50	-0.36	0.000	18.12	10.042	6.351	0.849	0.506	0.373	0.267	2
G 105-050	31671	4837	4.50	-1.59	0.007	11.39	11.120	6.433	0.743	0.490	0.226	0.154	2
G 192-043	32567	6085	4.50	-1.56	0.000	3.98	10.307	3.319	0.444	0.322	0.078	0.304	2
HD 49933	32851	6679	4.50	-0.88	0.022	33.45	5.779	3.402	0.366	0.248	0.135	0.455	2
HD 50778	33160	3980	1.25	-0.03	0.030	12.94	4.063	-0.360	1.377	0.848	0.720	0.425	1
HD 50420	33269	7412	3.40	0.30	0.022	3.75	6.000	-0.970	0.284	0.199	0.150	1.018	3
HD 50522	33449	5092	3.10	0.05	0.000	19.14	4.351	0.760	0.850	0.529	0.334	0.381	3
G 089-014	35756	5871	4.50	-1.85	0.000	5.87	10.397	4.233	0.477	0.347	0.063	0.316	2
G 088-027	36174	6015	4.50	-2.21	0.000	6.19	10.715	4.688	0.440	0.336	0.063	0.311	2
HD 58946	36366	6957	4.17	-0.31	0.002	54.06	4.200	2.824	0.317	0.213	0.156	0.614	1
G 090-003	36430	5786	4.50	-1.99	0.029	1.20	10.397	0.806	0.500	0.344	0.054	0.290	2
G 088-032	36513	6208	4.50	-2.59	0.000	3.07	10.785	3.236	0.350	0.309	0.051	0.357	2
HD 59984	36640	5928	4.50	-0.99	0.000	33.40	5.930	3.519	0.540	0.356	0.123	0.336	2
HD 59881	36641	7447	3.10	0.19	0.029	4.14	5.250	-1.675	0.190	0.099	0.182	1.191	3
HD 60298	36874	5781	4.00	-0.08	0.000	25.42	7.377	4.396	0.642	0.401	0.198	0.338	2
G 087-047	36936	5188	4.50	-0.88	0.000	9.97	10.308	5.303	0.660	0.427	0.173	0.233	2
HD 61064	37088	6358	3.21	0.44	0.000	16.11	5.138	1.175	0.442	0.284	0.178	0.643	3
HD 61421	37279	6601	4.08	0.02	0.000	285.93	0.400	2.681	0.432	0.272	0.167	0.532	1
G 112-036	37335	5082	4.50	-0.88	0.044	3.53	9.229	1.969	0.760	0.468	0.236	0.268	2
G 112-043	37671	6065	4.50	-1.61	0.007	3.08	10.201	2.833	0.526	0.332	0.075	0.337	2
HD 62345	37740	5001	2.60	-0.04	0.000	22.73	3.570	0.353	0.932	0.571	0.379	0.395	3
HD 62509	37826	4896	2.80	-0.01	0.001	96.74	1.100	1.088	0.990	0.610	0.427	0.420	1
HD 62721	37908	3961	1.67	-0.27	0.000	9.55	4.857	-0.210	1.425	0.896	0.727	0.460	3
HD 63336	38048	6440	4.00	0.00	0.000	33.06	5.476	3.077	0.478	0.313	0.162	0.412	2
HD 64096	38382	5727	4.00	0.00	0.000	59.98	5.152	4.050	0.600	0.380	0.196	0.316	2
HD 64090	38541	5441	4.50	-1.82	0.000	35.29	8.282	6.008	0.621	0.430	0.109	0.116	2
HD 64606	38625	5134	4.50	-0.65	0.000	52.01	7.427	6.010	0.739	0.452	0.219	0.210	2
HD 65583	39157	5242	4.50	-0.60	0.000	59.52	6.975	5.843	0.716	0.450	0.232	0.231	2
HD 67228	39780	5781	4.00	0.14	0.000	42.86	5.293	3.460	0.642	0.407	0.206	0.404	2
G 251-054	40068	5308	5.00	-1.73	0.000	3.91	10.010	2.971	0.564	0.402	0.082	0.234	2
HD 68017	40118	5512	4.00	-0.42	0.000	46.05	6.791	5.096	0.679	0.419	0.199	0.269	2
HD 69267	40526	4031	1.35	-0.21	0.004	11.23	3.518	-1.218	1.475	0.909	0.762	0.368	1
HD 233511	40778	5967	4.50	-1.64	0.000	10.36	9.716	4.807	0.484	0.339	0.071	0.258	2
HD 69897	40843	6242	4.00	-0.50	0.000	55.17	5.150	3.839	0.487	0.315	0.149	0.384	2
HD 70958	41211	6275	4.00	-0.41	0.000	36.75	5.610	3.436	0.478	0.313	0.139	0.396	2
G 051-010	41269	4579	4.50	-0.04	0.037	24.18	10.030	7.017	0.971	0.551	0.550	0.215	2
G 113-040	41661	4740	4.50	-1.13	0.029	11.03	11.919	7.153	0.880	0.520	0.397	0.153	2
HD 71369	41704	5176	2.60	0.03	0.015	17.76	3.400	-0.403	0.836	0.507	0.313	0.419	1
HD 72324	41940	4764	2.10	0.03	0.000	7.75	6.349	0.797	1.032	0.633	0.432	0.408	3
HD 73394	42550	4558	1.30	-1.40	0.000	2.18	7.700	-0.608	1.027	0.665	0.271	0.467	3
G 009-014	42563	5059	4.50	-0.76	0.044	18.88	10.170	6.560	0.740	0.436	0.329	0.245	2
HD 74000	42592	6224	4.50	-2.00	0.000	7.26	9.674	3.975	0.431	0.316	0.057	0.311	2
G 009-016	42887	6776	4.50	-1.31	0.000	6.59	9.322	3.414	0.316	0.234	0.101	0.506	2
HD 74739	43103	4911	2.15	-0.05	0.000	10.94	4.046	-0.775	1.007	0.612	0.395	0.414	3
G 009-031	43595	5569	4.50	-0.85	0.000	7.01	10.823	5.059	0.617	0.398	0.158	0.224	2
G 009-036	44033	5625	4.50	-1.18	0.000	5.99	11.934	5.827	0.584	0.381	0.124	0.195	2
HD 76932	44075	5727	4.50	-1.05	0.000	46.90	5.811	4.156	0.521	0.359	0.119	0.299	2
G 114-026	44124	5809	4.50	-1.47	0.000	12.37	9.653	5.122	0.481	0.349	0.076	0.250	2
G 115-049	44605	5950	4.50	-1.86	0.000	10.26	11.613	6.656	0.527	0.371	0.062	0.141	2
G 115-058	45069	6257	4.50	-1.65	0.000	5.17	12.112	5.667	0.490	0.325	0.074	0.341	2
HD 79452	45412	5050	2.20	-0.85	0.011	7.17	5.998	0.258	0.824	0.522	0.226	0.432	3
G 046-031	45554	5866	4.50	-0.79	0.000	3.79	10.867	3.763	0.523	0.350	0.122	0.274	2
HD 80218	45699	6087	4.00	-0.39	0.000	25.51	6.615	3.644	0.487	0.336	0.147	0.388	2
G 041-034	45990	5215	4.50	0.00	0.000	15.75	9.618	5.606	0.770	0.471	0.312	0.326	2
HD 81192	46155	4707	2.60	-0.64	0.007	8.17	6.545	1.091	0.923	0.587	0.265	0.452	3
HD 81809	46404	5611	4.00	-0.31	0.000	32.01	5.384	2.906	0.642	0.415	0.186	0.345	2
G 041-041	46516	6333	5.00	-2.89	0.000	1.04	11.141	1.235	0.390	0.313	0.049	0.383	2
HD 82590	46822	6005	2.75	-1.85	0.029	2.39	9.428	1.302	0.429	0.309	0.083	0.696	3
HD 82328	46853	6338	4.00	-0.01	0.000	74.15	3.200	2.521	0.475	0.314	0.153	0.463	2

Star ID	HIC	T_{eff}	log g	[Fe/H]	E$(b-y)$	π	V	M_V	$(B-V)_o$	$(b-y)_o$	m_o	c_o	Source
HD 82210	46977	5279	3.50	-0.08	0.024	30.89	4.561	1.989	0.748	0.466	0.258	0.349	1
HD 83212	47139	4455	1.25	-1.47	0.018	1.96	8.331	-0.209	0.990	0.676	0.244	0.569	3
HD 83769	47480	6678	4.00	-2.66	0.007	1.20	10.175	0.576	0.395	0.270	0.146	0.621	2
HD 233666	47599	5186	2.30	-1.40	0.004	1.22	9.330	-0.228	0.639	0.466	0.096	0.439	3
HD 84441	47908	5299	2.40	-0.13	0.007	13.01	2.989	-1.459	0.798	0.500	0.279	0.450	1
HD 84937	48152	6330	4.50	-2.49	0.000	12.44	8.342	3.804	0.399	0.302	0.054	0.369	2
BD+44 1910	48195	6063	4.50	-2.40	0.000	1.60	10.950	1.971	0.462	0.328	0.044	0.347	2
HD 85091	48215	5465	4.50	-0.60	0.000	23.35	7.614	4.421	0.610	0.400	0.170	0.295	2
HD 237846	48444	4985	1.90	-2.63	0.000	0.02	9.960	-8.565	0.835	0.515	0.030	0.360	3
HD 85503	48455	4500	2.40	0.16	0.000	24.52	3.871	0.828	1.222	0.760	0.640	0.385	3
HD 87140	49371	5157	3.01	-1.73	0.000	4.38	8.980	2.177	0.719	0.480	0.115	0.279	2
HD 88230	49908	3764	5.00	-1.00	0.000	205.22	6.550	8.161	1.326	0.790	0.741	0.032	2
HD 88725	50139	5669	4.50	-0.78	0.000	27.67	7.746	4.960	0.609	0.397	0.160	0.259	2
HD 88609	50173	4600	1.30	-2.60	0.000	0.63	8.609	-2.413	0.894	0.683	0.078	0.564	3
HD 89010	50319	5769	4.00	-0.03	0.000	32.94	5.960	3.539	0.655	0.418	0.209	0.374	2
HD 89254	50414	7040	3.76	0.09	0.000	17.86	5.254	1.509	0.336	0.190	0.199	0.812	3
HD 89449	50564	6374	4.21	0.09	0.003	47.24	4.792	3.152	0.448	0.296	0.167	0.461	1
HD 93529	52781	4825	2.00	-1.70	0.048	3.70	9.305	2.141	0.736	0.535	0.184	0.403	3
G 058-023	52958	5413	4.50	-1.04	0.000	11.16	9.940	5.178	0.600	0.407	0.138	0.219	2
HD 94028	53070	6001	4.50	-1.50	0.000	19.23	8.229	4.630	0.498	0.344	0.079	0.258	2
G 055-044	53169	4370	4.50	-0.23	0.000	23.94	9.766	6.686	1.048	0.607	0.548	0.162	2
HD 94247	53261	4231	2.30	-0.10	0.000	4.82	5.120	-1.465	1.355	0.828	0.618	0.394	3
HD 95345	53807	4490	2.75	-0.18	0.000	9.54	4.850	-0.262	1.144	0.710	0.510	0.420	3
HD 95735	54035	3828	5.00	-0.20	0.000	392.40	7.421	10.459	1.502	0.980	0.424	0.143	2
HD 95689	54061	4655	2.20	-0.19	0.001	26.38	1.800	-1.084	1.059	0.659	0.438	0.394	1
HD 95934	54136	7822	3.00	0.00	0.007	12.41	6.000	1.479	0.155	0.087	0.189	0.972	3
HD 96833	54539	4542	2.30	0.03	0.003	22.21	3.000	-0.267	1.140	0.700	0.525	0.395	1
G 010-004	54639	5192	4.50	-2.30	0.044	14.26	11.378	7.161	0.674	0.452	0.130	0.092	2
G 119-064	54772	6206	4.50	-1.71	0.000	8.11	9.795	4.315	0.432	0.319	0.073	0.319	2
GJ 421B	54966	3714	5.00	-1.50	0.000	48.47	9.923	8.397	1.340	0.777	0.727	0.054	2
HD 97916	55022	6393	4.00	-1.22	0.000	7.69	9.207	3.640	0.425	0.292	0.103	0.410	2
HD 98839	55560	4872	2.30	-0.03	0.000	6.63	4.989	-0.902	0.998	0.610	0.414	0.400	3
G 056-036	55592	5918	4.50	-1.03	0.000	8.72	9.973	4.673	0.494	0.351	0.099	0.285	2
HD 99747	56035	6634	4.50	-0.61	0.000	30.40	5.829	3.244	0.382	0.265	0.125	0.490	2
HD 99998	56127	3891	1.67	-0.39	0.000	5.40	4.744	-1.568	1.529	0.952	0.769	0.361	3
HD 100920	56647	4802	2.80	-0.24	0.000	18.31	4.312	0.613	0.983	0.600	0.382	0.414	1
HD 101013	56731	4874	2.00	-0.33	0.022	7.07	6.139	0.387	1.038	0.625	0.520	0.086	3
HD 101177	56809	5483	4.00	-0.13	0.000	42.94	6.474	4.454	0.566	0.371	0.182	0.310	2
HD 101501	56997	5552	4.60	-0.14	0.001	104.81	5.308	5.412	0.722	0.443	0.271	0.291	1
HD 101606	57029	6266	4.50	-0.82	0.000	24.42	5.744	2.669	0.440	0.312	0.119	0.402	2
G 121-012	57265	5957	4.50	-1.17	0.000	6.14	10.374	4.321	0.491	0.350	0.094	0.287	2
G 176-053	57450	5593	4.50	-1.54	0.000	13.61	9.909	5.579	0.582	0.398	0.099	0.179	2
HD 102634	57629	6311	4.00	0.12	0.000	29.26	6.153	3.481	0.518	0.329	0.176	0.439	2
HD 102870	57757	6147	4.22	0.13	0.001	91.74	3.602	3.403	0.516	0.353	0.188	0.416	1
HD 103095	57939	5029	4.50	-1.35	0.000	109.21	6.427	6.611	0.754	0.484	0.222	0.155	2
BD-01 2582	57983	5148	1.20	-2.20	0.004	2.98	9.600	1.961	0.720	0.472	0.121	0.208	3
HD 103545	58139	4666	2.00	-2.30	0.000	0.60	9.426	-1.689	0.844	0.583	0.090	0.438	3
HD 233891	58514	4911	2.05	-1.50	0.015	0.41	8.821	-3.136	0.778	0.542	0.158	0.485	3
HD 104556	58708	4370	4.00	-0.64	0.000	18.05	6.630	2.922	0.860	0.537	0.265	0.406	2
HD 104636	58752	7019	4.00	0.00	0.000	5.17	8.228	1.797	0.402	0.254	0.173	0.639	2
HD 104979	58948	4824	2.75	-0.38	0.000	19.08	4.124	0.523	0.967	0.598	0.368	0.307	3
HD 105452	59199	7003	4.00	-0.60	0.000	67.71	4.025	3.173	0.334	0.213	0.163	0.577	2
HD 105546	59239	5190	2.40	-1.40	0.000	1.96	8.619	0.071	0.660	0.477	0.097	0.457	3
HD 105601	59271	7481	4.00	0.00	0.000	8.56	7.394	2.052	0.307	0.179	0.219	0.775	2
HD 105755	59330	5806	4.00	-1.08	0.000	12.80	8.587	4.126	0.568	0.385	0.127	0.302	2
G 011-044	59376	5943	4.50	-1.80	0.000	4.76	11.096	4.478	0.449	0.334	0.054	0.263	2
HD 106038	59490	5960	4.50	-1.40	0.000	9.16	10.176	4.979	0.469	0.339	0.090	0.284	2
HD 106373	59672	6093	2.80	-2.48	0.044	2.22	8.928	0.642	0.382	0.295	0.045	0.722	3
HD 106516	59750	6208	4.50	-0.78	0.000	44.34	6.116	4.344	0.470	0.319	0.114	0.334	2
HD 107213	60098	6343	4.00	0.38	0.000	20.12	6.379	2.898	0.523	0.339	0.181	0.462	2
HD 107328	60172	4396	2.20	-0.47	0.000	11.43	4.970	0.260	1.172	0.718	0.483	0.516	3
HD 107760	60331	5323	4.00	-0.39	0.007	23.16	8.069	4.794	0.734	0.460	0.249	0.265	2
HD 108177	60632	6097	4.50	-1.98	0.000	10.95	9.670	4.857	0.445	0.331	0.060	0.285	2

Star ID	HIC	T_{eff}	log g	[Fe/H]	E$(b-y)$	π	V	M_V	$(B-V)_o$	$(b-y)_o$	m_o	c_o	Source
HD 108317	60719	5234	2.40	-2.30	0.000	4.53	8.042	1.310	0.607	0.448	0.053	0.306	3
HD 108381	60742	4681	2.60	0.17	0.006	19.18	4.350	0.764	1.120	0.652	0.482	0.265	1
HD 108577	60846	5020	2.00	-2.50	0.015	2.35	9.583	1.425	0.684	0.497	0.066	0.494	3
HD 108754	60956	5338	4.00	-0.50	0.000	19.20	9.008	5.407	0.703	0.436	0.217	0.250	2
HD 109358	61317	5861	4.45	-0.25	0.001	119.46	4.240	4.626	0.586	0.384	0.183	0.298	1
G 059-024	61361	6108	4.50	-2.69	0.000	4.91	12.010	5.465	0.448	0.332	0.054	0.225	2
G 059-027	61545	6107	4.50	-2.34	0.000	5.35	10.882	4.532	0.448	0.322	0.055	0.321	2
G 060-026	61802	5275	4.50	-1.24	0.000	4.55	9.804	3.080	0.652	0.439	0.127	0.244	2
HD 110184	61824	4250	0.90	-2.26	0.000	1.00	8.297	-1.730	1.147	0.818	0.173	0.706	3
HD 110281	61899	3950	2.00	0.00	0.011	1.74	9.347	0.573	1.570	1.031	0.506	0.640	3
HD 111631	62687	3748	5.00	0.10	0.000	92.75	8.455	8.327	1.409	0.824	0.728	0.015	2
HD 111812	62763	5761	3.00	-0.20	0.004	10.62	4.928	0.061	0.675	0.431	0.197	0.405	1
HD 111980	62882	5624	4.00	-1.12	0.015	12.48	8.361	3.841	0.530	0.355	0.111	0.293	2
G 060-048	63100	5795	4.50	-1.92	0.000	4.84	11.306	4.744	0.521	0.365	0.074	0.189	2
HD 112758	63366	5116	4.50	-0.29	0.000	47.60	7.548	5.928	0.769	0.476	0.300	0.266	2
BD+10 2495	63385	4939	2.00	-1.83	0.002	2.36	9.738	1.585	0.746	0.514	0.092	0.350	3
HD 113101	63548	5413	4.50	0.06	0.000	18.25	8.976	5.276	0.736	0.450	0.256	0.340	2
HD 114094	64103	5500	4.50	-0.17	0.000	14.41	9.675	5.463	0.702	0.429	0.233	0.290	2
HD 114095	64115	4541	4.50	-1.58	0.000	4.73	8.371	1.724	0.963	0.597	0.268	0.458	2
HD 114606	64345	5590	4.50	-0.34	0.000	16.36	8.727	4.789	0.622	0.409	0.164	0.289	2
G 061-038	64386	5516	4.50	-0.79	0.000	14.30	9.881	5.637	1.060	0.415	0.165	0.237	2
HD 114710	64394	6024	4.47	0.27	0.001	109.23	4.249	4.422	0.571	0.367	0.192	0.338	1
HD 114642	64407	6240	4.00	-0.15	0.000	30.72	5.034	2.477	0.460	0.310	0.148	0.476	3
HD 114762	64426	5884	4.00	-0.80	0.000	24.65	7.304	4.259	0.525	0.365	0.125	0.297	2
HD 115444	64786	4721	1.85	-2.70	0.000	3.55	8.975	1.711	0.749	0.586	0.056	0.467	3
HD 115604	64844	7141	3.75	0.30	0.000	11.39	4.719	0.003	0.306	0.176	0.232	0.915	3
G 014-045	64965	4480	4.50	-0.22	0.000	27.87	10.803	8.066	1.009	0.587	0.517	0.115	2
G 062-030	65040	5341	4.50	-0.75	0.000	15.43	9.778	5.712	0.654	0.418	0.174	0.246	2
G 063-026	65418	5970	4.50	-1.70	0.000	2.52	12.183	4.187	0.468	0.328	0.085	0.277	2
HD 117126	65708	5682	4.00	0.12	0.000	21.79	7.440	4.131	0.651	0.414	0.206	0.348	2
HD 117417	65774	4580	2.00	0.00	0.015	3.63	7.537	0.330	0.953	0.643	0.404	0.366	3
HD 118100	66252	4179	4.50	-0.07	0.000	50.54	9.299	7.758	1.210	0.692	0.641	0.112	2
G 062-052	66354	5209	4.50	-1.16	0.000	12.26	10.871	6.292	0.670	0.430	0.167	0.190	2
BD+18 2757	66378	4853	2.00	-2.60	0.000	0.28	9.800	-2.964	0.775	0.547	0.077	0.503	3
G 063-046	66665	5705	4.50	-0.83	0.000	7.44	9.376	3.728	0.598	0.382	0.139	0.283	2
G 064-012	66673	6468	5.00	-3.35	0.015	1.88	11.464	2.841	0.385	0.289	0.050	0.337	2
HD 118981	66708	5898	4.50	-0.08	0.000	14.44	8.214	4.008	0.567	0.373	0.162	0.365	2
HD 119516	66959	5476	2.50	-2.50	0.000	0.05	9.084	-7.455	0.661	0.404	0.066	0.512	3
HD 121135	67822	4934	2.00	-1.70	0.008	1.73	9.367	0.550	0.784	0.522	0.124	0.508	3
HD 121370	67927	6048	3.80	0.16	0.001	88.17	2.680	2.407	0.578	0.373	0.204	0.488	1
G 165-039	68321	6282	4.50	-2.41	0.000	5.37	10.062	3.700	0.410	0.309	0.055	0.354	2
HD 122405	68478	7671	3.00	0.00	0.011	9.59	6.100	1.139	0.178	0.096	0.204	0.987	3
G 065-022	68527	4971	4.50	-1.75	0.000	13.01	11.571	7.141	0.746	0.479	0.184	0.139	2
G 064-037	68592	6432	4.50	-2.51	0.007	2.88	11.143	3.427	0.387	0.296	0.049	0.338	2
HD 122563	68594	4572	1.60	-2.62	0.000	3.76	6.203	-0.944	0.853	0.639	0.091	0.543	3
HD 123710	68796	5768	4.50	-1.32	0.000	22.84	8.210	5.003	0.590	0.402	0.148	0.257	2
BD+09 2860	69468	5285	2.00	-2.60	0.003	4.97	10.838	4.312	0.706	0.448	0.084	0.461	3
HD 124358	69470	4688	1.75	-2.20	0.031	1.16	9.508	-0.178	0.874	0.598	0.135	0.523	3
HD 124897	69673	4321	1.59	-0.51	0.003	88.85	-0.050	-0.307	1.235	0.750	0.532	0.487	1
HD 124850	69701	6111	3.99	-0.41	0.002	46.74	4.087	2.418	0.508	0.335	0.163	0.439	1
G 166-022	70218	3972	5.00	-1.50	0.000	69.43	8.507	7.768	1.275	0.727	0.747	0.065	2
HD 126053	70319	5646	4.00	-0.29	0.000	56.82	6.262	5.023	0.639	0.405	0.188	0.281	2
HD 126587	70647	4794	2.00	-2.70	0.051	1.40	9.115	-0.159	0.704	0.546	0.068	0.380	3
HD 126681	70681	5541	4.50	-1.98	0.000	19.16	9.299	5.692	0.606	0.400	0.130	0.197	2
BD+18 2890	71087	5057	2.00	-1.61	0.022	1.52	9.834	0.749	0.788	0.484	0.123	0.377	3
HD 128167	71284	6696	4.26	-0.36	0.001	64.66	4.465	3.523	0.363	0.253	0.134	0.480	1
HD 128279	71458	5290	3.00	-2.22	0.037	5.96	8.038	1.896	0.590	0.429	0.069	0.253	3
HD 128429	71469	6349	4.00	-0.29	0.000	29.97	6.192	3.583	0.464	0.306	0.150	0.427	2
HD 128959	71761	5763	4.50	-0.88	0.037	7.24	9.260	3.519	0.556	0.376	0.148	0.350	2
HD 129312	71832	4854	2.00	-0.22	0.000	5.66	4.864	-1.376	0.992	0.625	0.401	0.379	3
G 066-022	71979	5071	4.50	-1.11	0.000	11.38	10.435	5.721	0.714	0.456	0.194	0.190	2
G 166-045	72461	6037	4.50	-2.33	0.007	10.28	9.730	4.790	0.427	0.325	0.055	0.287	2
G 066-030	72561	6211	4.50	-1.50	0.007	7.01	11.025	5.279	0.403	0.301	0.073	0.358	2

Star ID	HIC	T_{eff}	log g	[Fe/H]	E$(b-y)$	π	V	M_V	$(B-V)_o$	$(b-y)_o$	m_o	c_o	Source
HD 130948	72567	6019	4.00	0.20	0.000	55.73	5.874	4.590	0.576	0.374	0.191	0.321	2
HD 130952	72631	4708	2.50	-0.38	0.007	15.09	4.931	0.823	0.978	0.609	0.341	0.450	3
HD 131653	72998	5311	4.50	-0.50	0.000	20.29	9.510	6.046	0.716	0.442	0.225	0.252	2
HD 132142	73005	5098	4.50	-0.55	0.000	41.83	7.754	5.877	0.785	0.479	0.304	0.273	2
HD 131977	73184	4605	4.50	0.01	0.000	169.32	5.724	6.864	1.024	0.617	0.669	0.190	2
HD 132475	73385	5788	4.00	-1.53	0.022	10.85	8.561	3.727	0.480	0.371	0.083	0.282	2
BD+30 2611	73960	4209	1.00	-1.40	0.004	3.45	9.152	1.819	1.243	0.806	0.334	0.550	3
HD 134083	73996	6616	4.31	-0.01	0.004	50.70	4.940	3.455	0.423	0.283	0.161	0.445	1
HD 134169	74079	5870	4.00	-1.15	0.000	16.80	7.684	3.797	0.565	0.370	0.119	0.312	2
HD 134439	74235	4974	4.50	-1.52	0.000	34.14	9.060	6.736	0.770	0.486	0.216	0.163	2
HD 134440	74234	4746	4.50	-1.57	0.000	33.68	9.421	7.077	0.850	0.522	0.291	0.175	2
G 015-013	74419	5244	4.50	-1.88	0.051	7.96	12.296	6.815	0.694	0.440	0.181	0.132	2
HD 135722	74666	4832	2.60	-0.32	0.000	27.94	3.460	0.691	0.961	0.589	0.346	0.407	1
HD 136202	74975	6036	3.95	-0.13	0.000	40.46	5.060	3.075	0.540	0.348	0.170	0.427	3
HD 136512	75049	4677	2.70	-0.38	0.000	11.90	5.509	0.888	1.015	0.638	0.355	0.454	3
G 015-023	75839	5175	4.50	-1.42	0.000	27.55	10.924	8.141	0.709	0.452	0.177	0.161	2
HD 138290	75971	6831	4.00	0.01	0.000	19.73	6.573	3.046	0.380	0.240	0.160	0.508	2
HD 138716	76219	4742	3.20	-0.14	0.015	34.54	4.613	2.302	0.980	0.597	0.428	0.425	1
HD 138905	76333	4711	2.80	-0.44	0.007	21.42	3.914	0.564	0.997	0.601	0.387	0.395	3
HD 139225	76424	6662	2.50	0.00	0.000	20.40	5.800	2.478	0.354	0.222	0.160	0.681	3
HD 139195	76425	4958	3.00	-0.13	0.000	13.89	5.249	0.974	0.925	0.579	0.380	0.357	3
HD 139641	76534	4893	3.20	-0.55	0.010	20.00	5.262	1.755	0.873	0.551	0.268	0.404	3
HD 139798	76568	6782	4.00	-0.13	0.000	27.98	5.750	2.994	0.353	0.243	0.147	0.567	2
HD 139663	76742	4392	2.30	-0.10	0.051	8.55	4.958	-0.370	1.232	0.758	0.707	0.346	3
HD 140283	76976	5691	4.00	-2.37	0.000	17.44	7.216	3.408	0.484	0.379	0.040	0.293	2
HD 140573	77070	4556	2.60	0.18	0.004	44.54	2.630	0.874	1.161	0.711	0.573	0.450	1
HD 141004	77257	5940	4.31	0.05	0.001	85.08	4.422	4.069	0.602	0.382	0.193	0.364	1
HD 141531	77483	4461	1.00	-1.57	0.012	3.16	9.137	1.628	1.224	0.753	0.266	0.589	3
HD 141714	77512	5180	3.10	-0.32	0.000	19.71	4.604	1.063	0.794	0.509	0.223	0.415	3
G 016-013	77637	5507	4.50	-0.96	0.000	3.62	9.946	2.744	0.591	0.390	0.127	0.290	2
HD 142091	77655	4811	4.00	0.00	0.000	32.13	4.799	2.325	0.996	0.615	0.420	0.443	2
BD+05 3098	77739	4881	2.00	-2.60	0.028	2.48	10.537	2.502	0.742	0.517	0.075	0.385	3
HD 142373	77760	5802	4.33	-0.44	0.001	63.08	4.608	3.599	0.561	0.380	0.147	0.328	1
HD 142198	77853	4782	2.30	-0.24	0.026	20.02	4.140	0.637	0.968	0.594	0.407	0.416	1
HD 142860	78072	6246	4.24	-0.32	0.002	89.92	3.843	3.619	0.475	0.317	0.151	0.400	1
HD 143107	78159	4350	1.95	-0.05	0.011	14.20	4.137	-0.099	1.216	0.740	0.573	0.411	1
HD 144061	78217	5555	4.50	-0.78	0.000	34.35	7.251	4.940	0.654	0.408	0.181	0.275	2
HD 143761	78459	5777	4.00	-0.17	0.000	57.38	5.410	4.184	0.612	0.394	0.178	0.337	2
HD 144284	78527	6158	4.00	0.23	0.000	47.79	4.000	2.407	0.528	0.353	0.174	0.461	2
G 180-024	78640	6059	4.50	-1.67	0.000	8.03	9.878	4.384	0.481	0.342	0.067	0.277	2
HD 144515	78864	4867	4.50	-0.61	0.000	24.81	8.350	5.283	0.803	0.511	0.286	0.224	2
G 168-042	80003	5059	4.50	-1.46	0.007	9.12	11.542	6.320	0.713	0.464	0.170	0.184	2
G 180-058	80679	5168	4.50	-2.32	0.000	10.30	11.318	6.364	0.735	0.489	0.075	0.091	2
BD+11 2998	80822	5385	2.50	-1.15	0.035	3.25	9.063	1.619	0.624	0.425	0.098	0.508	3
HD 148816	80837	5851	5.00	-0.75	0.000	24.34	7.286	4.202	0.545	0.367	0.125	0.306	2
HD 149144	81046	5364	4.50	-1.79	0.000	16.70	10.172	6.294	0.789	0.473	0.287	0.166	2
BD+09 3223	81078	5363	2.00	-2.30	0.044	1.88	9.256	0.621	0.560	0.426	0.053	0.471	3
HD 149414	81170	4966	5.00	-1.34	0.000	20.71	9.611	6.181	0.736	0.474	0.202	0.159	2
HD 150177	81580	6038	4.00	-0.63	0.000	23.02	6.333	3.141	0.492	0.334	0.119	0.395	2
HD 150682	81729	6474	3.00	0.00	0.000	23.35	5.920	2.761	0.402	0.269	0.152	0.462	3
HD 152156	82536	5289	4.50	-1.70	0.095	7.81	9.735	4.193	0.687	0.409	0.117	0.424	2
HD 152598	82587	6886	3.00	0.00	0.000	33.30	5.365	2.952	0.319	0.211	0.161	0.632	3
HD 152311	82621	5535	4.00	0.00	0.000	35.73	5.867	3.625	0.685	0.434	0.219	0.400	2
HD 154363	83591	4314	4.50	0.00	0.000	92.98	7.698	7.542	1.100	0.659	0.626	0.176	2
HD 155646	84217	6162	3.95	-0.14	0.007	14.55	6.651	2.464	0.494	0.323	0.161	0.480	3
HD 156026	84478	4345	5.00	-0.23	0.000	167.56	6.295	7.451	1.144	0.653	0.673	0.132	2
HD 157089	84905	5662	4.00	-0.58	0.000	25.88	6.961	4.015	0.571	0.380	0.143	0.324	2
HD 157482	84949	5309	2.00	0.00	0.000	15.53	5.564	1.506	0.667	0.437	0.212	0.434	3
HD 157728	85157	7397	2.00	0.00	0.000	23.37	5.700	2.543	0.229	0.136	0.188	0.809	3
HD 157881	85295	4065	4.50	0.40	0.000	129.54	7.506	8.102	1.359	0.783	0.744	0.045	2
HD 157999	85355	4075	1.20	0.01	0.063	2.78	4.322	-3.440	1.394	0.896	0.682	0.317	1
HD 158226	85378	5794	4.50	-0.68	0.000	14.51	8.498	4.288	0.626	0.383	0.156	0.316	2
BD+17 3248	85487	5236	1.80	-2.04	0.040	3.67	9.356	2.163	0.618	0.452	0.069	0.442	3

Star ID	HIC	T_{eff}	log g	[Fe/H]	$E(b-y)$	π	V	M_V	$(B-V)_o$	$(b-y)_o$	m_o	c_o	Source
HD 158809	85757	5418	4.50	-0.59	0.000	13.31	8.152	3.771	0.663	0.424	0.163	0.298	2
HD 159222	85810	5770	4.00	0.00	0.000	42.20	6.528	4.647	0.639	0.406	0.216	0.364	2
HD 159332	85912	6096	3.95	-0.24	0.000	27.26	5.660	2.828	0.505	0.330	0.143	0.467	3
HD 159561	86032	7923	4.00	0.00	0.000	69.84	2.080	1.301	0.155	0.093	0.168	1.039	2
G 170-056	86321	5952	4.50	-1.25	0.000	8.93	9.765	4.524	0.480	0.350	0.090	0.319	2
HD 160693	86431	5771	4.50	-0.71	0.000	18.32	8.393	4.705	0.576	0.383	0.145	0.291	2
G 020-008	86443	5891	5.00	-2.59	0.007	8.35	9.954	4.548	0.448	0.345	0.050	0.256	2
HD 160910	86623	6488	4.00	-0.13	0.000	28.15	5.500	2.787	0.387	0.258	0.155	0.541	3
HD 161096	86742	4603	2.50	0.18	0.011	39.78	2.764	0.758	1.153	0.705	0.565	0.445	1
HD 161797	86974	5527	4.10	0.30	0.001	119.05	3.413	3.799	0.748	0.467	0.272	0.407	1
g 020-015	87062	5682	4.50	-2.79	0.073	10.34	10.590	5.673	0.505	0.378	0.059	0.256	2
HD 162208	87118	7953	4.00	0.00	0.000	5.84	7.630	1.442	0.194	0.111	0.186	0.941	2
HD 161903	87149	7521	4.00	0.00	0.000	10.02	7.739	2.744	0.309	0.176	0.186	0.875	2
HD 162211	87194	4518	2.80	0.04	0.015	15.94	5.063	1.102	1.121	0.696	0.461	0.382	3
G 183-011	87693	6441	4.50	-2.05	0.000	6.47	9.858	3.825	0.442	0.323	0.048	0.308	2
G 154-034	87788	5469	4.50	-1.86	0.037	13.47	11.320	6.947	0.641	0.434	0.082	0.085	2
HD 164058	87833	3955	1.20	-0.23	0.007	22.10	2.240	-1.038	1.512	0.934	0.813	0.371	1
HD 163810	88010	5493	4.50	-1.50	0.015	11.88	9.636	5.004	0.596	0.409	0.118	0.199	2
HD 164507	88217	5490	2.00	0.00	0.000	22.20	6.284	3.012	0.747	0.463	0.230	0.402	3
HD 165195	88527	4237	1.50	-2.20	0.095	2.20	7.326	-0.978	1.102	0.824	0.184	0.701	3
HD 165341	88601	4978	4.50	-0.17	0.000	196.62	4.016	5.498	0.860	0.508	0.390	0.262	2
HD 165760	88765	4969	2.95	-0.15	0.015	13.71	4.635	0.325	0.931	0.577	0.380	0.426	3
HD 166208	88788	4994	2.65	0.06	0.007	8.98	4.997	-0.234	0.903	0.587	0.307	0.526	3
G 020-024	88827	6464	4.50	-0.91	0.088	5.42	11.125	4.760	0.334	0.274	0.064	0.354	2
HD 166233	88964	6661	2.00	0.00	0.007	19.62	5.712	2.173	0.353	0.220	0.183	0.647	3
HD 166620	88972	4947	4.50	-0.25	0.000	90.11	6.377	6.154	0.876	0.518	0.406	0.295	2
HD 166161	88977	4974	2.31	-1.21	0.201	3.25	8.138	0.679	0.601	0.484	0.142	0.454	3
HD 166285	89000	6312	3.90	-0.22	0.007	21.30	5.674	2.312	0.480	0.306	0.150	0.449	3
G 140-046	89215	4980	4.50	-1.44	0.000	17.00	10.348	6.522	0.755	0.474	0.261	0.141	2
HD 168009	89474	5781	4.00	0.00	0.000	44.08	6.308	4.521	0.641	0.410	0.203	0.345	2
HD 167858	89601	7038	4.00	0.17	0.000	15.98	6.643	2.638	0.312	0.201	0.162	0.683	2
HD 168322	89604	4785	2.00	-0.30	0.007	9.36	6.132	0.976	0.967	0.603	0.300	0.502	3
HD 170737	90659	5075	3.00	-0.91	0.026	8.28	8.127	2.720	0.768	0.477	0.244	0.281	3
G 141-019	90957	5138	4.50	-2.39	0.037	3.57	10.578	3.333	0.617	0.469	0.022	0.246	2
HD 171620	91058	6109	4.50	-0.65	0.000	19.12	7.562	3.957	0.511	0.340	0.131	0.341	2
HD 172323	91115	5835	4.00	0.27	0.000	18.76	8.096	4.466	0.564	0.360	0.180	0.324	2
G 206-034	91129	6191	5.00	-3.10	0.029	3.59	11.409	4.165	0.408	0.311	0.039	0.254	2
HD 171369	91132	7120	3.00	0.00	0.007	10.71	6.481	1.639	0.270	0.160	0.187	0.828	3
HD 171496	91182	4485	1.50	-1.12	0.078	5.57	8.510	2.219	0.972	0.687	0.185	0.422	3
HD 349063	91410	5531	4.00	-0.45	0.000	16.23	9.320	5.382	0.646	0.415	0.196	0.251	2
HD 173417	91883	6655	3.00	0.00	0.000	19.27	5.500	2.104	0.360	0.242	0.154	0.693	3
HD 175305	92167	5041	2.50	-1.45	0.018	6.18	7.197	1.135	0.738	0.486	0.158	0.286	3
HD 173764	92175	4702	2.20	0.00	0.080	4.73	4.210	-2.406	0.978	0.629	0.380	0.412	1
HD 175179	92781	5676	2.00	-0.75	0.037	11.85	9.074	4.419	0.536	0.345	0.162	0.260	3
HD 175190	92845	4283	1.00	-0.40	0.015	12.07	4.997	0.409	1.328	0.809	0.721	0.231	3
HD 175617	92960	5465	4.50	-0.48	0.000	13.38	10.130	5.752	0.702	0.441	0.208	0.281	2
HD 178428	93966	5603	4.00	0.00	0.000	47.72	6.085	4.474	0.705	0.437	0.247	0.358	2
HD 179626	94449	5597	4.50	-1.21	0.000	7.52	9.210	3.561	0.538	0.373	0.095	0.293	2
HD 180262	94624	4840	2.00	0.21	0.029	5.32	5.586	-0.790	1.027	0.637	0.405	0.406	3
HD 180809	94713	4501	1.72	-0.20	0.036	4.24	4.350	-2.513	1.209	0.751	0.576	0.324	1
HD 181096	94755	6285	4.17	-0.28	0.000	23.57	6.010	2.882	0.479	0.322	0.139	0.444	3
HD 181276	94779	4947	2.85	-0.10	0.000	26.48	3.800	0.915	0.950	0.578	0.388	0.429	3
HD 180928	94929	4008	1.40	-0.60	0.029	6.31	6.074	0.090	1.380	0.871	0.576	0.522	3
G 125-004	94931	5004	4.50	-0.42	0.000	28.28	8.865	6.127	0.806	0.488	0.303	0.268	2
G 022-024	95059	4700	4.50	-0.47	0.000	18.16	10.537	6.826	0.889	0.534	0.408	0.236	2
HD 182572	95447	5518	4.00	0.41	0.000	66.01	5.169	4.268	0.761	0.470	0.287	0.408	2
HD 182807	95492	6062	4.00	0.24	0.000	36.05	6.203	3.975	0.528	0.345	0.149	0.367	2
G 125-013	95996	5896	4.50	-0.87	0.000	9.55	10.234	5.120	0.510	0.360	0.074	0.219	2
HD 184400	96062	6559	4.00	0.00	0.000	9.13	8.518	3.312	0.460	0.291	0.170	0.473	2
HD 185144	96100	5253	4.50	-0.25	0.002	173.41	4.672	5.865	0.783	0.470	0.322	0.266	1
HD 338529	96115	6341	4.31	-2.10	0.000	6.93	9.378	3.574	0.390	0.300	0.054	0.374	2
HD 184499	96185	5750	4.00	-0.69	0.000	31.29	6.631	4.097	0.595	0.390	0.143	0.314	2
HD 184406	96229	4456	2.20	0.08	0.005	29.50	4.440	1.799	1.169	0.711	0.563	0.417	1

Star ID	HIC	T_{eff}	log g	[Fe/H]	E$(b-y)$	π	V	M_V	$(B-V)_o$	$(b-y)_o$	m_o	c_o	Source
HD 184266	96248	5587	1.85	-1.57	0.037	3.28	7.597	0.169	0.498	0.388	0.068	0.603	3
HD 232078	96599	3654	0.50	-1.10	0.117	1.61	8.711	-0.396	1.840	1.320	0.403	0.604	3
HD 185758	96757	5429	2.40	0.00	0.038	6.89	4.384	-1.419	0.725	0.454	0.272	0.459	1
HD 186408	96895	5826	4.30	0.00	0.004	46.25	5.978	4.316	0.638	0.406	0.214	0.369	1
HD 186427	96901	5664	4.40	0.00	0.004	46.70	6.234	4.597	0.656	0.412	0.225	0.351	1
HD 186478	97192	4598	0.95	-2.63	0.057	1.34	9.173	-0.224	0.893	0.632	0.097	0.491	3
HD 187111	97468	4271	0.75	-1.87	0.081	1.99	7.747	-0.796	1.060	0.749	0.245	0.597	3
HD 188056	97635	4374	1.80	-0.05	0.007	16.96	5.014	1.177	1.276	0.799	0.696	0.344	3
HD 187923	97767	5648	2.00	0.06	0.000	36.15	6.161	3.951	0.642	0.417	0.192	0.341	3
HD 188262	97904	4850	4.50	0.00	0.000	0.40	7.695	-4.290	0.789	0.589	0.138	0.444	2
HD 188350	97980	7946	2.00	0.00	0.022	9.45	5.615	0.477	0.068	0.071	0.085	1.130	3
HD 188510	98020	5564	4.00	-1.80	0.000	25.32	8.832	5.847	0.599	0.416	0.107	0.148	2
HD 188512	98036	5098	3.56	-0.08	0.003	72.95	3.724	3.025	0.851	0.517	0.307	0.342	1
BD-18 5550	98339	4668	1.10	-2.90	0.073	1.90	9.300	0.674	0.615	0.612	-0.008	0.394	3
G 023-020	98492	5278	4.50	-1.83	0.000	9.09	11.580	6.383	0.673	0.451	0.069	0.289	2
HD 189558	98532	5663	4.00	-1.30	0.000	14.76	7.753	3.565	0.571	0.386	0.111	0.284	2
HD 189849	98543	7804	3.60	0.01	0.011	14.67	4.670	0.492	0.169	0.086	0.205	1.062	3
HD 190360	98767	5572	4.00	0.26	0.000	62.92	5.745	4.724	0.749	0.461	0.274	0.380	2
HD 190404	98792	5001	4.50	-0.18	0.000	64.17	7.277	6.317	0.815	0.492	0.322	0.249	2
G 024-003	98989	5859	4.50	-1.78	0.000	5.31	10.473	4.085	0.510	0.363	0.057	0.271	2
HD 191046	99041	4574	2.00	-0.42	0.081	2.40	7.023	-1.089	1.040	0.636	0.429	0.461	3
HD 345957	99423	5788	4.50	-1.45	0.000	9.38	8.897	3.751	0.487	0.372	0.078	0.289	2
HD 191849	99701	3562	5.00	-1.50	0.000	161.17	7.950	9.006	1.431	0.879	0.569	0.128	2
HD 192718	99938	5737	2.00	0.00	0.011	17.28	8.401	4.578	0.565	0.365	0.152	0.304	3
HD 192947	100064	4978	3.00	0.05	0.000	30.01	3.583	0.966	0.883	0.571	0.382	0.410	3
G 024-013	100279	5558	4.50	-1.10	0.000	10.19	10.145	5.181	0.621	0.411	0.123	0.267	2
HD 193495	100345	4878	2.00	-0.78	0.000	9.48	3.088	-2.066	0.790	0.516	0.212	0.335	3
HD 193901	100568	5750	4.50	-1.13	0.000	22.88	8.660	5.447	0.554	0.381	0.103	0.217	2
HD 229274	100660	5414	4.50	-2.46	0.000	1.87	9.058	0.409	0.622	0.435	0.108	0.453	2
G 186-026	100682	6428	4.50	-3.40	0.007	7.49	10.829	5.202	0.417	0.299	0.044	0.337	2
HD 194598	100792	6017	4.00	-1.37	0.000	17.94	8.355	4.599	0.503	0.342	0.092	0.273	2
HD 195725	101093	7774	4.00	0.14	0.007	24.04	4.245	1.115	0.189	0.097	0.225	0.997	3
HD 195636	101379	5384	3.40	-2.79	0.044	0.74	9.551	-1.114	0.581	0.423	0.023	0.464	3
BD-17 6036	101740	4860	1.75	-2.60	0.036	1.65	10.525	1.607	0.791	0.545	0.066	0.380	3
HD 197076	102040	5761	4.00	0.00	0.000	47.65	6.438	4.820	0.611	0.397	0.187	0.326	2
HD 197461	102281	6877	3.50	-0.20	0.000	16.03	4.380	0.455	0.302	0.191	0.162	0.853	3
HD 198149	102422	4996	3.34	-0.17	0.009	69.73	3.410	2.627	0.900	0.544	0.369	0.373	1
HD 197989	102488	4725	2.80	-0.10	0.000	45.26	2.480	0.759	1.021	0.627	0.417	0.425	3
BD+04 4551	102718	5819	4.50	-1.80	0.000	1.64	9.694	0.664	0.541	0.362	0.074	0.276	2
HD 198809	103004	5135	2.85	-0.13	0.000	15.06	4.560	0.449	0.835	0.510	0.310	0.390	3
HD 198802	103077	5686	4.00	0.00	0.000	22.17	6.387	3.109	0.661	0.415	0.207	0.376	2
HD 199191	103092	4798	2.25	-0.70	0.029	6.90	7.130	1.344	0.920	0.552	0.309	0.410	3
HD 199305	103096	3630	5.00	-1.50	0.000	141.95	8.554	9.311	1.483	0.911	0.518	0.201	2
HD 199611	103359	6794	2.00	0.00	0.000	18.75	5.700	2.195	0.337	0.224	0.167	0.708	3
HD 200077	103641	5870	4.00	0.09	0.000	25.60	6.578	3.621	0.584	0.364	0.171	0.368	2
HD 200580	103987	5747	4.50	-0.48	0.000	17.83	7.327	3.566	0.547	0.364	0.149	0.305	2
HD 201091	104214	4463	4.50	-0.05	0.001	287.13	5.211	7.490	1.068	0.657	0.679	0.132	1
HD 201092	104217	4252	4.60	-0.05	0.001	285.42	6.043	8.327	1.308	0.790	0.675	0.067	1
HD 201601	104521	7429	4.00	0.07	0.000	28.38	4.703	1.965	0.262	0.148	0.240	0.754	3
HD 201891	104659	5909	4.50	-1.22	0.000	28.26	7.383	4.626	0.525	0.358	0.104	0.262	2
HD 201889	104660	5635	4.00	-1.10	0.000	17.95	8.060	4.330	0.595	0.388	0.148	0.281	2
HD 202314	104822	4767	2.00	0.00	0.044	1.34	6.141	-3.184	1.045	0.655	0.422	0.351	3
HD 203608	105858	6065	4.31	-0.81	0.001	108.50	4.229	4.387	0.492	0.330	0.125	0.313	1
HD 204155	105888	5771	4.50	-0.90	0.000	13.02	8.501	4.063	0.572	0.378	0.131	0.311	2
HD 204613	105969	5781	3.75	-0.50	0.015	16.61	8.275	4.362	0.623	0.380	0.215	0.278	3
BD-03 5215	105993	5487	2.30	-1.57	0.032	2.11	10.187	1.791	0.675	0.404	0.089	0.495	3
G 026-009	106335	4853	4.33	-0.91	0.000	20.26	9.804	6.253	0.954	0.584	0.350	0.182	2
HD 205512	106551	4715	2.00	0.25	0.021	12.76	4.878	0.399	1.056	0.653	0.491	0.371	1
G 126-019	106947	5267	4.50	-0.20	0.000	17.66	9.509	5.745	0.756	0.459	0.278	0.281	2
HD 206739	107337	4647	1.70	-1.59	0.023	0.69	8.560	-2.246	0.969	0.601	0.193	0.433	3
HD 207978	107975	6252	4.10	-0.60	0.000	36.15	5.524	3.311	0.426	0.299	0.122	0.425	3
G 188-030	108200	5264	4.50	-1.99	0.007	10.60	11.000	6.197	0.676	0.457	0.114	0.128	2
HD 208787	108400	5958	2.00	0.00	0.007	12.11	7.897	3.306	0.520	0.343	0.164	0.411	3

Star ID	HIC	T_{eff}	log g	[Fe/H]	$E(b-y)$	π	V	M_V	$(B-V)_o$	$(b-y)_o$	m_o	c_o	Source
G 018-028	109067	5411	4.50	-0.84	0.000	21.52	9.556	6.214	0.672	0.423	0.180	0.223	2
HD 210334	109303	5261	2.00	-0.50	0.000	23.79	6.130	2.992	0.763	0.476	0.226	0.347	3
HD 210459	109410	6209	2.00	0.00	0.000	12.96	4.270	-0.157	0.471	0.303	0.178	0.776	3
HD 210460	109439	5304	4.50	-0.53	0.000	18.01	6.182	2.458	0.688	0.445	0.213	0.330	2
G 126-062	109558	5941	4.50	-1.80	0.000	8.43	9.478	4.089	0.459	0.329	0.070	0.337	2
HD 211391	110003	4956	2.80	-0.07	0.011	17.04	4.175	0.327	0.964	0.583	0.423	0.395	1
HD 211476	110035	5862	4.50	0.05	0.000	32.55	7.047	4.603	0.606	0.388	0.177	0.323	2
G 018-039	110140	5976	4.50	-1.34	0.000	3.97	10.392	3.374	0.489	0.346	0.073	0.286	2
HD 212943	110882	4588	1.05	-0.33	0.000	20.39	4.791	1.327	1.039	0.639	0.421	0.424	3
G 018-054	111195	5762	4.50	-1.52	0.000	8.99	10.712	5.479	0.520	0.366	0.075	0.275	2
HD 214362	111730	5727	2.50	-2.20	0.006	1.45	9.111	-0.093	0.497	0.364	0.062	0.594	3
G 067-008	111783	5273	4.50	-0.09	0.000	16.15	9.494	5.541	0.764	0.461	0.276	0.305	2
HD 215257	112229	5730	4.50	-0.90	0.000	23.66	7.411	4.280	0.515	0.355	0.119	0.306	2
HD 215664	112417	6711	2.00	0.00	0.000	18.79	5.800	2.210	0.358	0.222	0.178	0.731	3
HD 215648	112447	6085	4.00	-0.31	0.000	61.54	4.203	3.146	0.502	0.331	0.147	0.407	3
HD 216143	112796	4486	1.50	-2.20	0.013	3.14	7.825	0.285	0.934	0.675	0.161	0.564	3
HD 216777	113231	5592	4.50	-0.42	0.000	28.72	8.019	5.301	0.659	0.410	0.193	0.278	2
HD 217357	113576	3746	5.00	-1.50	0.000	122.80	7.849	8.326	1.379	0.798	0.700	0.057	2
HD 218502	114271	6296	3.75	-1.85	0.022	14.33	8.278	4.031	0.381	0.290	0.067	0.356	3
HD 218732	114426	4058	2.00	0.00	0.073	1.23	8.460	-1.090	1.490	0.977	0.455	0.593	3
HD 218804	114430	6116	4.10	-0.28	0.000	35.39	6.000	3.654	0.450	0.302	0.145	0.442	3
HD 219134	114622	4896	4.50	0.00	0.002	153.24	5.540	6.497	0.997	0.574	0.554	0.268	1
G 190-015	114661	5115	5.00	-3.00	0.007	14.09	11.021	6.765	0.679	0.471	0.065	0.079	2
HD 219617	114962	6012	5.00	-1.63	0.000	12.04	8.175	3.563	0.481	0.344	0.078	0.246	2
HD 219615	114971	4826	2.50	-0.44	0.000	24.92	3.699	0.683	0.916	0.561	0.306	0.431	3
HD 219571	114996	6530	3.93	-0.33	0.001	45.40	3.996	2.275	0.408	0.266	0.147	0.564	1
G 029-023	115167	6102	4.50	-2.02	0.000	3.26	10.230	2.776	0.456	0.339	0.059	0.332	2
HD 220657	115623	5897	3.92	-0.12	0.007	18.83	4.420	0.794	0.607	0.383	0.190	0.459	1
G 217-008	115704	6134	4.50	-1.91	0.007	8.85	10.487	5.225	0.459	0.323	0.067	0.254	2
HD 221170	115949	4410	1.10	-2.16	0.044	2.30	7.703	-0.521	0.967	0.703	0.140	0.554	3
HD 221503	116215	4101	5.00	0.00	0.000	71.70	8.583	7.868	1.290	0.723	0.756	0.065	2
G 190-034	116351	5318	4.50	-0.01	0.000	21.01	9.076	5.662	0.792	0.470	0.316	0.305	2
HD 221950	116495	6311	4.50	-0.70	0.000	32.27	5.689	3.224	0.449	0.305	0.124	0.389	2
HD 222107	116584	4578	2.80	-0.60	0.000	38.74	3.790	1.751	0.984	0.625	0.314	0.408	3
HD 222766	117041	5440	4.50	-0.90	0.000	8.46	10.112	4.747	0.671	0.426	0.190	0.244	2
HD 224342	118071	5520	2.00	0.00	0.037	2.26	6.000	-2.219	0.662	0.437	0.177	0.580	3

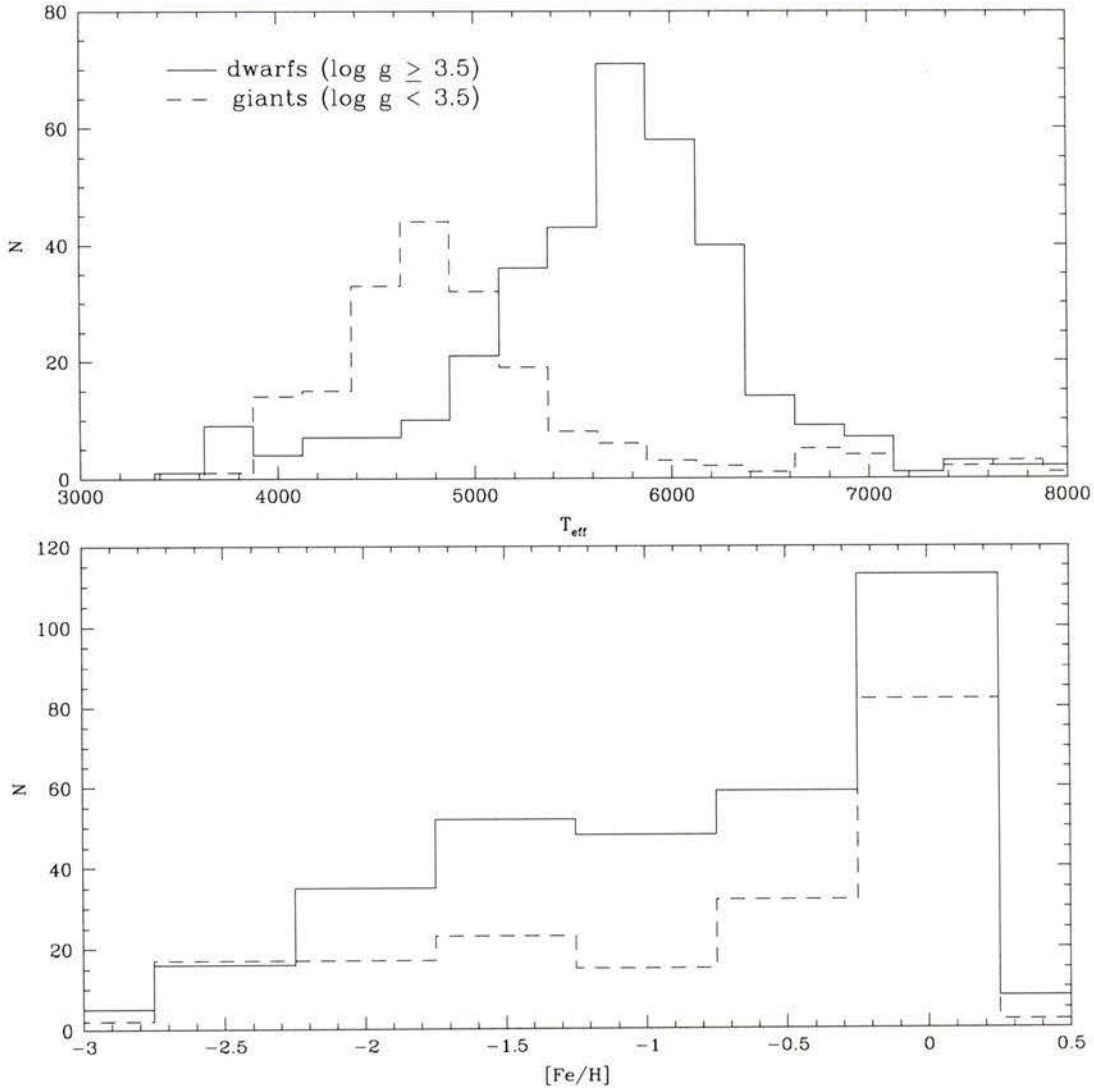

Figure A.1: Histograms showing the number distribution of field stars from Table A.1 in terms of T_{eff} and [Fe/H]. All dwarf stars in the sample are represented by the solid lines while dashed lines are the giant stars.

Appendix B

The Calibrated Strömgren Colors

The following appendix presents the entire Strömgren grid of colors calculated using the methods discussed in Chapter 2 and subsequently placed onto the observational system using the calibrations derived in Chapter 3. The Strömgren indices $(b-y)$, m_1, and c_1 are tabulated according to the effective temperatures, surface gravities, and metal abundances listed in each table.

Table B.1:

[M/H] = 0.5

T_{eff}	$\log g$	$(b-y)$	m_1	c_1
3000	5.00	1.249	1.081	0.367
3000	4.50	1.276	0.856	0.458
3000	4.00	1.291	0.758	0.484
3000	3.50	1.302	0.724	0.510
3000	3.00	1.315	0.735	0.539
3000	2.50	1.336	0.791	0.546
3000	2.00	1.369	0.851	0.559
3000	1.50	1.368	0.972	0.571
3000	1.00	1.379	1.136	0.516
3000	0.50	1.434	1.274	0.367
3000	0.00	1.520	1.407	0.172
3250	5.00	1.157	0.771	0.440
3250	4.50	1.161	0.702	0.432
3250	4.00	1.167	0.668	0.459
3250	3.50	1.177	0.647	0.502
3250	3.00	1.187	0.678	0.525
3250	2.50	1.175	0.752	0.545
3250	2.00	1.187	0.830	0.559
3250	1.50	1.231	0.931	0.539
3250	1.00	1.294	1.061	0.487
3250	0.50	1.368	1.189	0.470
3250	0.00	1.450	1.323	0.258
3500	5.00	1.050	0.715	0.454
3500	4.50	1.052	0.691	0.418
3500	4.00	1.056	0.674	0.418
3500	3.50	1.039	0.692	0.423
3500	3.00	1.040	0.708	0.455
3500	2.50	1.071	0.739	0.460
3500	2.00	1.109	0.800	0.450
3500	1.50	1.154	0.910	0.422
3500	1.00	1.204	1.025	0.420
3500	0.50	1.257	1.171	0.423
3500	0.00	1.308	1.286	0.410
3750	5.00	0.957	0.725	0.140
3750	4.50	0.948	0.708	0.159
3750	4.00	0.926	0.722	0.167
3750	3.50	0.935	0.716	0.186
3750	3.00	0.959	0.719	0.201
3750	2.50	0.987	0.752	0.210
3750	2.00	1.018	0.805	0.224
3750	1.50	1.054	0.892	0.232
3750	1.00	1.093	1.014	0.222
3750	0.50	1.135	1.125	0.252
3750	0.00	1.178	1.198	0.254
4000	5.00	0.856	0.776	-0.039
4000	4.50	0.832	0.780	0.008
4000	4.00	0.838	0.765	0.070
4000	3.50	0.856	0.744	0.123
4000	3.00	0.876	0.734	0.176
4000	2.50	0.898	0.760	0.208
4000	2.00	0.924	0.815	0.216
4000	1.50	0.956	0.886	0.196
4000	1.00	0.992	0.975	0.156
4000	0.50	1.035	1.068	0.123
4000	0.00	1.082	1.135	0.085
4250	5.00	0.749	0.838	0.043
4250	4.50	0.750	0.810	0.089
4250	4.00	0.761	0.787	0.140
4250	3.50	0.775	0.758	0.189
4250	3.00	0.792	0.753	0.239
4250	2.50	0.813	0.759	0.262
4250	2.00	0.839	0.784	0.259
4250	1.50	0.871	0.832	0.242
4250	1.00	0.909	0.882	0.217
4250	0.50	0.952	0.938	0.185
4250	0.00	0.999	0.972	0.161
4500	5.00	0.670	0.826	0.126
4500	4.50	0.677	0.798	0.168
4500	4.00	0.687	0.759	0.220
4500	3.50	0.701	0.717	0.261
4500	3.00	0.720	0.689	0.288
4500	2.50	0.743	0.682	0.293
4500	2.00	0.770	0.705	0.287
4500	1.50	0.800	0.738	0.273
4500	1.00	0.832	0.777	0.254
4500	0.50	0.866	0.818	0.240
4500	0.00	0.900	0.853	0.222
4750	5.00	0.600	0.723	0.200
4750	4.50	0.615	0.677	0.243
4750	4.00	0.631	0.614	0.284
4750	3.50	0.649	0.580	0.312
4750	3.00	0.666	0.572	0.322
4750	2.50	0.688	0.564	0.325
4750	2.00	0.706	0.592	0.319
4750	1.50	0.728	0.621	0.313
4750	1.00	0.750	0.655	0.304
4750	0.50	0.771	0.693	0.293
4750	0.00	0.791	0.740	0.283
5000	5.00	0.544	0.593	0.278
5000	4.50	0.557	0.548	0.308
5000	4.00	0.573	0.508	0.332
5000	3.50	0.590	0.476	0.350
5000	3.00	0.606	0.460	0.360
5000	2.50	0.621	0.460	0.364
5000	2.00	0.634	0.459	0.365
5000	1.50	0.645	0.492	0.364
5000	1.00	0.654	0.538	0.362
5000	0.50	0.662	0.592	0.363
5000	0.00	0.669	0.651	0.362
5250	5.00	0.498	0.464	0.322
5250	4.50	0.512	0.434	0.343
5250	4.00	0.526	0.401	0.370
5250	3.50	0.538	0.374	0.382
5250	3.00	0.545	0.361	0.391
5250	2.50	0.549	0.372	0.397
5250	2.00	0.551	0.397	0.402
5250	1.50	0.553	0.417	0.405
5250	1.00	0.554	0.463	0.406
5250	0.50	0.555	0.515	0.407
5250	0.00	0.556	0.579	0.407
5500	5.00	0.460	0.359	0.357
5500	4.50	0.472	0.328	0.380
5500	4.00	0.479	0.309	0.406
5500	3.50	0.481	0.300	0.430
5500	3.00	0.480	0.301	0.447
5500	2.50	0.477	0.316	0.460
5500	2.00	0.474	0.319	0.470
5500	1.50	0.471	0.345	0.472
5500	1.00	0.467	0.389	0.470
5500	0.50	0.462	0.437	0.468
5500	0.00	0.456	0.494	0.466
5750	5.00	0.421	0.286	0.371
5750	4.50	0.427	0.260	0.396
5750	4.00	0.428	0.245	0.424
5750	3.50	0.425	0.243	0.449
5750	3.00	0.420	0.251	0.467
5750	2.50	0.413	0.267	0.484
5750	2.00	0.405	0.289	0.494
5750	1.50	0.398	0.298	0.496
5750	1.00	0.389	0.333	0.494
5750	0.50	0.379	0.369	0.492
5750	0.00	0.366	0.411	0.491
6000	5.00	0.383	0.236	0.383
6000	4.50	0.385	0.215	0.416
6000	4.00	0.381	0.208	0.445
6000	3.50	0.374	0.214	0.469
6000	3.00	0.365	0.225	0.493
6000	2.50	0.355	0.241	0.512
6000	2.00	0.346	0.258	0.522
6000	1.50	0.335	0.273	0.524
6000	1.00	0.320	0.299	0.522
6000	0.50	0.306	0.326	0.519
6000	0.00	0.286	0.360	0.515
6250	5.00	0.346	0.213	0.409
6250	4.50	0.345	0.197	0.449
6250	4.00	0.340	0.192	0.486
6250	3.50	0.331	0.196	0.521
6250	3.00	0.319	0.209	0.553
6250	2.50	0.308	0.222	0.579
6250	2.00	0.295	0.241	0.603
6500	5.00	0.311	0.200	0.431
6500	4.50	0.310	0.188	0.486
6500	4.00	0.304	0.183	0.539
6500	3.50	0.294	0.188	0.589
6500	3.00	0.281	0.198	0.636
6500	2.50	0.266	0.213	0.677
6500	2.00	0.249	0.232	0.705
6750	5.00	0.279	0.190	0.455
6750	4.50	0.276	0.180	0.527
6750	4.00	0.269	0.178	0.599
6750	3.50	0.257	0.183	0.661
6750	3.00	0.242	0.192	0.733
6750	2.50	0.223	0.205	0.801
6750	2.00	0.200	0.222	0.855
7000	5.00	0.250	0.183	0.480
7000	4.50	0.245	0.177	0.578
7000	4.00	0.236	0.177	0.668
7000	3.50	0.221	0.182	0.756
7000	3.00	0.202	0.191	0.842
7000	2.50	0.179	0.199	0.919
7000	2.00	0.153	0.210	0.983
7250	5.00	0.222	0.183	0.515
7250	4.50	0.215	0.178	0.636
7250	4.00	0.202	0.179	0.740
7250	3.50	0.185	0.185	0.844
7250	3.00	0.162	0.198	0.932
7250	2.50	0.135	0.201	1.016
7250	2.00	0.119	0.179	1.083
7500	5.00	0.196	0.186	0.548
7500	4.50	0.186	0.183	0.702
7500	4.00	0.170	0.184	0.821
7500	3.50	0.149	0.187	0.936
7500	3.00	0.122	0.196	1.031
7500	2.50	0.103	0.184	1.109
7500	2.00	0.091	0.161	1.176
7750	5.00	0.171	0.189	0.570
7750	4.50	0.157	0.187	0.742
7750	4.00	0.138	0.186	0.890
7750	3.50	0.111	0.189	1.026
7750	3.00	0.090	0.176	1.143
7750	2.50	0.077	0.158	1.225
7750	2.00	0.068	0.138	1.280
8000	5.00	0.146	0.195	0.600
8000	4.50	0.129	0.194	0.773
8000	4.00	0.104	0.192	0.967
8000	3.50	0.083	0.177	1.123
8000	3.00	0.067	0.159	1.249
8000	2.50	0.056	0.138	1.337
8000	2.00	0.049	0.117	1.386

[M/H] = 0.0

T_{eff}	log g	$(b-y)$	m_1	c_1
3000.	5.00	1.320	1.124	-0.241
3000.	4.50	1.320	0.968	-0.167
3000.	4.00	1.330	0.804	-0.082
3000.	3.50	1.335	0.745	-0.004
3000.	3.00	1.343	0.737	0.063
3000.	2.50	1.358	0.784	0.117
3000.	2.00	1.388	0.869	0.139
3000.	1.50	1.426	0.948	0.126
3000.	1.00	1.440	1.067	0.083
3000.	0.50	1.487	1.140	0.027
3000.	0.00	1.574	1.168	-0.011
3250.	5.00	1.198	0.864	-0.184
3250.	4.50	1.196	0.750	-0.108
3250.	4.00	1.198	0.682	-0.029
3250.	3.50	1.204	0.665	0.035
3250.	3.00	1.214	0.679	0.091
3250.	2.50	1.223	0.724	0.139
3250.	2.00	1.219	0.816	0.163
3250.	1.50	1.252	0.914	0.152
3250.	1.00	1.307	1.002	0.112
3250.	0.50	1.376	1.055	0.058
3250.	0.00	1.452	1.086	0.022
3500.	5.00	1.086	0.271	0.520
3500.	4.50	1.085	0.305	0.528
3500.	4.00	1.088	0.363	0.507
3500.	3.50	1.088	0.462	0.471
3500.	3.00	1.069	0.608	0.426
3500.	2.50	1.076	0.717	0.378
3500.	2.00	1.108	0.810	0.363
3500.	1.50	1.148	0.889	0.321
3500.	1.00	1.194	0.992	0.223
3500.	0.50	1.245	1.090	0.119
3500.	0.00	1.304	1.141	0.049
3750.	5.00	0.988	0.467	0.366
3750.	4.50	0.986	0.469	0.406
3750.	4.00	0.973	0.519	0.411
3750.	3.50	0.945	0.601	0.415
3750.	3.00	0.954	0.649	0.427
3750.	2.50	0.978	0.734	0.397
3750.	2.00	1.006	0.826	0.368
3750.	1.50	1.037	0.911	0.326
3750.	1.00	1.072	1.009	0.239
3750.	0.50	1.113	1.105	0.160
3750.	0.00	1.165	1.194	0.069
4000.	5.00	0.889	0.713	0.101
4000.	4.50	0.861	0.708	0.171
4000.	4.00	0.843	0.702	0.245
4000.	3.50	0.846	0.708	0.294
4000.	3.00	0.865	0.726	0.321
4000.	2.50	0.885	0.768	0.333
4000.	2.00	0.908	0.825	0.311
4000.	1.50	0.935	0.908	0.270
4000.	1.00	0.970	0.995	0.211
4000.	0.50	1.009	1.078	0.143
4000.	0.00	1.056	1.147	0.076
4250.	5.00	0.768	0.794	0.028
4250.	4.50	0.750	0.780	0.099
4250.	4.00	0.752	0.756	0.162
4250.	3.50	0.766	0.739	0.215
4250.	3.00	0.783	0.730	0.247
4250.	2.50	0.799	0.738	0.280
4250.	2.00	0.821	0.761	0.286
4250.	1.50	0.849	0.805	0.276
4250.	1.00	0.881	0.845	0.269
4250.	0.50	0.915	0.894	0.259
4250.	0.00	0.963	0.922	0.243
4500.	5.00	0.659	0.712	0.094
4500.	4.50	0.660	0.677	0.161
4500.	4.00	0.674	0.640	0.221
4500.	3.50	0.689	0.617	0.270
4500.	3.00	0.707	0.607	0.309
4500.	2.50	0.726	0.612	0.331
4500.	2.00	0.748	0.629	0.337
4500.	1.50	0.771	0.668	0.331
4500.	1.00	0.797	0.700	0.315
4500.	0.50	0.828	0.732	0.305
4500.	0.00	0.865	0.757	0.291
4750.	5.00	0.585	0.593	0.171
4750.	4.50	0.595	0.559	0.222
4750.	4.00	0.609	0.526	0.274
4750.	3.50	0.626	0.502	0.315
4750.	3.00	0.642	0.493	0.348
4750.	2.50	0.658	0.493	0.373
4750.	2.00	0.674	0.504	0.375
4750.	1.50	0.691	0.529	0.367
4750.	1.00	0.714	0.562	0.357
4750.	0.50	0.739	0.599	0.344
4750.	0.00	0.770	0.628	0.330
5000.	5.00	0.529	0.473	0.225
5000.	4.50	0.539	0.443	0.269
5000.	4.00	0.552	0.414	0.316
5000.	3.50	0.564	0.391	0.353
5000.	3.00	0.576	0.380	0.379
5000.	2.50	0.587	0.383	0.389
5000.	2.00	0.597	0.394	0.392
5000.	1.50	0.608	0.423	0.387
5000.	1.00	0.621	0.457	0.377
5000.	0.50	0.637	0.493	0.367
5000.	0.00	0.658	0.537	0.348
5250	5.00	0.487	0.367	0.248
5250	4.50	0.495	0.341	0.298
5250	4.00	0.505	0.317	0.338
5250	3.50	0.514	0.296	0.374
5250	3.00	0.520	0.287	0.394
5250	2.50	0.524	0.291	0.406
5250	2.00	0.526	0.311	0.409
5250	1.50	0.529	0.340	0.403
5250	1.00	0.534	0.376	0.397
5250	0.50	0.543	0.410	0.388
5250	0.00	0.557	0.445	0.370
5500	5.00	0.449	0.287	0.254
5500	4.50	0.455	0.264	0.308
5500	4.00	0.460	0.244	0.354
5500	3.50	0.464	0.230	0.392
5500	3.00	0.465	0.228	0.410
5500	2.50	0.463	0.236	0.423
5500	2.00	0.461	0.254	0.428
5500	1.50	0.460	0.279	0.426
5500	1.00	0.460	0.308	0.418
5500	0.50	0.462	0.341	0.404
5500	0.00	0.467	0.371	0.390
5750	5.00	0.413	0.234	0.262
5750	4.50	0.416	0.213	0.320
5750	4.00	0.417	0.201	0.371
5750	3.50	0.417	0.192	0.415
5750	3.00	0.415	0.194	0.444
5750	2.50	0.410	0.202	0.468
5750	2.00	0.404	0.218	0.482
5750	1.50	0.398	0.238	0.496
5750	1.00	0.393	0.259	0.498
5750	0.50	0.388	0.281	0.496
5750	0.00	0.380	0.313	0.486
6000	5.00	0.378	0.203	0.267
6000	4.50	0.379	0.181	0.330
6000	4.00	0.379	0.171	0.396
6000	3.50	0.377	0.166	0.449
6000	3.00	0.372	0.167	0.490
6000	2.50	0.365	0.175	0.528
6000	2.00	0.356	0.190	0.563
6000	1.50	0.346	0.205	0.595
6000	1.00	0.337	0.222	0.623
6000	0.50	0.324	0.244	0.648
6000	0.00	0.310	0.268	0.670
6250	5.00	0.343	0.179	0.278
6250	4.50	0.343	0.163	0.346
6250	4.00	0.342	0.152	0.414
6250	3.50	0.339	0.147	0.487
6250	3.00	0.334	0.146	0.546
6250	2.50	0.325	0.155	0.599
6250	2.00	0.314	0.170	0.652
6500	5.00	0.313	0.171	0.299
6500	4.50	0.310	0.157	0.371
6500	4.00	0.308	0.148	0.455
6500	3.50	0.305	0.142	0.537
6500	3.00	0.298	0.143	0.607
6500	2.50	0.287	0.150	0.683
6500	2.00	0.272	0.164	0.745
6750	5.00	0.284	0.170	0.335
6750	4.50	0.279	0.159	0.416
6750	4.00	0.276	0.150	0.504
6750	3.50	0.270	0.148	0.603
6750	3.00	0.260	0.151	0.682
6750	2.50	0.245	0.157	0.759
6750	2.00	0.226	0.167	0.824
7000	5.00	0.256	0.171	0.389
7000	4.50	0.252	0.162	0.478
7000	4.00	0.245	0.157	0.574
7000	3.50	0.236	0.152	0.675
7000	3.00	0.222	0.156	0.766
7000	2.50	0.203	0.161	0.856
7000	2.00	0.176	0.169	0.928
7250	5.00	0.232	0.175	0.447
7250	4.50	0.225	0.167	0.546
7250	4.00	0.215	0.162	0.653
7250	3.50	0.200	0.163	0.761
7250	3.00	0.182	0.163	0.859
7250	2.50	0.158	0.162	0.954
7250	2.00	0.136	0.149	1.049
7500	5.00	0.208	0.177	0.510
7500	4.50	0.198	0.173	0.611
7500	4.00	0.183	0.171	0.724
7500	3.50	0.165	0.172	0.844
7500	3.00	0.142	0.166	0.953
7500	2.50	0.121	0.154	1.055
7500	2.00	0.108	0.132	1.146
7750	5.00	0.183	0.184	0.577
7750	4.50	0.171	0.182	0.692
7750	4.00	0.150	0.179	0.817
7750	3.50	0.131	0.172	0.939
7750	3.00	0.111	0.160	1.055
7750	2.50	0.095	0.142	1.163
7750	2.00	0.087	0.121	1.233
8000	5.00	0.165	0.188	0.639
8000	4.50	0.146	0.190	0.780
8000	4.00	0.121	0.191	0.909
8000	3.50	0.098	0.178	1.039
8000	3.00	0.085	0.156	1.161
8000	2.50	0.076	0.134	1.264
8000	2.00	0.071	0.112	1.330

[M/H] = −0.5

T_{eff}	log g	$(b-y)$	m_1	c_1
3000	5.00	1.315	0.948	-0.221
3000	4.50	1.315	0.794	-0.094
3000	4.00	1.311	0.676	-0.010
3000	3.50	1.306	0.587	0.068
3000	3.00	1.308	0.565	0.109
3000	2.50	1.319	0.562	0.134
3000	2.00	1.341	0.605	0.155
3000	1.50	1.389	0.661	0.136
3000	1.00	1.432	0.733	0.126
3000	0.50	1.488	0.781	0.132
3000	0.00	1.582	0.783	0.169
3250	5.00	1.189	0.666	-0.198
3250	4.50	1.177	0.538	-0.049
3250	4.00	1.169	0.480	0.048
3250	3.50	1.169	0.468	0.096
3250	3.00	1.174	0.490	0.125
3250	2.50	1.186	0.508	0.154
3250	2.00	1.190	0.580	0.163
3250	1.50	1.206	0.651	0.157
3250	1.00	1.266	0.704	0.183
3250	0.50	1.346	0.739	0.199
3250	0.00	1.435	0.746	0.246
3500	5.00	1.065	0.550	-0.161
3500	4.50	1.058	0.500	-0.066
3500	4.00	1.055	0.485	-0.003
3500	3.50	1.054	0.479	0.057
3500	3.00	1.045	0.514	0.093
3500	2.50	1.022	0.586	0.111
3500	2.00	1.044	0.637	0.115
3500	1.50	1.089	0.697	0.108
3500	1.00	1.145	0.754	0.142
3500	0.50	1.211	0.808	0.159
3500	0.00	1.287	0.821	0.214
3750	5.00	0.960	0.529	-0.009
3750	4.50	0.954	0.505	0.056
3750	4.00	0.944	0.492	0.126
3750	3.50	0.914	0.529	0.166
3750	3.00	0.889	0.579	0.203
3750	2.50	0.905	0.612	0.172
3750	2.00	0.935	0.654	0.194
3750	1.50	0.971	0.719	0.204
3750	1.00	1.013	0.796	0.204
3750	0.50	1.066	0.881	0.210
3750	0.00	1.132	0.924	0.222
4000	5.00	0.857	0.561	0.004
4000	4.50	0.836	0.544	0.043
4000	4.00	0.797	0.564	0.082
4000	3.50	0.778	0.575	0.123
4000	3.00	0.787	0.586	0.169
4000	2.50	0.802	0.616	0.202
4000	2.00	0.822	0.650	0.228
4000	1.50	0.849	0.714	0.245
4000	1.00	0.887	0.781	0.247
4000	0.50	0.938	0.837	0.257
4000	0.00	1.005	0.861	0.274
4250	5.00	0.736	0.607	0.036
4250	4.50	0.698	0.602	0.094
4250	4.00	0.681	0.586	0.144
4250	3.50	0.684	0.568	0.199
4250	3.00	0.692	0.562	0.248
4250	2.50	0.706	0.568	0.280
4250	2.00	0.725	0.595	0.304
4250	1.50	0.751	0.629	0.325
4250	1.00	0.788	0.673	0.343
4250	0.50	0.837	0.714	0.362
4250	0.00	0.901	0.737	0.381
4500	5.00	0.615	0.593	0.151
4500	4.50	0.601	0.552	0.200
4500	4.00	0.600	0.508	0.247
4500	3.50	0.605	0.483	0.279
4500	3.00	0.615	0.464	0.302
4500	2.50	0.632	0.459	0.329
4500	2.00	0.651	0.471	0.353
4500	1.50	0.676	0.495	0.379
4500	1.00	0.708	0.525	0.404
4500	0.50	0.749	0.559	0.429
4500	0.00	0.801	0.584	0.456
4750	5.00	0.538	0.488	0.208
4750	4.50	0.536	0.440	0.245
4750	4.00	0.538	0.399	0.277
4750	3.50	0.544	0.374	0.312
4750	3.00	0.555	0.357	0.344
4750	2.50	0.571	0.354	0.379
4750	2.00	0.589	0.364	0.415
4750	1.50	0.610	0.379	0.459
4750	1.00	0.636	0.402	0.508
4750	0.50	0.668	0.430	0.561
4750	0.00	0.707	0.453	0.613
5000	5.00	0.487	0.370	0.238
5000	4.50	0.488	0.335	0.267
5000	4.00	0.490	0.309	0.302
5000	3.50	0.495	0.288	0.331
5000	3.00	0.504	0.273	0.374
5000	2.50	0.515	0.266	0.422
5000	2.00	0.529	0.274	0.481
5000	1.50	0.544	0.295	0.553
5000	1.00	0.562	0.317	0.619
5000	0.50	0.584	0.348	0.689
5000	0.00	0.613	0.379	0.759
5250	5.00	0.447	0.287	0.250
5250	4.50	0.448	0.258	0.278
5250	4.00	0.449	0.237	0.314
5250	3.50	0.452	0.219	0.351
5250	3.00	0.456	0.210	0.407
5250	2.50	0.463	0.208	0.478
5250	2.00	0.472	0.215	0.564
5250	1.50	0.482	0.231	0.655
5250	1.00	0.492	0.253	0.749
5250	0.50	0.506	0.279	0.852
5250	0.00	0.523	0.307	0.953
5500	5.00	0.411	0.220	0.260
5500	4.50	0.411	0.196	0.289
5500	4.00	0.411	0.178	0.327
5500	3.50	0.411	0.168	0.383
5500	3.00	0.412	0.166	0.448
5500	2.50	0.415	0.172	0.534
5500	2.00	0.419	0.181	0.620
5500	1.50	0.423	0.195	0.728
5500	1.00	0.427	0.213	0.839
5500	0.50	0.433	0.238	0.948
5500	0.00	0.440	0.264	1.060
5750	5.00	0.376	0.173	0.269
5750	4.50	0.375	0.153	0.307
5750	4.00	0.374	0.139	0.356
5750	3.50	0.372	0.131	0.417
5750	3.00	0.370	0.129	0.493
5750	2.50	0.370	0.131	0.581
5750	2.00	0.369	0.139	0.694
5750	1.50	0.367	0.152	0.803
5750	1.00	0.366	0.167	0.908
5750	0.50	0.365	0.184	1.028
5750	0.00	0.366	0.206	1.144
6000	5.00	0.345	0.144	0.280
6000	4.50	0.343	0.128	0.329
6000	4.00	0.339	0.117	0.398
6000	3.50	0.335	0.111	0.473
6000	3.00	0.332	0.108	0.559
6000	2.50	0.329	0.109	0.652
6000	2.00	0.325	0.115	0.753
6000	1.50	0.319	0.127	0.867
6000	1.00	0.313	0.143	1.010
6000	0.50	0.305	0.160	1.148
6000	0.00	0.298	0.176	1.278
6250	5.00	0.315	0.130	0.290
6250	4.50	0.311	0.117	0.354
6250	4.00	0.305	0.110	0.449
6250	3.50	0.300	0.103	0.545
6250	3.00	0.297	0.097	0.641
6250	2.50	0.293	0.096	0.739
6250	2.00	0.287	0.099	0.824
6500	5.00	0.288	0.118	0.322
6500	4.50	0.281	0.109	0.410
6500	4.00	0.274	0.103	0.518
6500	3.50	0.269	0.098	0.622
6500	3.00	0.265	0.092	0.733
6500	2.50	0.259	0.091	0.835
6500	2.00	0.250	0.094	0.917
6750	5.00	0.260	0.114	0.353
6750	4.50	0.251	0.110	0.463
6750	4.00	0.242	0.107	0.589
6750	3.50	0.236	0.103	0.713
6750	3.00	0.230	0.099	0.830
6750	2.50	0.221	0.097	0.940
6750	2.00	0.207	0.098	1.022
7000	5.00	0.233	0.116	0.401
7000	4.50	0.222	0.116	0.524
7000	4.00	0.211	0.114	0.665
7000	3.50	0.204	0.109	0.814
7000	3.00	0.194	0.107	0.946
7000	2.50	0.181	0.105	1.062
7000	2.00	0.158	0.105	1.145
7250	5.00	0.206	0.125	0.452
7250	4.50	0.195	0.125	0.597
7250	4.00	0.183	0.124	0.753
7250	3.50	0.173	0.120	0.924
7250	3.00	0.160	0.114	1.061
7250	2.50	0.138	0.111	1.186
7250	2.00	0.113	0.103	1.265
7500	5.00	0.181	0.135	0.511
7500	4.50	0.169	0.134	0.670
7500	4.00	0.157	0.130	0.838
7500	3.50	0.144	0.125	1.016
7500	3.00	0.122	0.120	1.179
7500	2.50	0.097	0.116	1.310
7500	2.00	0.083	0.101	1.408
7750	5.00	0.157	0.145	0.588
7750	4.50	0.147	0.142	0.759
7750	4.00	0.131	0.139	0.916
7750	3.50	0.111	0.134	1.108
7750	3.00	0.085	0.123	1.276
7750	2.50	0.070	0.107	1.415
7750	2.00	0.062	0.088	1.503
8000	5.00	0.141	0.150	0.663
8000	4.50	0.126	0.147	0.842
8000	4.00	0.104	0.143	1.003
8000	3.50	0.077	0.136	1.197
8000	3.00	0.061	0.117	1.383
8000	2.50	0.052	0.097	1.512
8000	2.00	0.047	0.076	1.613

T_{eff}	$\log g$	$(b-y)$	m_1	c_1
		[M/H] = −1.0		
3000	5.00	1.351	0.880	-0.083
3000	4.50	1.346	0.710	0.021
3000	4.00	1.337	0.560	0.138
3000	3.50	1.328	0.484	0.195
3000	3.00	1.325	0.458	0.237
3000	2.50	1.333	0.470	0.307
3000	2.00	1.352	0.532	0.383
3000	1.50	1.389	0.603	0.414
3000	1.00	1.460	0.639	0.422
3000	0.50	1.526	0.649	0.435
3000	0.00	1.621	0.622	0.432
3250	5.00	1.214	0.603	0.191
3250	4.50	1.197	0.480	0.268
3250	4.00	1.185	0.399	0.309
3250	3.50	1.181	0.382	0.305
3250	3.00	1.185	0.406	0.276
3250	2.50	1.197	0.447	0.283
3250	2.00	1.218	0.507	0.316
3250	1.50	1.231	0.592	0.359
3250	1.00	1.277	0.651	0.404
3250	0.50	1.359	0.636	0.456
3250	0.00	1.454	0.594	0.518
3500	5.00	1.078	0.467	0.235
3500	4.50	1.067	0.399	0.283
3500	4.00	1.062	0.359	0.303
3500	3.50	1.062	0.370	0.272
3500	3.00	1.063	0.420	0.212
3500	2.50	1.051	0.493	0.208
3500	2.00	1.044	0.573	0.246
3500	1.50	1.083	0.636	0.285
3500	1.00	1.143	0.673	0.338
3500	0.50	1.216	0.707	0.392
3500	0.00	1.300	0.676	0.485
3750	5.00	0.963	0.416	0.277
3750	4.50	0.956	0.385	0.286
3750	4.00	0.949	0.377	0.286
3750	3.50	0.934	0.404	0.262
3750	3.00	0.898	0.475	0.234
3750	2.50	0.896	0.528	0.246
3750	2.00	0.920	0.580	0.290
3750	1.50	0.954	0.634	0.341
3750	1.00	0.999	0.676	0.396
3750	0.50	1.057	0.732	0.454
3750	0.00	1.133	0.737	0.521
4000	5.00	0.856	0.432	0.252
4000	4.50	0.841	0.426	0.240
4000	4.00	0.810	0.445	0.227
4000	3.50	0.775	0.480	0.220
4000	3.00	0.775	0.496	0.233
4000	2.50	0.786	0.521	0.263
4000	2.00	0.802	0.555	0.312
4000	1.50	0.827	0.604	0.377
4000	1.00	0.865	0.652	0.442
4000	0.50	0.921	0.679	0.503
4000	0.00	0.999	0.665	0.584
4250	5.00	0.740	0.448	0.208
4250	4.50	0.705	0.451	0.215
4250	4.00	0.675	0.465	0.215
4250	3.50	0.672	0.459	0.217
4250	3.00	0.677	0.462	0.216
4250	2.50	0.686	0.468	0.257
4250	2.00	0.703	0.488	0.327
4250	1.50	0.728	0.511	0.407
4250	1.00	0.763	0.538	0.489
4250	0.50	0.815	0.562	0.571
4250	0.00	0.885	0.565	0.662
4500	5.00	0.621	0.429	0.140
4500	4.50	0.597	0.418	0.162
4500	4.00	0.593	0.404	0.175
4500	3.50	0.594	0.397	0.187
4500	3.00	0.601	0.394	0.215
4500	2.50	0.612	0.393	0.276
4500	2.00	0.627	0.401	0.354
4500	1.50	0.650	0.414	0.443
4500	1.00	0.682	0.422	0.524
4500	0.50	0.724	0.436	0.610
4500	0.00	0.781	0.445	0.694
4750	5.00	0.539	0.354	0.148
4750	4.50	0.538	0.325	0.171
4750	4.00	0.539	0.308	0.191
4750	3.50	0.540	0.301	0.215
4750	3.00	0.543	0.300	0.248
4750	2.50	0.552	0.300	0.321
4750	2.00	0.565	0.304	0.400
4750	1.50	0.584	0.311	0.477
4750	1.00	0.609	0.319	0.556
4750	0.50	0.640	0.329	0.647
4750	0.00	0.680	0.337	0.745
5000	5.00	0.494	0.262	0.157
5000	4.50	0.493	0.239	0.181
5000	4.00	0.493	0.224	0.207
5000	3.50	0.493	0.218	0.240
5000	3.00	0.495	0.219	0.287
5000	2.50	0.499	0.224	0.358
5000	2.00	0.508	0.228	0.432
5000	1.50	0.521	0.237	0.514
5000	1.00	0.538	0.248	0.605
5000	0.50	0.560	0.259	0.706
5000	0.00	0.586	0.270	0.808
5250	5.00	0.449	0.209	0.167
5250	4.50	0.448	0.189	0.194
5250	4.00	0.448	0.177	0.226
5250	3.50	0.447	0.172	0.272
5250	3.00	0.447	0.173	0.331
5250	2.50	0.450	0.176	0.409
5250	2.00	0.456	0.180	0.498
5250	1.50	0.465	0.186	0.607
5250	1.00	0.475	0.196	0.711
5250	0.50	0.485	0.208	0.824
5250	0.00	0.496	0.225	0.944
5500	5.00	0.414	0.164	0.180
5500	4.50	0.412	0.149	0.202
5500	4.00	0.410	0.139	0.250
5500	3.50	0.408	0.133	0.308
5500	3.00	0.406	0.133	0.389
5500	2.50	0.405	0.137	0.491
5500	2.00	0.405	0.144	0.603
5500	1.50	0.406	0.155	0.721
5500	1.00	0.409	0.164	0.845
5500	0.50	0.412	0.175	0.972
5500	0.00	0.416	0.188	1.115
5750	5.00	0.381	0.130	0.189
5750	4.50	0.377	0.118	0.220
5750	4.00	0.373	0.109	0.283
5750	3.50	0.369	0.106	0.367
5750	3.00	0.365	0.104	0.467
5750	2.50	0.362	0.104	0.595
5750	2.00	0.359	0.110	0.718
5750	1.50	0.357	0.118	0.859
5750	1.00	0.354	0.128	0.998
5750	0.50	0.352	0.139	1.143
5750	0.00	0.347	0.154	1.287
6000	5.00	0.349	0.108	0.198
6000	4.50	0.344	0.098	0.253
6000	4.00	0.339	0.092	0.335
6000	3.50	0.334	0.086	0.441
6000	3.00	0.328	0.084	0.569
6000	2.50	0.323	0.084	0.715
6000	2.00	0.318	0.088	0.863
6000	1.50	0.312	0.096	1.018
6000	1.00	0.305	0.107	1.163
6000	0.50	0.297	0.120	1.313
6000	0.00	0.285	0.139	1.451
6250	5.00	0.321	0.097	0.215
6250	4.50	0.313	0.091	0.292
6250	4.00	0.305	0.086	0.398
6250	3.50	0.300	0.079	0.525
6250	3.00	0.291	0.079	0.664
6250	2.50	0.285	0.077	0.812
6250	2.00	0.278	0.078	0.970
6500	5.00	0.293	0.088	0.253
6500	4.50	0.285	0.083	0.356
6500	4.00	0.277	0.081	0.483
6500	3.50	0.267	0.080	0.625
6500	3.00	0.259	0.078	0.775
6500	2.50	0.252	0.074	0.937
6500	2.00	0.245	0.071	1.112
6750	5.00	0.267	0.085	0.306
6750	4.50	0.257	0.086	0.431
6750	4.00	0.246	0.086	0.575
6750	3.50	0.236	0.085	0.728
6750	3.00	0.226	0.083	0.892
6750	2.50	0.216	0.080	1.071
6750	2.00	0.206	0.074	1.261
7000	5.00	0.241	0.091	0.369
7000	4.50	0.229	0.093	0.510
7000	4.00	0.215	0.096	0.663
7000	3.50	0.203	0.095	0.828
7000	3.00	0.192	0.091	1.007
7000	2.50	0.179	0.085	1.201
7000	2.00	0.162	0.076	1.402
7250	5.00	0.216	0.100	0.436
7250	4.50	0.200	0.104	0.586
7250	4.00	0.186	0.106	0.748
7250	3.50	0.172	0.106	0.927
7250	3.00	0.158	0.100	1.119
7250	2.50	0.141	0.091	1.322
7250	2.00	0.119	0.078	1.541
7500	5.00	0.190	0.113	0.501
7500	4.50	0.173	0.118	0.660
7500	4.00	0.157	0.119	0.834
7500	3.50	0.142	0.114	1.024
7500	3.00	0.124	0.105	1.225
7500	2.50	0.104	0.092	1.443
7500	2.00	0.085	0.079	1.609
7750	5.00	0.164	0.128	0.593
7750	4.50	0.148	0.129	0.752
7750	4.00	0.131	0.127	0.937
7750	3.50	0.113	0.122	1.135
7750	3.00	0.091	0.112	1.327
7750	2.50	0.073	0.093	1.502
7750	2.00	0.066	0.074	1.645
8000	5.00	0.143	0.139	0.662
8000	4.50	0.125	0.139	0.840
8000	4.00	0.105	0.134	1.031
8000	3.50	0.083	0.126	1.217
8000	3.00	0.063	0.109	1.399
8000	2.50	0.053	0.089	1.552
8000	2.00	0.048	0.069	1.668

[M/H] = −1.5

T_{eff}	log g	$(b-y)$	m_1	c_1
3000	5.00	1.437	1.128	-0.391
3000	4.50	1.421	0.968	-0.285
3000	4.00	1.399	0.796	-0.145
3000	3.50	1.380	0.656	-0.027
3000	3.00	1.370	0.568	0.029
3000	2.50	1.376	0.509	0.083
3000	2.00	1.395	0.479	0.098
3000	1.50	1.432	0.471	0.131
3000	1.00	1.500	0.472	0.161
3000	0.50	1.612	0.440	0.187
3000	0.00	1.723	0.409	0.215
3250	5.00	1.264	0.816	-0.052
3250	4.50	1.244	0.685	0.045
3250	4.00	1.222	0.590	0.114
3250	3.50	1.210	0.521	0.151
3250	3.00	1.211	0.478	0.162
3250	2.50	1.223	0.459	0.142
3250	2.00	1.248	0.463	0.142
3250	1.50	1.294	0.477	0.144
3250	1.00	1.345	0.485	0.182
3250	0.50	1.427	0.472	0.218
3250	0.00	1.530	0.445	0.247
3500	5.00	1.110	0.636	0.095
3500	4.50	1.091	0.552	0.149
3500	4.00	1.080	0.503	0.172
3500	3.50	1.076	0.469	0.186
3500	3.00	1.080	0.462	0.168
3500	2.50	1.088	0.474	0.141
3500	2.00	1.094	0.516	0.146
3500	1.50	1.128	0.550	0.168
3500	1.00	1.185	0.572	0.214
3500	0.50	1.259	0.565	0.259
3500	0.00	1.357	0.537	0.307
3750	5.00	0.976	0.535	0.179
3750	4.50	0.964	0.482	0.215
3750	4.00	0.953	0.461	0.222
3750	3.50	0.944	0.463	0.208
3750	3.00	0.935	0.474	0.191
3750	2.50	0.935	0.497	0.174
3750	2.00	0.952	0.532	0.175
3750	1.50	0.988	0.566	0.212
3750	1.00	1.051	0.585	0.263
3750	0.50	1.125	0.598	0.324
3750	0.00	1.219	0.587	0.373
4000	5.00	0.860	0.449	0.223
4000	4.50	0.842	0.425	0.239
4000	4.00	0.826	0.421	0.240
4000	3.50	0.815	0.429	0.226
4000	3.00	0.811	0.447	0.214
4000	2.50	0.817	0.475	0.203
4000	2.00	0.836	0.498	0.223
4000	1.50	0.869	0.523	0.264
4000	1.00	0.916	0.550	0.323
4000	0.50	0.988	0.548	0.409
4000	0.00	1.080	0.525	0.476
4250	5.00	0.742	0.385	0.242
4250	4.50	0.718	0.381	0.241
4250	4.00	0.701	0.384	0.241
4250	3.50	0.694	0.390	0.227
4250	3.00	0.694	0.393	0.230
4250	2.50	0.707	0.396	0.239
4250	2.00	0.729	0.396	0.269
4250	1.50	0.759	0.399	0.334
4250	1.00	0.802	0.404	0.417
4250	0.50	0.862	0.414	0.507
4250	0.00	0.934	0.426	0.608
4500	5.00	0.635	0.322	0.226
4500	4.50	0.617	0.314	0.227
4500	4.00	0.607	0.306	0.226
4500	3.50	0.605	0.298	0.226
4500	3.00	0.608	0.289	0.228
4500	2.50	0.618	0.285	0.255
4500	2.00	0.636	0.285	0.311
4500	1.50	0.662	0.290	0.391
4500	1.00	0.697	0.300	0.491
4500	0.50	0.745	0.310	0.596
4500	0.00	0.803	0.320	0.702
4750	5.00	0.556	0.252	0.208
4750	4.50	0.549	0.237	0.215
4750	4.00	0.545	0.224	0.222
4750	3.50	0.544	0.213	0.237
4750	3.00	0.548	0.203	0.252
4750	2.50	0.556	0.199	0.291
4750	2.00	0.569	0.200	0.360
4750	1.50	0.586	0.207	0.458
4750	1.00	0.611	0.217	0.557
4750	0.50	0.643	0.229	0.675
4750	0.00	0.684	0.242	0.783
5000	5.00	0.501	0.183	0.167
5000	4.50	0.497	0.167	0.185
5000	4.00	0.493	0.155	0.207
5000	3.50	0.492	0.147	0.232
5000	3.00	0.495	0.143	0.274
5000	2.50	0.500	0.143	0.336
5000	2.00	0.505	0.148	0.422
5000	1.50	0.514	0.155	0.528
5000	1.00	0.529	0.165	0.641
5000	0.50	0.549	0.176	0.759
5000	0.00	0.574	0.189	0.877
5250	5.00	0.461	0.138	0.140
5250	4.50	0.456	0.128	0.165
5250	4.00	0.451	0.119	0.197
5250	3.50	0.448	0.114	0.243
5250	3.00	0.445	0.113	0.314
5250	2.50	0.445	0.114	0.399
5250	2.00	0.448	0.117	0.507
5250	1.50	0.453	0.124	0.624
5250	1.00	0.462	0.132	0.752
5250	0.50	0.472	0.143	0.880
5250	0.00	0.482	0.158	1.016
5500	5.00	0.424	0.111	0.136
5500	4.50	0.419	0.102	0.168
5500	4.00	0.414	0.093	0.215
5500	3.50	0.408	0.087	0.284
5500	3.00	0.403	0.085	0.372
5500	2.50	0.399	0.087	0.484
5500	2.00	0.398	0.092	0.611
5500	1.50	0.400	0.099	0.745
5500	1.00	0.404	0.106	0.889
5500	0.50	0.407	0.116	1.034
5500	0.00	0.412	0.129	1.177
5750	5.00	0.390	0.094	0.143
5750	4.50	0.383	0.084	0.188
5750	4.00	0.376	0.077	0.256
5750	3.50	0.370	0.072	0.342
5750	3.00	0.365	0.069	0.442
5750	2.50	0.360	0.069	0.576
5750	2.00	0.356	0.073	0.719
5750	1.50	0.353	0.078	0.870
5750	1.00	0.350	0.086	1.027
5750	0.50	0.347	0.096	1.180
5750	0.00	0.342	0.110	1.328
6000	5.00	0.357	0.077	0.171
6000	4.50	0.349	0.070	0.229
6000	4.00	0.342	0.065	0.310
6000	3.50	0.335	0.061	0.420
6000	3.00	0.328	0.060	0.547
6000	2.50	0.321	0.059	0.700
6000	2.00	0.315	0.061	0.856
6000	1.50	0.309	0.066	1.024
6000	1.00	0.303	0.074	1.187
6000	0.50	0.295	0.086	1.342
6000	0.00	0.286	0.100	1.502
6250	5.00	0.324	0.076	0.207
6250	4.50	0.315	0.072	0.282
6250	4.00	0.307	0.070	0.376
6250	3.50	0.299	0.068	0.507
6250	3.00	0.292	0.066	0.654
6250	2.50	0.284	0.065	0.805
6250	2.00	0.277	0.063	0.966
6500	5.00	0.292	0.080	0.243
6500	4.50	0.285	0.078	0.336
6500	4.00	0.277	0.076	0.464
6500	3.50	0.269	0.074	0.612
6500	3.00	0.258	0.074	0.766
6500	2.50	0.249	0.073	0.928
6500	2.00	0.242	0.067	1.107
6750	5.00	0.267	0.084	0.291
6750	4.50	0.259	0.083	0.412
6750	4.00	0.247	0.085	0.560
6750	3.50	0.238	0.083	0.720
6750	3.00	0.226	0.082	0.885
6750	2.50	0.215	0.079	1.064
6750	2.00	0.204	0.073	1.256
7000	5.00	0.244	0.091	0.354
7000	4.50	0.233	0.093	0.496
7000	4.00	0.219	0.097	0.658
7000	3.50	0.204	0.099	0.823
7000	3.00	0.190	0.098	1.000
7000	2.50	0.177	0.092	1.195
7000	2.00	0.162	0.082	1.404
7250	5.00	0.221	0.101	0.425
7250	4.50	0.205	0.107	0.582
7250	4.00	0.188	0.113	0.747
7250	3.50	0.170	0.115	0.922
7250	3.00	0.155	0.112	1.115
7250	2.50	0.139	0.102	1.323
7250	2.00	0.121	0.089	1.545
7500	5.00	0.197	0.116	0.496
7500	4.50	0.177	0.125	0.661
7500	4.00	0.157	0.131	0.834
7500	3.50	0.141	0.126	1.023
7500	3.00	0.122	0.120	1.227
7500	2.50	0.105	0.105	1.447
7500	2.00	0.089	0.095	1.615
7750	5.00	0.173	0.131	0.565
7750	4.50	0.153	0.138	0.737
7750	4.00	0.132	0.140	0.940
7750	3.50	0.115	0.133	1.138
7750	3.00	0.093	0.124	1.332
7750	2.50	0.076	0.108	1.509
7750	2.00	0.068	0.090	1.652
8000	5.00	0.151	0.145	0.626
8000	4.50	0.130	0.149	0.834
8000	4.00	0.108	0.148	1.034
8000	3.50	0.087	0.138	1.221
8000	3.00	0.065	0.124	1.407
8000	2.50	0.054	0.106	1.580
8000	2.00	0.049	0.086	1.674

T_{eff}	$\log g$	$(b-y)$	m_1	c_1
		[M/H] = −2.0		
3000	5.00	1.606	1.253	-0.930
3000	4.50	1.536	1.062	-0.703
3000	4.00	1.496	0.896	-0.528
3000	3.50	1.453	0.750	-0.343
3000	3.00	1.428	0.619	-0.161
3000	2.50	1.431	0.512	0.014
3000	2.00	1.452	0.455	0.117
3000	1.50	1.493	0.428	0.222
3000	1.00	1.558	0.411	0.320
3000	0.50	1.671	0.378	0.408
3000	0.00	1.818	0.319	0.477
3250	5.00	1.325	0.925	-0.480
3250	4.50	1.297	0.784	-0.343
3250	4.00	1.271	0.651	-0.210
3250	3.50	1.256	0.541	-0.081
3250	3.00	1.252	0.461	0.050
3250	2.50	1.261	0.414	0.145
3250	2.00	1.283	0.397	0.202
3250	1.50	1.322	0.397	0.258
3250	1.00	1.403	0.390	0.350
3250	0.50	1.510	0.389	0.447
3250	0.00	1.631	0.343	0.539
3500	5.00	1.147	0.736	-0.247
3500	4.50	1.119	0.612	-0.113
3500	4.00	1.100	0.511	-0.011
3500	3.50	1.091	0.442	0.069
3500	3.00	1.092	0.408	0.131
3500	2.50	1.103	0.405	0.182
3500	2.00	1.117	0.428	0.223
3500	1.50	1.153	0.457	0.296
3500	1.00	1.223	0.466	0.395
3500	0.50	1.323	0.441	0.501
3500	0.00	1.434	0.404	0.607
3750	5.00	0.984	0.569	-0.060
3750	4.50	0.968	0.479	0.033
3750	4.00	0.957	0.426	0.095
3750	3.50	0.951	0.404	0.133
3750	3.00	0.944	0.412	0.163
3750	2.50	0.947	0.427	0.233
3750	2.00	0.966	0.447	0.308
3750	1.50	1.011	0.459	0.391
3750	1.00	1.077	0.465	0.507
3750	0.50	1.169	0.445	0.622
3750	0.00	1.281	0.402	0.717
4000	5.00	0.851	0.435	0.067
4000	4.50	0.840	0.387	0.109
4000	4.00	0.828	0.360	0.144
4000	3.50	0.816	0.348	0.178
4000	3.00	0.810	0.355	0.219
4000	2.50	0.817	0.366	0.279
4000	2.00	0.844	0.371	0.377
4000	1.50	0.887	0.372	0.482
4000	1.00	0.951	0.359	0.615
4000	0.50	1.036	0.338	0.745
4000	0.00	1.130	0.306	0.862
4250	5.00	0.740	0.303	0.146
4250	4.50	0.725	0.295	0.154
4250	4.00	0.714	0.287	0.165
4250	3.50	0.706	0.282	0.192
4250	3.00	0.705	0.274	0.238
4250	2.50	0.717	0.268	0.312
4250	2.00	0.741	0.263	0.423
4250	1.50	0.778	0.257	0.548
4250	1.00	0.833	0.254	0.687
4250	0.50	0.903	0.253	0.832
4250	0.00	0.982	0.251	0.980
4500	5.00	0.648	0.238	0.160
4500	4.50	0.638	0.228	0.170
4500	4.00	0.628	0.217	0.177
4500	3.50	0.625	0.209	0.198
4500	3.00	0.629	0.200	0.232
4500	2.50	0.640	0.192	0.305
4500	2.00	0.659	0.186	0.422
4500	1.50	0.686	0.183	0.550
4500	1.00	0.725	0.182	0.679
4500	0.50	0.773	0.183	0.808
4500	0.00	0.828	0.185	0.926
4750	5.00	0.577	0.179	0.164
4750	4.50	0.570	0.165	0.170
4750	4.00	0.565	0.153	0.185
4750	3.50	0.562	0.145	0.207
4750	3.00	0.561	0.137	0.242
4750	2.50	0.565	0.132	0.320
4750	2.00	0.577	0.129	0.413
4750	1.50	0.594	0.128	0.521
4750	1.00	0.622	0.130	0.638
4750	0.50	0.652	0.133	0.761
4750	0.00	0.692	0.137	0.872
5000	5.00	0.521	0.132	0.150
5000	4.50	0.513	0.117	0.167
5000	4.00	0.508	0.105	0.183
5000	3.50	0.504	0.097	0.210
5000	3.00	0.501	0.092	0.274
5000	2.50	0.502	0.090	0.367
5000	2.00	0.507	0.091	0.470
5000	1.50	0.517	0.094	0.587
5000	1.00	0.535	0.098	0.711
5000	0.50	0.553	0.103	0.840
5000	0.00	0.579	0.108	0.965
5250	5.00	0.475	0.094	0.146
5250	4.50	0.468	0.083	0.166
5250	4.00	0.462	0.075	0.194
5250	3.50	0.456	0.069	0.242
5250	3.00	0.452	0.067	0.318
5250	2.50	0.449	0.068	0.416
5250	2.00	0.449	0.071	0.523
5250	1.50	0.451	0.075	0.665
5250	1.00	0.457	0.080	0.795
5250	0.50	0.468	0.086	0.928
5250	0.00	0.483	0.092	1.076
5500	5.00	0.433	0.078	0.149
5500	4.50	0.426	0.069	0.172
5500	4.00	0.417	0.063	0.205
5500	3.50	0.410	0.059	0.279
5500	3.00	0.404	0.057	0.373
5500	2.50	0.400	0.058	0.483
5500	2.00	0.396	0.061	0.613
5500	1.50	0.396	0.065	0.747
5500	1.00	0.399	0.070	0.883
5500	0.50	0.405	0.076	1.033
5500	0.00	0.411	0.082	1.177
5750	5.00	0.396	0.071	0.139
5750	4.50	0.387	0.065	0.170
5750	4.00	0.379	0.061	0.229
5750	3.50	0.372	0.059	0.320
5750	3.00	0.365	0.058	0.434
5750	2.50	0.358	0.059	0.567
5750	2.00	0.352	0.062	0.718
5750	1.50	0.348	0.066	0.860
5750	1.00	0.345	0.071	1.006
5750	0.50	0.344	0.076	1.165
5750	0.00	0.344	0.082	1.325
6000	5.00	0.360	0.066	0.144
6000	4.50	0.351	0.062	0.198
6000	4.00	0.343	0.059	0.281
6000	3.50	0.335	0.057	0.385
6000	3.00	0.327	0.056	0.522
6000	2.50	0.318	0.057	0.682
6000	2.00	0.310	0.060	0.847
6000	1.50	0.302	0.064	1.006
6000	1.00	0.297	0.068	1.176
6000	0.50	0.291	0.073	1.327
6000	0.00	0.286	0.079	1.480
6250	5.00	0.326	0.070	0.173
6250	4.50	0.318	0.065	0.245
6250	4.00	0.310	0.063	0.344
6250	3.50	0.300	0.063	0.473
6250	3.00	0.292	0.062	0.625
6250	2.50	0.282	0.063	0.780
6250	2.00	0.274	0.066	0.940
6500	5.00	0.296	0.077	0.214
6500	4.50	0.287	0.075	0.308
6500	4.00	0.278	0.073	0.433
6500	3.50	0.269	0.072	0.583
6500	3.00	0.259	0.071	0.741
6500	2.50	0.249	0.070	0.903
6500	2.00	0.239	0.067	1.080
6750	5.00	0.272	0.084	0.267
6750	4.50	0.263	0.083	0.385
6750	4.00	0.252	0.084	0.533
6750	3.50	0.240	0.085	0.698
6750	3.00	0.227	0.085	0.864
6750	2.50	0.215	0.083	1.041
6750	2.00	0.203	0.078	1.233
7000	5.00	0.250	0.094	0.331
7000	4.50	0.240	0.094	0.471
7000	4.00	0.226	0.097	0.639
7000	3.50	0.210	0.100	0.809
7000	3.00	0.193	0.103	0.984
7000	2.50	0.177	0.100	1.175
7000	2.00	0.162	0.090	1.386
7250	5.00	0.229	0.104	0.400
7250	4.50	0.216	0.107	0.562
7250	4.00	0.197	0.114	0.735
7250	3.50	0.179	0.118	0.909
7250	3.00	0.160	0.117	1.099
7250	2.50	0.142	0.110	1.310
7250	2.00	0.119	0.103	1.533
7500	5.00	0.208	0.115	0.470
7500	4.50	0.189	0.122	0.644
7500	4.00	0.169	0.131	0.820
7500	3.50	0.147	0.134	1.008
7500	3.00	0.128	0.128	1.214
7500	2.50	0.105	0.116	1.436
7500	2.00	0.084	0.107	1.605
7750	5.00	0.184	0.129	0.538
7750	4.50	0.161	0.140	0.719
7750	4.00	0.139	0.147	0.903
7750	3.50	0.116	0.145	1.101
7750	3.00	0.094	0.135	1.318
7750	2.50	0.073	0.121	1.502
7750	2.00	0.062	0.106	1.643
8000	5.00	0.159	0.145	0.631
8000	4.50	0.135	0.155	0.814
8000	4.00	0.114	0.156	1.003
8000	3.50	0.090	0.148	1.203
8000	3.00	0.066	0.135	1.397
8000	2.50	0.055	0.116	1.550
8000	2.00	0.048	0.097	1.650

T_{eff}	$\log g$	$(b-y)$	m_1	c_1
		[M/H] = −2.5		
3000	5.00	1.666	1.246	-0.625
3000	4.50	1.606	1.106	-0.655
3000	4.00	1.548	0.958	-0.582
3000	3.50	1.513	0.766	-0.403
3000	3.00	1.486	0.596	-0.166
3000	2.50	1.481	0.456	0.108
3000	2.00	1.496	0.368	0.327
3000	1.50	1.534	0.321	0.498
3000	1.00	1.593	0.291	0.605
3000	0.50	1.680	0.292	0.630
3000	0.00	1.805	0.307	0.570
3250	5.00	1.374	1.056	-0.501
3250	4.50	1.336	0.873	-0.435
3250	4.00	1.303	0.704	-0.337
3250	3.50	1.281	0.542	-0.148
3250	3.00	1.272	0.412	0.043
3250	2.50	1.281	0.330	0.228
3250	2.00	1.306	0.290	0.371
3250	1.50	1.357	0.270	0.496
3250	1.00	1.455	0.265	0.588
3250	0.50	1.586	0.232	0.632
3250	0.00	1.709	0.194	0.645
3500	5.00	1.151	0.785	-0.265
3500	4.50	1.127	0.623	-0.203
3500	4.00	1.110	0.473	-0.109
3500	3.50	1.098	0.362	0.021
3500	3.00	1.097	0.306	0.134
3500	2.50	1.108	0.296	0.251
3500	2.00	1.137	0.308	0.330
3500	1.50	1.184	0.325	0.413
3500	1.00	1.267	0.318	0.524
3500	0.50	1.392	0.269	0.597
3500	0.00	1.511	0.213	0.640
3750	5.00	0.988	0.544	-0.082
3750	4.50	0.975	0.417	0.004
3750	4.00	0.965	0.329	0.069
3750	3.50	0.957	0.288	0.130
3750	3.00	0.954	0.290	0.163
3750	2.50	0.958	0.310	0.239
3750	2.00	0.978	0.332	0.322
3750	1.50	1.027	0.340	0.411
3750	1.00	1.111	0.326	0.520
3750	0.50	1.214	0.292	0.624
3750	0.00	1.340	0.230	0.701
4000	5.00	0.866	0.319	0.136
4000	4.50	0.858	0.284	0.133
4000	4.00	0.851	0.261	0.149
4000	3.50	0.844	0.257	0.173
4000	3.00	0.843	0.259	0.208
4000	2.50	0.850	0.269	0.286
4000	2.00	0.875	0.277	0.386
4000	1.50	0.917	0.280	0.475
4000	1.00	0.980	0.279	0.596
4000	0.50	1.059	0.272	0.680
4000	0.00	1.159	0.244	0.770
4250	5.00	0.771	0.222	0.208
4250	4.50	0.765	0.206	0.205
4250	4.00	0.755	0.204	0.205
4250	3.50	0.743	0.210	0.224
4250	3.00	0.738	0.215	0.264
4250	2.50	0.746	0.216	0.347
4250	2.00	0.766	0.218	0.442
4250	1.50	0.805	0.220	0.549
4250	1.00	0.860	0.225	0.660
4250	0.50	0.925	0.230	0.770
4250	0.00	0.992	0.235	0.862
4500	5.00	0.683	0.158	0.207
4500	4.50	0.674	0.154	0.201
4500	4.00	0.663	0.153	0.206
4500	3.50	0.655	0.155	0.219
4500	3.00	0.652	0.154	0.240
4500	2.50	0.655	0.156	0.294
4500	2.00	0.667	0.158	0.376
4500	1.50	0.691	0.162	0.479
4500	1.00	0.731	0.167	0.589
4500	0.50	0.780	0.173	0.715
4500	0.00	0.836	0.178	0.814
4750	5.00	0.608	0.114	0.199
4750	4.50	0.598	0.108	0.194
4750	4.00	0.587	0.104	0.208
4750	3.50	0.579	0.102	0.230
4750	3.00	0.576	0.105	0.254
4750	2.50	0.575	0.107	0.311
4750	2.00	0.582	0.112	0.379
4750	1.50	0.596	0.117	0.481
4750	1.00	0.624	0.121	0.592
4750	0.50	0.656	0.127	0.715
4750	0.00	0.693	0.133	0.843
5000	5.00	0.543	0.085	0.168
5000	4.50	0.534	0.079	0.172
5000	4.00	0.524	0.074	0.190
5000	3.50	0.516	0.074	0.225
5000	3.00	0.510	0.075	0.261
5000	2.50	0.508	0.078	0.332
5000	2.00	0.510	0.081	0.419
5000	1.50	0.520	0.085	0.538
5000	1.00	0.534	0.089	0.660
5000	0.50	0.554	0.094	0.796
5000	0.00	0.582	0.100	0.921

T_{eff}	$\log g$	$(b-y)$	m_1	c_1
5250	5.00	0.486	0.065	0.159
5250	4.50	0.476	0.060	0.174
5250	4.00	0.467	0.057	0.192
5250	3.50	0.457	0.056	0.232
5250	3.00	0.449	0.056	0.293
5250	2.50	0.446	0.058	0.389
5250	2.00	0.445	0.060	0.506
5250	1.50	0.448	0.063	0.622
5250	1.00	0.453	0.066	0.765
5250	0.50	0.463	0.072	0.910
5250	0.00	0.478	0.078	1.055
5500	5.00	0.441	0.056	0.145
5500	4.50	0.429	0.053	0.178
5500	4.00	0.419	0.051	0.215
5500	3.50	0.410	0.051	0.273
5500	3.00	0.403	0.051	0.362
5500	2.50	0.399	0.053	0.478
5500	2.00	0.395	0.055	0.602
5500	1.50	0.393	0.058	0.747
5500	1.00	0.396	0.061	0.896
5500	0.50	0.401	0.066	1.061
5500	0.00	0.407	0.071	1.210
5750	5.00	0.400	0.051	0.150
5750	4.50	0.389	0.048	0.196
5750	4.00	0.380	0.046	0.241
5750	3.50	0.372	0.045	0.330
5750	3.00	0.364	0.045	0.439
5750	2.50	0.356	0.046	0.571
5750	2.00	0.350	0.048	0.715
5750	1.50	0.347	0.052	0.876
5750	1.00	0.345	0.057	1.041
5750	0.50	0.343	0.063	1.210
5750	0.00	0.344	0.068	1.377
6000	5.00	0.364	0.045	0.158
6000	4.50	0.356	0.043	0.219
6000	4.00	0.347	0.041	0.290
6000	3.50	0.338	0.040	0.389
6000	3.00	0.329	0.041	0.526
6000	2.50	0.320	0.042	0.673
6000	2.00	0.312	0.045	0.834
6000	1.50	0.304	0.050	1.007
6000	1.00	0.296	0.055	1.181
6000	0.50	0.289	0.061	1.354
6000	0.00	0.283	0.066	1.516
6250	5.00	0.330	0.050	0.181
6250	4.50	0.322	0.047	0.253
6250	4.00	0.313	0.047	0.350
6250	3.50	0.304	0.047	0.480
6250	3.00	0.295	0.048	0.636
6250	2.50	0.284	0.049	0.792
6250	2.00	0.272	0.051	0.952
6500	5.00	0.299	0.059	0.223
6500	4.50	0.291	0.057	0.316
6500	4.00	0.282	0.057	0.439
6500	3.50	0.272	0.057	0.591
6500	3.00	0.262	0.058	0.752
6500	2.50	0.250	0.059	0.916
6500	2.00	0.239	0.058	1.093
6750	5.00	0.271	0.072	0.277
6750	4.50	0.265	0.068	0.392
6750	4.00	0.256	0.068	0.540
6750	3.50	0.243	0.071	0.709
6750	3.00	0.229	0.073	0.878
6750	2.50	0.216	0.072	1.055
6750	2.00	0.203	0.066	1.247
7000	5.00	0.247	0.084	0.338
7000	4.50	0.239	0.082	0.476
7000	4.00	0.226	0.085	0.647
7000	3.50	0.210	0.088	0.822
7000	3.00	0.193	0.090	0.997
7000	2.50	0.177	0.089	1.188
7000	2.00	0.162	0.080	1.401
7250	5.00	0.225	0.095	0.404
7250	4.50	0.213	0.097	0.565
7250	4.00	0.195	0.104	0.744
7250	3.50	0.176	0.108	0.919
7250	3.00	0.160	0.105	1.108
7250	2.50	0.140	0.100	1.321
7250	2.00	0.120	0.093	1.546
7500	5.00	0.203	0.108	0.474
7500	4.50	0.185	0.115	0.650
7500	4.00	0.164	0.122	0.829
7500	3.50	0.146	0.121	1.015
7500	3.00	0.127	0.116	1.222
7500	2.50	0.107	0.101	1.446
7500	2.00	0.085	0.092	1.620
7750	5.00	0.180	0.122	0.545
7750	4.50	0.158	0.132	0.728
7750	4.00	0.135	0.138	0.913
7750	3.50	0.116	0.132	1.110
7750	3.00	0.097	0.119	1.327
7750	2.50	0.074	0.104	1.515
7750	2.00	0.063	0.085	1.657
8000	5.00	0.155	0.139	0.611
8000	4.50	0.131	0.148	0.813
8000	4.00	0.110	0.149	1.028
8000	3.50	0.091	0.136	1.223
8000	3.00	0.071	0.116	1.419
8000	2.50	0.055	0.098	1.573
8000	2.00	0.048	0.080	1.683

T_{eff}	$\log g$	$(b-y)$	m_1	c_1
		[M/H] = −3.0		
3000	5.00	1.746	1.259	-2.185
3000	4.50	1.706	1.099	-1.785
3000	4.00	1.668	0.922	-1.370
3000	3.50	1.633	0.746	-0.969
3000	3.00	1.607	0.581	-0.550
3000	2.50	1.600	0.434	-0.165
3000	2.00	1.614	0.324	0.116
3000	1.50	1.647	0.258	0.282
3000	1.00	1.695	0.223	0.388
3000	0.50	1.765	0.240	0.410
3000	0.00	1.865	0.240	0.340
3250	5.00	1.422	1.149	-1.665
3250	4.50	1.395	0.980	-1.358
3250	4.00	1.364	0.814	-1.004
3250	3.50	1.341	0.631	-0.604
3250	3.00	1.331	0.468	-0.223
3250	2.50	1.340	0.348	0.064
3250	2.00	1.368	0.280	0.242
3250	1.50	1.420	0.240	0.354
3250	1.00	1.510	0.201	0.452
3250	0.50	1.653	0.141	0.567
3250	0.00	1.787	0.098	0.660
3500	5.00	1.164	0.918	-1.077
3500	4.50	1.143	0.742	-0.762
3500	4.00	1.128	0.559	-0.412
3500	3.50	1.116	0.411	-0.101
3500	3.00	1.120	0.313	0.119
3500	2.50	1.136	0.274	0.253
3500	2.00	1.178	0.261	0.337
3500	1.50	1.252	0.255	0.416
3500	1.00	1.354	0.229	0.530
3500	0.50	1.487	0.170	0.648
3500	0.00	1.597	0.139	0.672
3750	5.00	0.989	0.571	-0.414
3750	4.50	0.974	0.423	-0.161
3750	4.00	0.965	0.313	0.044
3750	3.50	0.964	0.250	0.185
3750	3.00	0.973	0.228	0.274
3750	2.50	0.994	0.237	0.328
3750	2.00	1.035	0.251	0.372
3750	1.50	1.099	0.243	0.454
3750	1.00	1.189	0.218	0.591
3750	0.50	1.294	0.186	0.689
3750	0.00	1.417	0.134	0.723
4000	5.00	0.846	0.311	0.056
4000	4.50	0.844	0.236	0.165
4000	4.00	0.843	0.196	0.231
4000	3.50	0.843	0.182	0.284
4000	3.00	0.847	0.192	0.316
4000	2.50	0.861	0.208	0.343
4000	2.00	0.891	0.215	0.396
4000	1.50	0.947	0.207	0.492
4000	1.00	1.032	0.175	0.611
4000	0.50	1.118	0.148	0.715
4000	0.00	1.204	0.130	0.765
4250	5.00	0.753	0.167	0.241
4250	4.50	0.750	0.144	0.265
4250	4.00	0.746	0.134	0.279
4250	3.50	0.741	0.136	0.298
4250	3.00	0.740	0.148	0.311
4250	2.50	0.747	0.161	0.339
4250	2.00	0.772	0.166	0.418
4250	1.50	0.816	0.162	0.491
4250	1.00	0.876	0.152	0.578
4250	0.50	0.946	0.136	0.669
4250	0.00	1.011	0.124	0.750
4500	5.00	0.681	0.097	0.276
4500	4.50	0.671	0.095	0.263
4500	4.00	0.662	0.093	0.263
4500	3.50	0.655	0.096	0.274
4500	3.00	0.653	0.102	0.297
4500	2.50	0.657	0.110	0.336
4500	2.00	0.673	0.115	0.368
4500	1.50	0.699	0.119	0.444
4500	1.00	0.737	0.124	0.497
4500	0.50	0.784	0.121	0.574
4500	0.00	0.834	0.121	0.679
4750	5.00	0.612	0.067	0.232
4750	4.50	0.603	0.063	0.225
4750	4.00	0.593	0.062	0.231
4750	3.50	0.584	0.063	0.246
4750	3.00	0.578	0.066	0.267
4750	2.50	0.576	0.074	0.303
4750	2.00	0.583	0.080	0.343
4750	1.50	0.596	0.089	0.435
4750	1.00	0.623	0.091	0.543
4750	0.50	0.657	0.092	0.658
4750	0.00	0.695	0.095	0.775
5000	5.00	0.550	0.045	0.157
5000	4.50	0.541	0.043	0.163
5000	4.00	0.530	0.045	0.171
5000	3.50	0.520	0.044	0.197
5000	3.00	0.511	0.045	0.235
5000	2.50	0.508	0.047	0.296
5000	2.00	0.509	0.051	0.378
5000	1.50	0.518	0.059	0.498
5000	1.00	0.535	0.067	0.620
5000	0.50	0.556	0.070	0.755
5000	0.00	0.585	0.071	0.887
5250	5.00	0.496	0.034	0.148
5250	4.50	0.485	0.034	0.159
5250	4.00	0.474	0.033	0.180
5250	3.50	0.463	0.034	0.211
5250	3.00	0.454	0.035	0.261
5250	2.50	0.450	0.034	0.341
5250	2.00	0.450	0.035	0.459
5250	1.50	0.451	0.044	0.597
5250	1.00	0.457	0.052	0.744
5250	0.50	0.468	0.059	0.896
5250	0.00	0.484	0.064	1.044
5500	5.00	0.447	0.030	0.159
5500	4.50	0.436	0.028	0.167
5500	4.00	0.425	0.027	0.190
5500	3.50	0.414	0.027	0.237
5500	3.00	0.407	0.026	0.314
5500	2.50	0.401	0.026	0.427
5500	2.00	0.396	0.030	0.573
5500	1.50	0.393	0.038	0.720
5500	1.00	0.397	0.043	0.871
5500	0.50	0.403	0.048	1.030
5500	0.00	0.411	0.054	1.193
5750	5.00	0.404	0.029	0.149
5750	4.50	0.393	0.028	0.173
5750	4.00	0.382	0.028	0.219
5750	3.50	0.373	0.028	0.293
5750	3.00	0.366	0.026	0.404
5750	2.50	0.360	0.027	0.542
5750	2.00	0.353	0.031	0.697
5750	1.50	0.348	0.035	0.856
5750	1.00	0.346	0.037	1.024
5750	0.50	0.344	0.042	1.195
5750	0.00	0.343	0.047	1.358
6000	5.00	0.367	0.030	0.152
6000	4.50	0.355	0.031	0.197
6000	4.00	0.344	0.032	0.271
6000	3.50	0.336	0.031	0.377
6000	3.00	0.328	0.031	0.511
6000	2.50	0.320	0.031	0.660
6000	2.00	0.309	0.036	0.822
6000	1.50	0.303	0.038	0.988
6000	1.00	0.296	0.043	1.165
6000	0.50	0.289	0.049	1.354
6000	0.00	0.285	0.052	1.523
6250	5.00	0.334	0.035	0.175
6250	4.50	0.320	0.039	0.246
6250	4.00	0.311	0.039	0.342
6250	3.50	0.301	0.040	0.471
6250	3.00	0.290	0.042	0.629
6250	2.50	0.280	0.043	0.786
6250	2.00	0.270	0.043	0.948
6500	5.00	0.302	0.045	0.216
6500	4.50	0.291	0.047	0.308
6500	4.00	0.281	0.048	0.430
6500	3.50	0.271	0.048	0.582
6500	3.00	0.259	0.049	0.746
6500	2.50	0.249	0.048	0.911
6500	2.00	0.239	0.046	1.089
6750	5.00	0.272	0.055	0.269
6750	4.50	0.264	0.055	0.383
6750	4.00	0.255	0.055	0.529
6750	3.50	0.242	0.057	0.700
6750	3.00	0.230	0.056	0.872
6750	2.50	0.216	0.056	1.050
6750	2.00	0.203	0.052	1.242
7000	5.00	0.247	0.065	0.330
7000	4.50	0.241	0.063	0.465
7000	4.00	0.230	0.063	0.636
7000	3.50	0.214	0.067	0.815
7000	3.00	0.195	0.071	0.990
7000	2.50	0.178	0.070	1.181
7000	2.00	0.163	0.062	1.396
7250	5.00	0.225	0.073	0.395
7250	4.50	0.217	0.072	0.554
7250	4.00	0.200	0.077	0.736
7250	3.50	0.178	0.085	0.912
7250	3.00	0.159	0.085	1.100
7250	2.50	0.144	0.076	1.314
7250	2.00	0.121	0.068	1.540
7500	5.00	0.203	0.084	0.465
7500	4.50	0.189	0.088	0.641
7500	4.00	0.166	0.096	0.822
7500	3.50	0.146	0.098	1.008
7500	3.00	0.130	0.090	1.214
7500	2.50	0.108	0.085	1.439
7500	2.00	0.085	0.079	1.619
7750	5.00	0.180	0.099	0.537
7750	4.50	0.160	0.106	0.722
7750	4.00	0.137	0.111	0.906
7750	3.50	0.118	0.107	1.101
7750	3.00	0.099	0.098	1.319
7750	2.50	0.077	0.089	1.513
7750	2.00	0.067	0.074	1.660
8000	5.00	0.155	0.116	0.607
8000	4.50	0.132	0.124	0.803
8000	4.00	0.112	0.122	1.010
8000	3.50	0.090	0.114	1.216
8000	3.00	0.067	0.104	1.409
8000	2.50	0.055	0.087	1.569
8000	2.00	0.049	0.070	1.686

Appendix C

Strömgren Photometry of NGC 188 and NGC 6819

The photometric observations of NGC 188 and NGC 6819 in the *uvby* filter set were obtained over three separate runs in September/October 1999 using the 1.8 meter Plaskett Telescope at the Dominion Astrophysical Observatory. The thinned SITe-5 CCD detector used for the observations was composed of an array of 1024 x 1024 pixels and yielded an effective field of view of $9.2' \times 9.2'$. The log of the cluster observations providing such information as the date, filter/exposure combinations, and airmass is given in Table C.1.[1] Atmospheric conditions throughout each of the 7 nights remained quite stable and lead to photometric skies for all three runs with average nightly seeing ranging between $2.05''$ and $2.73''$.

All initial science images were pre-processed using a number of bias frames and sky flats taken during the evening and morning twilight of each night. A total of 20 individual bias frames per night were median combined into a single master bias which was subsequently subtracted from the rest of the images. In addition, a medianed master flat for each Strömgren filter was produced from no fewer than 10 sky flats per night and used to account for the effects of pixel-to-pixel variations and gradients

[1] Due to the fact that the filter wheel on the telescope could only accommodate two Strömgren filters at a time, observations were limited to using a combination of *uy* and *vb* filters on separate nights.

Table C.1: Journal of *uvby* observations for NGC 188 and NGC 6819.

Date	Cluster	Filter	Exposures	Airmass
1999 Sept 2...	NGC 6819	y	3 x 30 s	1.0
		y	2 x 120 s	1.6
		y	3 x 180 s	1.2
		y	1 x 300 s	1.0
		u	3 x 1200 s	1.4-1.5
		u	4 x 1800 s	1.0-1.2
	NGC 188	y	3 x 180 s	1.3
		u	3 x 1800 s	1.3
1999 Sept 3...	NGC 6819	b	3 x 160 s	1.0
		b	3 x 240 s	1.0
		b	1 x 400 s	1.0
		b	1 x 600 s	1.0
		v	1 x 360 s	1.0
		v	1 x 480 s	1.0
		v	3 x 600 s	1.0
		v	3 x 960 s	1.0
	NGC 188	b	3 x 240 s	1.3
		v	3 x 900 s	1.3
1999 Sept 11...	NGC 6819	y	3 x 120 s	1.4
		y	3 x 180 s	1.1
		u	3 x 1200 s	1.4-1.6
		u	3 x 1800 s	1.0-1.1
1999 Sept 12...	NGC 6819	y	30 x 60 s	1.6-1.8
1999 Sept 13...	NGC 6819	y	2 x 120 s	1.1
		y	3 x 180 s	1.0
		u	2 x 1800 s	1.0
1999 Sept 30...	NGC 6819	b	2 x 250 s	1.0
		v	2 x 900 s	1.0
	NGC 188	b	6 x 250 s	1.3
		v	6 x 900 s	1.3
1999 Oct 1.....	NGC 6819	y	2 x 120 s	1.0
		y	3 x 180 s	1.0
		u	2 x 1800 s	1.1
	NGC 188	y	9 x 180 s	1.3
		u	5 x 1800 s	1.3

in each image.

Several bright and isolated Strömgren standard stars taken from the lists of Crawford & Barnes (1970b) and Perry, Olsen, & Crawford (1987) were observed in conjunction with the cluster images to derive the transformations between instrumental magnitudes and the standard *uvby* system. To account for uncertainties in the timing of the camera shutter, all standard stars (as well as the cluster fields) required integration times of at least five seconds. This fact posed a problem, however, for these bright field standards because they saturated the chip in this minimum exposure time. To avoid saturation, the telescope was defocused by a small amount to allow the light from each standard star to be distributed over a larger area in the image. During the reduction process, the instrumental magnitudes for each standard were derived using aperture photometry while taking into careful consideration an aperture size which would be large enough to account for broad distribution of light over a large number of pixels, but small enough to both limit the amount of sky as well as ensure that light from neighboring stars did not enter into the aperture. After inspection of all standards on all frames, it was concluded that apertures with radii between of 25-30 pixels were sufficient enough for such considerations. Despite this, 5 standards were eventually discarded from subsequent photometric reductions because either their light distributions extended beyond the edge of the largest aperture or there was light contamination from other nearby defocused stars.

In addition to the primary field standards mentioned above, a number of stars from the open cluster NGC 752 were also observed and used as secondary standards (Crawford and Barnes, 1970a). These cluster stars were chosen largely because they were faint enough to avoid saturation of the chip without defocussing the camera. This fact allowed for a direct investigation of any possible differences between color transformations derived from the defocused standards and the cluster standards. The inclusion of the stars from NGC 752 also led to an slight increase in the color range for the standard transformations. In total, no fewer than 21 standard stars were used for

each night of observation to derive the transformation coefficients in every Strömgren filter (see below).

Images taken of both NGC 188 and NGC 6819 focused primarily on the cluster centers in order to maximize the number of stars. Due to the relative sparseness of NGC 188, however, additional observations of the four quadrants surrounding the cluster center were made in all four Strömgren filters. The photometric reduction of the cluster frames was performed using point spread function (PSF) photometry as part of the DAOPHOT II suite of programs (Stetson 1987). In summary, between 70 and 95 uncrowded and unsaturated stars in each cluster frame were used to construct a high signal-to-noise PSF. This PSF was then fitted to all stars detected on an individual frame under the assumption it was allowed to vary quadratically across the image. To ensure that the majority of stars had been detected, the resulting subtracted image from the PSF fitting routine was scanned for any faint and/or blended stellar images which were not detected during the initial run.

After all the cluster frames were reduced in the manner mentioned above, a set of coordinate transformations were derived to refer positions of each star on each frame to the coordinate system of a single master frame. These coordinate transformations along with a list of stellar positions on each frame were then fed into the multiple-PSF fitting ALLFRAME algorithm (Stetson 1994) which yielded the final PSF photometry for all detected stars and all frames. A total of 40 relatively bright and isolated stars were then selected from the photometry files and used to derive the aperture corrections. These corrections, defined as the net differences between a star's profile-fitted magnitude and its total magnitude as measured through a generously large aperture (typically containing $> 99\%$ of the total light), were determined by constructing a set of empirical growth curves using the DAOGROW program (Stetson 1990). For this procedure, all neighboring stars were first subtracted from the frames leaving only the 40 selected stars. The analysis proceeds by measuring stellar magnitudes through a set of concentric apertures centered on each star and selecting only those magnitudes

which had errors less than 0.01 mag to define the growth curve. The final aperture corrections were subsequently determined from the overall convergence of a large number of stellar growth curves and applied to the instrumental PSF magnitudes for each star.

The final step in the photometric reduction process is the transformation of the raw, instrumental magnitudes derived from PSF fitting and aperture corrections to the standard *uvby* system. After examination of the residuals between the standard and observed magnitudes for all standard stars and testing their dependence against any parameter that could correlate with the residuals (i.e. airmass, exposure time, photometric color, etc.), the final adopted transformation equations took the following form for each Strömgren filter:

$$m_{inst} = M_{std} + AX + B(v-y)_{std} + C \tag{C.1}$$

where M_{std} and m_{inst} are the standard and instrumental *uvby* magnitudes for each star in question and X and $(v-y)_{std}$ are the airmass and photometric color of the standard star, respectively. The three coefficients listed in the above equation (A, B, and C) were solved by the method of simultaneous least-square fitting. Table C.2 provides the values of these coefficients for each night of observation. Once the transformation coefficients were derived, a number of bright isolated stars in each cluster were transformed to the standard system to serve as local zero-point standards. These local standards were then used to transform the instrumental magnitudes of all other detected stars in all cluster frames to the standard *uvby* system.

Table C.2: The transformation coefficients for the Strömgren standard star observations. For all Strömgren filters the transformation equations took the form $m_{inst} = M_{std} + AX + B(v-y)_{std} + C$. Columns 6, 7, and 8 provide the number of standard stars (N) together with their range in $(v-y)$ color and airmass (X) which were used to derive the transformations while column 9 denotes the rms (σ) of the resulting standard star residuals.

Date	Filter	A	B	C	N	$(v-y)$	X	σ
Sept 2	u	0.737 ± 0.012	-0.137 ± 0.013	6.107 ± 0.016	22	0.72−1.75	1.0−2.0	0.019
	y	0.209 ± 0.009	-0.030 ± 0.007	4.139 ± 0.009	21	-	-	0.011
Sept 3	v	0.416 ± 0.020	-0.007 ± 0.018	5.384 ± 0.023	24	0.64−1.76	1.0−2.1	0.032
	b	0.385 ± 0.014	-0.059 ± 0.013	4.515 ± 0.017	26	-	-	0.024
Sept 11	u	0.827 ± 0.031	-0.119 ± 0.018	6.190 ± 0.022	28	0.50−2.10	1.0−2.2	0.044
	y	0.216 ± 0.020	-0.021 ± 0.011	4.174 ± 0.014	29	-	-	0.028
Sept 12	u	0.715 ± 0.049	-0.101 ± 0.025	6.161 ± 0.024	24	0.55−1.98	1.0−1.7	0.031
	y	0.195 ± 0.027	-0.024 ± 0.014	4.152 ± 0.013	24	-	-	0.022
Sept 13	u	0.668 ± 0.013	-0.118 ± 0.008	6.139 ± 0.010	33	0.25−2.10	1.0−2.0	0.021
	y	0.154 ± 0.010	-0.032 ± 0.006	4.154 ± 0.008	33	-	-	0.017
Sept 30	v	0.340 ± 0.014	0.010 ± 0.010	5.302 ± 0.010	43	0.25−2.10	1.0−2.0	0.029
	b	0.098 ± 0.018	-0.056 ± 0.012	4.454 ± 0.011	43	-	-	0.030
Oct 1	u	0.762 ± 0.014	-0.128 ± 0.014	6.090 ± 0.014	43	0.25−2.10	1.0−2.0	0.038
	y	0.203 ± 0.013	-0.027 ± 0.011	4.150 ± 0.011	41	-	-	0.030

In regards to the photometric accuracy of the final calibrated photometry, Figure C.1 presents the computed residuals of the standard stars for each Strömgren filter. In all four panels, the plotted residual is computed as the difference between the observed magnitude (based on its weighted average over all nights the standard was observed) and the actual standard magnitude. Furthermore, filled circles are used to represent the bright field standards while open circles give the residuals for the secondary standard stars observed in NGC 752. The figure shows that there are no systematic trends of the residuals with magnitude. Furthermore, the secondary standard stars observed in NGC 752 not only extend down to fainter magnitudes in each filter, but also exhibit no obvious differences in residuals from the primary standards.

Samples of the final standard *uvby* photometry for both NGC 188 and NGC 6819 are provided in Tables C.3 and C.4. Since the photometry given here is the first of its kind published to date, no direct comparison between the present data and previous Strömgren studies of these two clusters can be presented. Both clusters, however, have been extensively surveyed in the past few years using broadband filters, and the photometric studies of Rosvick & Vandenberg (1998) for NGC 6819 and Sarajedini et al. (1999) for NGC 188 yield a large number of stars in common with the present study. Given that Strömgren y magnitudes are often equated to broadband V, Figure C.2 examines the differences between y and V for stars in common between the present photometry and the two studies mentioned above. For each cluster, the comparison involves stars selected on the criteria that their photometric uncertainties are less than 0.015 mag in both y and V. For NGC 6819 the average difference between magnitudes denoted in the panel is negligible while it is just slightly less 0.01 mag for NGC 188. For both clusters, there appears to be quite good agreement between the Strömgren y and broadband V magnitudes with no obvious trends in the data, though there is an increased scatter toward fainter stars.

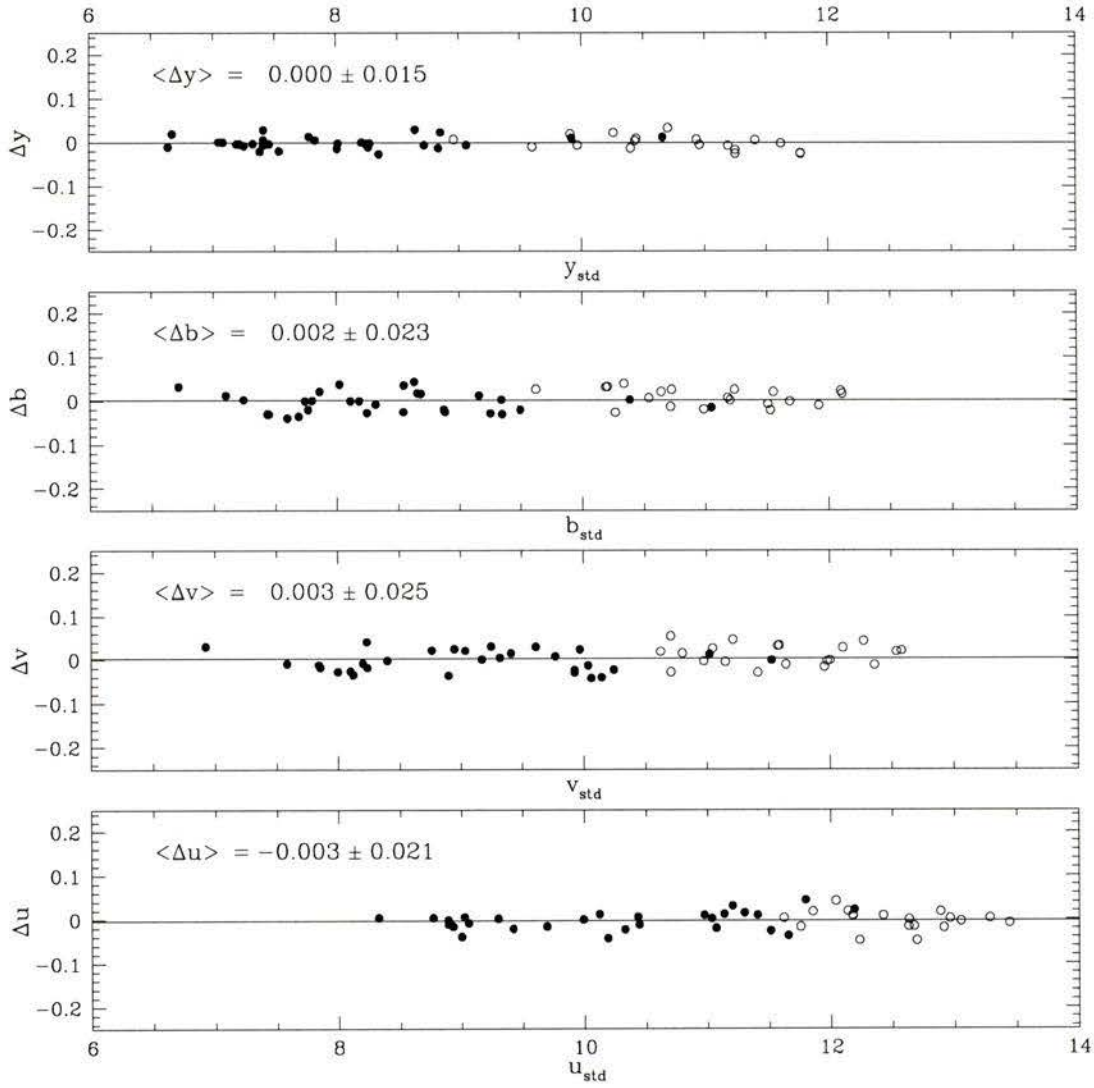

Figure C.1: Residuals between the computed and standard magnitudes for 51 standard stars observed in conjunction with the cluster observations. Each panel plots the residual versus standard magnitude for each Strömgren filter along with their computed means and standard deviations. Solid circles indicate field standards while open circles are the secondary standard stars observed in the open cluster NGC 752.

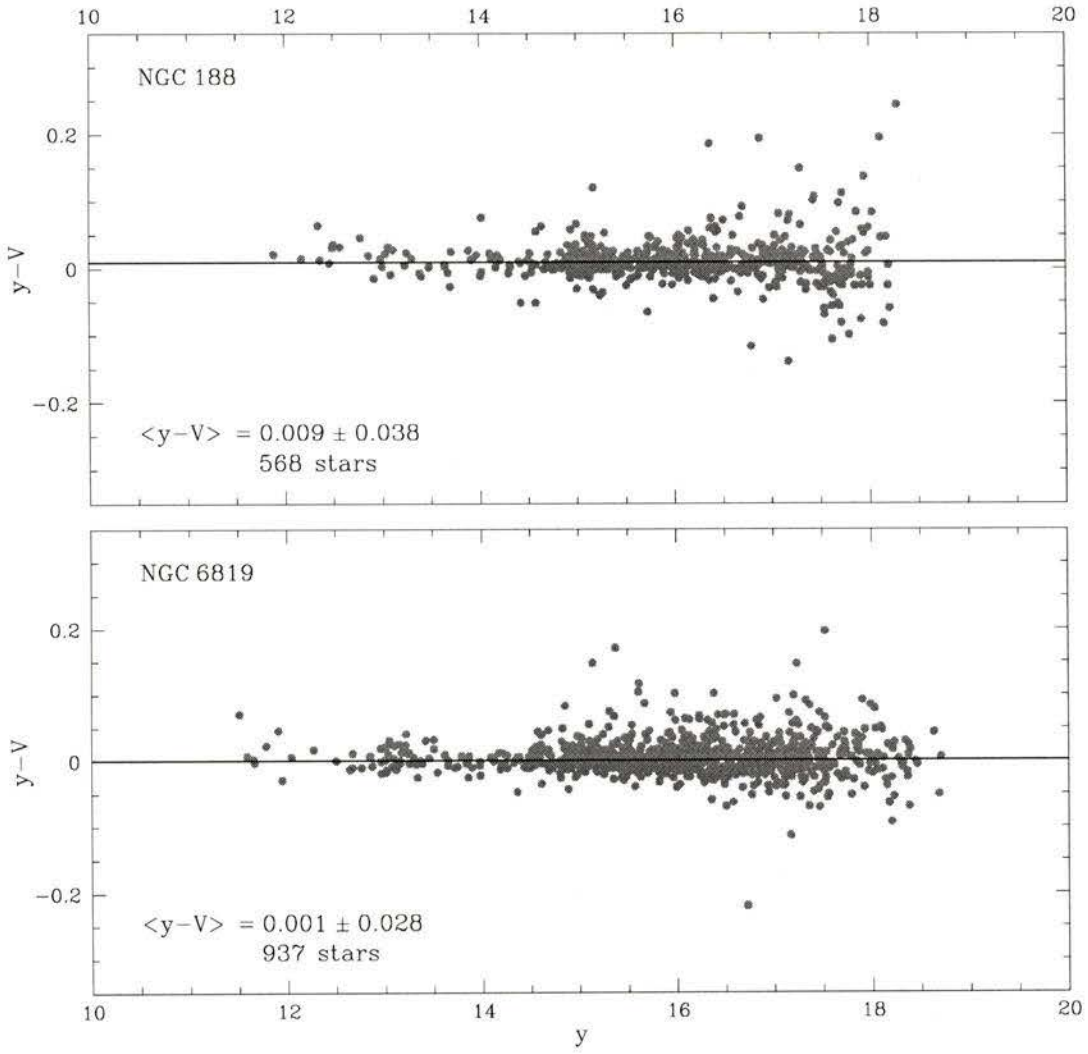

Figure C.2: A comparison between Strömgren y magnitudes derived in this study and broadband V magnitudes taken from the studies of Sarajedini et al. (1999) for NGC 188 and Rosvick & VandenBerg (1998) for NGC 6819. The computed averages are based on the number of stars indicated in each panel which have photometric uncertainties less than 0.015 mag in both y and V.

Table C.3: A sample of the final *uvby* photometry for a total of 1128 stars detected in NGC 188. For each star listed in the first column, the global CCD x and y positions, individual u, v, b, and y magnitudes on the standard system along with their corresponding mean errors, and the number of detections are given the remaining columns.

Star ID	X pos.	Y pos.	u	σ_u	v	σ_v	b	σ_b	y	σ_y	n_u	n_v	n_b	n_y
2	50.72	476.58	14.846	0.0227	13.594	0.0052	12.723	0.0095	12.123	0.0249	5	6	6	7
4	304.48	228.73	15.959	0.0075	14.358	0.0043	13.126	0.0022	12.410	0.0033	5	6	7	7
6	162.93	26.64	14.075	0.0112	13.273	0.0042	12.761	0.0062	12.363	0.0031	5	6	6	7
7	381.80	495.53	16.358	0.0348	14.635	0.0097	13.207	0.0079	12.459	0.0061	5	6	6	6
9	340.94	74.28	15.145	0.0067	14.282	0.0041	13.729	0.0069	13.301	0.0028	5	6	7	7
16	167.34	187.71	16.988	0.0148	15.479	0.0053	14.362	0.0020	13.672	0.0022	5	6	6	7
17	135.24	200.31	17.276	0.0159	15.721	0.0037	14.469	0.0044	13.697	0.0034	5	6	6	7
19	334.11	300.22	17.155	0.0052	15.673	0.0079	14.571	0.0046	13.910	0.0043	6	7	8	8
20	212.66	239.64	15.131	0.0404	14.636	0.0236	14.372	0.0196	14.156	0.0184	6	8	9	9
21	418.39	350.15	15.604	0.0097	14.698	0.0062	14.237	0.0062	13.919	0.0031	6	6	6	8
22	312.46	305.16	17.027	0.0184	16.019	0.0051	15.407	0.0047	14.942	0.0057	6	7	8	8
23	311.14	302.83	16.089	0.0133	15.114	0.0073	14.683	0.0077	14.357	0.0155	6	7	8	8
24	415.31	194.60	16.648	0.0141	15.466	0.0144	14.623	0.0121	14.017	0.0055	5	6	7	7
26	474.82	332.58	16.961	0.0237	15.590	0.0131	14.587	0.0064	14.005	0.0025	6	3	3	8
27	214.51	241.32	17.194	0.1942	16.167	0.0491	15.648	0.0693	15.135	0.0189	6	8	9	9
28	245.77	332.39	15.743	0.0057	14.797	0.0140	14.347	0.0139	14.018	0.0088	7	7	7	9
30	338.28	152.36	17.286	0.0054	15.833	0.0041	14.753	0.0013	14.100	0.0039	5	6	7	7
31	266.63	107.51	17.267	0.0083	15.845	0.0079	14.769	0.0062	14.117	0.0024	5	6	7	7
32	164.12	348.09	15.206	0.0106	14.243	0.0032	13.800	0.0032	13.479	0.0023	5	6	6	7
33	384.39	272.38	17.378	0.0113	15.918	0.0050	14.848	0.0042	14.200	0.0024	5	7	8	7

Table C.4: Same as Table C.3 but for a sample of 3151 stars in NGC 6819.

Star ID	X pos.	Y pos.	u	σ_u	v	σ_v	b	σ_b	y	σ_y	n_u	n_v	n_b	n_y
1	83.39	210.32	14.529	0.0133	12.122	0.0068	11.751	0.0074	10.331	0.0038	15	10	10	54
2	276.85	262.71	16.457	0.0260	14.044	0.0446	12.690	0.0489	11.505	0.0021	17	10	10	56
3	337.09	415.74	16.667	0.0027	14.395	0.0043	12.741	0.0033	11.585	0.0011	17	10	10	56
4	345.78	289.60	15.078	0.0012	13.507	0.0027	12.372	0.0032	11.653	0.0014	17	10	10	56
5	344.46	317.49	15.602	0.0010	13.849	0.0019	12.490	0.0043	11.661	0.0013	17	10	10	56
6	322.88	494.93	16.828	0.0055	15.482	0.3759	13.088	0.0652	11.908	0.0028	17	10	10	56
7	282.65	271.75	16.491	0.0017	14.456	0.0027	12.750	0.0023	11.716	0.0015	17	10	10	56
8	143.01	170.55	16.692	0.0089	14.601	0.0036	12.848	0.0049	11.781	0.0015	17	10	10	56
9	322.24	378.96	16.053	0.0033	14.352	0.0020	12.902	0.0015	11.945	0.0008	17	10	10	56
10	213.04	366.56	16.520	0.0041	14.574	0.0032	13.009	0.0022	12.041	0.0011	17	10	10	56
11	182.57	317.65	16.429	0.0042	14.585	0.0014	13.157	0.0024	12.268	0.0011	17	10	10	56
13	412.00	489.73	15.632	0.0049	14.183	0.0033	13.149	0.0090	12.500	0.0010	17	10	10	56
14	199.62	100.64	18.001	0.0075	15.716	0.0050	13.813	0.0045	12.599	0.0021	17	10	10	56
15	177.44	360.19	16.644	0.0022	14.875	0.0033	13.500	0.0017	12.669	0.0008	17	10	10	56
16	295.31	300.26	14.698	0.0039	13.280	0.0025	12.883	0.0047	12.640	0.0026	17	10	10	56
17	265.41	318.39	16.313	0.0038	14.711	0.0019	13.483	0.0032	12.667	0.0018	17	10	10	56
19	230.93	335.97	15.988	0.0027	14.575	0.0024	13.505	0.0011	12.761	0.0011	17	10	10	56
20	232.18	323.64	16.534	0.0029	14.875	0.0020	13.628	0.0024	12.845	0.0019	17	10	10	56
21	275.10	184.28	16.160	0.0017	14.635	0.0026	13.554	0.0023	12.848	0.0007	17	10	10	56
23	306.68	279.81	16.346	0.0017	14.738	0.0036	13.609	0.0037	12.870	0.0012	17	10	10	56

Bibliography

Allende Prieto, C. and Lambert, D. L.: 2000, *Astron. J.* **119**, 2445

Alonso, A., Arribas, S., and Martínez-Roger, C.: 1996a, *Astron. & Astrophys. Supp.* **117**, 227

Alonso, A., Arribas, S., and Martinez-Roger, C.: 1996b, *Astron. & Astrophys.* **313**, 873

Alonso, A., Arribas, S., and Martínez-Roger, C.: 1999, *Astron. & Astrophys. Supp.* **139**, 335

Anders, E. and Grevesse, N.: 1989, *Geochim. Cosmochim. Acta* **53**, 197

Anthony-Twarog, B. J. and Twarog, B. A.: 1994, *Astron. J.* **107**, 1577

Anthony-Twarog, B. J. and Twarog, B. A.: 2000, *Astron. J.* **120**, 3111

Axer, M., Fuhrmann, K., and Gehren, T.: 1994, *Astron. & Astrophys.* **291**, 895

Bell, K. L. and Berrington, K. A.: 1987, *J. Phys. B: At. Mol. Phys.* **20**, L353

Bell, R. A., Balachandran, S. C., and Bautista, M.: 2001, *Astrophys. J. Letters* **546**, L65

Bell, R. A. and Gustafsson, B.: 1978, *Astron. & Astrophys. Supp.* **34**, 229+

Bell, R. A. and Gustafsson, B.: 1989, *M.N.R.A.S.* **236**, 653

Bell, R. A., Paltoglou, G., and Tripicco, M. J.: 1994, *M.N.R.A.S.* **268**, 771+

Bergbusch, P. A. and VandenBerg, D. A.: 2001, *Astrophys. J.* **556**, 322

Bessell, M. S., Castelli, F., and Plez, B.: 1998, *Astron. & Astrophys.* **333**, 231

Blackwell, D. E. and Lynas-Gray, A. E.: 1994, *Astron. & Astrophys.* **282**, 899

Blackwell, D. E. and Shallis, M. J.: 1977, *M.N.R.A.S.* **180**, 177

Boesgaard, A. M.: 1989, *Astrophys. J.* **336**, 798

Boesgaard, A. M. and Friel, E. D.: 1990, *Astrophys. J.* **351**, 467

Bolte, M.: 1992, *Astrophys. J. Supp.* **82**, 145

Bonifacio, P., Caffau, E., and Molaro, P.: 2000, *Astron. & Astrophys. Supp.* **145**, 473

Bragaglia, A., Carretta, E., Gratton, R. G., Tosi, M., Bonanno, G., Bruno, P., Calì, A., Claudi, R., Cosentino, R., Desidera, S., Farisato, G., Rebeschini, M., and Scuderi, S.: 2001, *Astron. J.* **121**, 327

Briley, M. M., Grundahl, F., and Andersen, M. I.: 1999, in *American Astronomical Society Meeting*, Vol. 195, pp 0303+

Caputo, F., Chieffi, A., Castellani, V., Collados, M., Roger, C. M., and Paez, E.: 1990, *Astron. J.* **99**, 261

Carbon, D. F., Barbuy, B., Kraft, R. P., Friel, E. D., and Suntzeff, N. B.: 1987, *Pub. Astron. Soc. Pacific* **99**, 335

Carney, B. W.: 1996, *Pub. Astron. Soc. Pacific* **108**, 900+

Carretta, E. and Gratton, R. G.: 1997, *Astron. & Astrophys. Supp.* **121**, 95

Carretta, E., Gratton, R. G., Clementini, G., and Fusi Pecci, F.: 2000, *Astrophys. J.* **533**, 215

Castelli, F.: 1991, *Astron. & Astrophys.* **251**, 106

Castelli, F., Gratton, R. G., and Kurucz, R. L.: 1997, *Astron. & Astrophys.* **318**, 841

Castelli, F. and Kurucz, R. L.: 1994, *Astron. & Astrophys.* **281**, 817

Cayrel, R., Cayrel de Strobel, G., and Campbell, B.: 1985, *Astron. & Astrophys.* **146**, 249

Clementini, G., Gratton, R. G., Carretta, E., and Sneden, C.: 1999, *M.N.R.A.S.* **302**, 22

Crawford, D. L. and Barnes, J. V.: 1970a, *Astron. J.* **75**, 946+

Crawford, D. L. and Barnes, J. V.: 1970b, *Astron. J.* **75**, 978+

Crawford, D. L. and Perry, C. L.: 1966, *Astron. J.* **71**, 206+

de Bruijne, J. H. J., Hoogerwerf, R., and de Zeeuw, P. T.: 2001, *Astron. & Astrophys.* **367**, 111

Dinescu, D. I., Demarque, P., Guenther, D. B., and Pinsonneault, M. H.: 1995, *Astron. J.* **109**, 2090+

Dreiling, L. A. and Bell, R. A.: 1980, *Astrophys. J.* **241**, 736

Eggen, O. J.: 1982, *Astrophys. J. Supp.* **50**, 221

Fan, X., Burstein, D., Chen, J. ., Zhu, J., Jiang, Z., Wu, H., Yan, H., Zheng, Z., Zhou, X., Fang, L. ., Chen, F., Deng, Z., Chu, Y., Hester, J. J., Windhorst, A., Li, Y., Lu, P., Sun, W. ., Chen, W. ., Tsay, W. ., Chiueh, T. ., Chou, C. ., Ko, C. ., Lin, T. ., Guo, H. ., and Byun, Y. .: 1996, *Astron. J.* **112**, 628+

Fernley, J., Barnes, T. G., Skillen, I., Hawley, S. L., Hanley, C. J., Evans, D. W., Solano, E., and Garrido, R.: 1998, *Astron. & Astrophys.* **330**, 515

Friel, E. D. and Janes, K. A.: 1993, *Astron. & Astrophys.* **267**, 75

Fuhrmann, K.: 1998, *Astron. & Astrophys.* **330**, 626

Fulbright, J. P.: 2000, *Astron. J.* **120**, 1841

Gratton, R. G.: 1998, *M.N.R.A.S.* **296**, 739

Gratton, R. G., Carretta, E., and Castelli, F.: 1996, *Astron. & Astrophys.* **314**, 191

Gratton, R. G., Fusi Pecci, F., Carretta, E., Clementini, G., Corsi, C. E., and Lattanzi, M.: 1997, *Astrophys. J.* **491**, 749+

Gratton, R. G., Sneden, C., Carretta, E., and Bragaglia, A.: 2000, *Astron. & Astrophys.* **354**, 169

Grebel, E. K. and Richtler, T.: 1992, *Astron. & Astrophys.* **253**, 359

Grevesse, N., Lambert, D. L., Sauval, A. J., van Dishoeck, E. F., Farmer, C. B., and Norton, R. H.: 1990, *Astron. & Astrophys.* **232**, 225

Grevesse, N., Lambert, D. L., Sauval, A. J., van Dishoek, E. F., Farmer, C. B., and Norton, R. H.: 1991, *Astron. & Astrophys.* **242**, 488

Grundahl, F. and Andersen, M. I.: 1999, *Astrophys & Space Science* **265**, 197

Grundahl, F., Vandenberg, D. A., and Andersen, M. I.: 1998, *Astrophys. J. Letters*

500, L179

Grundahl, F., VandenBerg, D. A., Bell, R. A., Andersen, M. I., and Stetson, P. B.: 2000a, *Astron. J.* **120**, 1884

Grundahl, F., Vandenberg, D. A., Stetson, P. B., Andersen, M. I., and Briley, M.: 2000b, in *The Galactic Halo : From Globular Cluster to Field Stars, Proceedings of the 35th Liege International Astrophysics Colloquium, held 5-8 July, 1999. Edited by A. Noels, P. Magain, D. Caro, E. Jehin, G. Parmentier, and A. A. Thoul. Liege, Belgium : Institut d'Astrophysique et de Geophysique, 2000., p.503*, pp 503+

Gustafsson, B., Bell, R. A., Eriksson, K., and Nordlund, A.: 1975, *Astron. & Astrophys.* **42**, 407

Hauck, B. and Mermilliod, M.: 1998, *Astron. & Astrophys. Supp.* **129**, 431

Hayes, D. S. and Latham, D. W.: 1975, *Astrophys. J.* **197**, 593

Henyey, L., Vardya, M. S., and Bodenheimer, P.: 1965, *Astrophys. J.* **142**, 841+

Hesser, J. E., Harris, W. E., Vandenberg, D. A., Allwright, J. W. B., Shott, P., and Stetson, P. B.: 1987, *Pub. Astron. Soc. Pacific* **99**, 739

Hilker, M.: 2000, *Astron. & Astrophys.* **355**, 994

Hilker, M. and Richtler, T.: 2000, *Astron. & Astrophys.* **362**, 895

Hobbs, L. M., Thorburn, J. A., and Rodriguez-Bell, T.: 1990, *Astron. J.* **100**, 710

Houdashelt, M. L., Bell, R. A., and Sweigart, A. V.: 2000a, *Astron. J.* **119**, 1448

Houdashelt, M. L., Bell, R. A., Sweigart, A. V., and Wing, R. F.: 2000b, *Astron. J.* **119**, 1424

Johnson, H. L. and Morgan, W. W.: 1951, *Astrophys. J.* **114**, 522+

Johnson, H. L. and Morgan, W. W.: 1953, *Astrophys. J.* **117**, 313+

Johnson, J. A. and Bolte, M.: 1998, *Astron. J.* **115**, 693+

Kalirai, J. S., Richer, H. B., Fahlman, G. G., Cuillandre, J., Ventura, P., D'Antona, F., Bertin, E., Marconi, G., and Durrell, P. R.: 2001, *Astron. J.* **122**, 266

Kaluzny, J., Krzeminski, W., Mazur, B., Wysocka, A., and Stepien, K.: 1997, *Acta*

Astronomica **47**, 249

Kaluzny, J., Kubiak, M., Szymanski, M., Udalski, A., Krzeminski, W., Mateo, M., and Stanek, K. Z.: 1998, *Astron. & Astrophys. Supp.* **128**, 19

King, J. R.: 1997, *Astron. J.* **113**, 2302+

Kraft, R. P., Sneden, C., Smith, G. H., Shetrone, M. D., and Fulbright, J.: 1998, *Astron. J.* **115**, 1500

Kurucz, R.: 1993, *ATLAS9 Stellar Atmosphere Programs and 2 km/s grid. Kurucz CD-ROM No. 13. Cambridge, Mass.: Smithsonian Astrophysical Observatory, 1993.* 13

Kurucz, R. L.: 1991, in *Presicsion Photometry: Astrophysics of the Galaxy*, pp 27–44

Layden, A. C., Hanson, R. B., Hawley, S. L., Klemola, A. R., and Hanley, C. J.: 1996, *Astron. J.* **112**, 2110+

Lindoff, U.: 1972, *Astron. & Astrophys. Supp.* **7**, 497+

Manduca, A. and Bell, R. A.: 1979, *Pub. Astron. Soc. Pacific* **91**, 848

Meibom, S.: 2000, *Astron. & Astrophys.* **361**, 929

Meléndez, J., Barbuy, B., and Spite, F. .: 2001, *Astrophys. J.* **556**, 858

Montgomery, K. A., Marschall, L. A., and Janes, K. A.: 1993, *Astron. J.* **106**, 181

Moon, T. T. and Dworetsky, M. M.: 1985, *M.N.R.A.S.* **217**, 305

Napiwotzki, R., Schoenberner, D., and Wenske, V.: 1993, *Astron. & Astrophys.* **268**, 653

Nissen, P. E., Hoeg, E., and Schuster, W. J.: 1997, *ESA SP-402: Hipparcos - Venice '97* **402**, 225

Nissen, P. E., Twarog, B. A., and Crawford, D. L.: 1987, *Astron. J.* **93**, 634

Perry, C. L., Olsen, E. H., and Crawford, D. L.: 1987, *Pub. Astron. Soc. Pacific* **99**, 1184

Perryman, M. A. C., Brown, A. G. A., Lebreton, Y., Gomez, A., Turon, C., de Strobel, G. C., Mermilliod, J. C., Robichon, N., Kovalevsky, J., and Crifo, F.: 1998, *Astron. & Astrophys.* **331**, 81

Perryman, M. A. C., Lindegren, L., Kovalevsky, J., Hoeg, E., Bastian, U., Bernacca, P. L., Crézé, M., Donati, F., Grenon, M., van Leeuwen, F., van der Marel, H., Mignard, F., Murray, C. A., Le Poole, R. S., Schrijver, H., Turon, C., Arenou, F., Froeschlé, M., and Petersen, C. S.: 1997, *Astron. & Astrophys.* **323**, L49

Reglero, V., Fabregat, J., and Suso, J.: 1992, *Astron. & Astrophys. Supp.* **92**, 565

Reid, I. N.: 1997, *Astron. J.* **114**, 161+

Relyea, L. J. and Kurucz, R. L.: 1978, *Astrophys. J. Supp.* **37**, 45

Richter, P., Hilker, M., and Richtler, T.: 1999, *Astron. & Astrophys.* **350**, 476

Rosvick, J. M. and Vandenberg, D. A.: 1998, *Astron. J.* **115**, 1516

Ryan, S. G., Norris, J. E., and Beers, T. C.: 1999, *Astrophys. J.* **523**, 654

Salaris, M. and Weiss, A.: 1997, *Astron. & Astrophys.* **327**, 107

Sarajedini, A., von Hippel, T., Kozhurina-Platais, V., and Demarque, P.: 1999, *Astron. J.* **118**, 2894

Saxner, M. and Hammarback, G.: 1985, *Astron. & Astrophys.* **151**, 372

Schlegel, D. J., Finkbeiner, D. P., and Davis, M.: 1998, *Astrophys. J.* **500**, 525+

Schuster, W. J. and Nissen, P. E.: 1989, *Astron. & Astrophys.* **221**, 65

Shetrone, M. D. and Sandquist, E. L.: 2000, *Astron. J.* **120**, 1913

Sneden, C., Kraft, R. P., Prosser, C. F., and Langer, G. E.: 1991, *Astron. J.* **102**, 2001

Spiesman, W. J.: 1992, *Astrophys. J. Letters* **397**, L103

Stetson, P. B.: 1987, *Pub. Astron. Soc. Pacific* **99**, 191

Stetson, P. B.: 1990, *Pub. Astron. Soc. Pacific* **102**, 932

Stetson, P. B. and Harris, W. E.: 1988, *Astron. J.* **96**, 909

Strömgren, B.: 1963, *Quart. Jour. Royal Astron. Society* **4**, 8+

Strömgren, B.: 1966, *Ann. Rev. Astron. & Astrophys* **4**, 433+

Tautvaisiene, G., Edvardsson, B., Tuominen, I., and Ilyin, I.: 2000, *Astron. & Astrophys.* **360**, 499

Taylor, B. J.: 1994, *Pub. Astron. Soc. Pacific* **106**, 452

Thévenin, F. and Idiart, T. P.: 1999, *Astrophys. J.* **521**, 753

Twarog, B. A. and Anthony-Twarog, B. J.: 1989, *Astron. J.* **97**, 759

VandenBerg, D. A.: 2000, *Astrophys. J. Supp.* **129**, 315

VandenBerg, D. A. and Bell, R. A.: 1985, *Astrophys. J. Supp.* **58**, 561

VandenBerg, D. A., Swenson, F. J., Rogers, F. J., Iglesias, C. A., and Alexander, D. R.: 2000, *Astrophys. J.* **532**, 430

Wishart, A. W.: 1979, *M.N.R.A.S.* **187**, 59P

Zhao, G. and Magain, P.: 1990, *Astron. & Astrophys.* **238**, 242

Zinn, R. and West, M. J.: 1984, *Astrophys. J. Supp.* **55**, 45

Zoccali, M., Renzini, A., Ortolani, S., Bragaglia, A., Bohlin, R., Carretta, E., Ferraro, F. R., Gilmozzi, R., Holberg, J. B., Marconi, G., Rich, R. M., and Wesemael, F.: 2001, *Astrophys. J.* **553**, 733

VITA

Surname: Clem Given Names: James Lewis

Place of Birth: Ozark, Arkansas, United States of America

Educational Institutions Attended:

University of Arkansas	1994 – 1998
University of Victoria	1998 – 2001

Degrees Awarded:

B.Sc. (Magna Cum Laude), University of Arkansas	1998

Honors and Awards:

Newell Corporation Scholarship	1994 – 1998
Fulbright College of Arts & Sciences Academic Scholarship	1996 – 1998
Rear Admiral William C. Bryson Scholarship in Astronomy	1996 – 1998
J. Harry & Catherine H. Wood Scholarship	1997 – 1998
Phi Beta Kappa Member	1998 – 2001

University of Victoria Partial Copyright License

Title of Dissertation:

Strömgren Color-Temperature Relations for Cool Stars

Author: [redacted]

James Lewis Clem
November 15, 2001